Ministry of Environment
of Denmark
Environmental
Protection Agency

Mapping groundwater vulnerability to pesticide contamination through fractured clays

CLAYFRAC

Pesticide Research
no 206

January 2022

Publisher: The Danish Environmental Protection Agency

Authors:
Jens Aamand, GEUS
Nora Badawi, GEUS
Peter Roll Jakobsen, GEUS
Peter R. Jørgensen, PJ-Bluetech ApS
Klaus Mosthaf, DTU
Lars Troldborg, GEUS
Massimo Rolle, DTU

ISBN: 978-87-7038-375-2

Contents

1.	**PREFACE**	**6**
2.	**SUMMARY AND CONCLUSION**	**7**
3.	**INTRODUCTION**	**10**
3.1	Selection of Field sites	12
4.	**METHODS**	**14**
4.1	The excavations and characterization methods	14
4.2	Sorption and degradation	16
4.2.1	Sampling	16
4.2.2	Degradation	17
4.2.3	Sorption	18
4.3	Hydrology and LUC columns	19
4.3.1	LUC samples acquisition and laboratory setup	19
4.3.2	Laboratory procedures and experiments	21
4.3.3	Matrix permeability, porosity, and texture	23
4.3.4	Identification and mapping of preferential flow in fractures and macropores	24
4.3.5	Calculation of apertures for fracture and fracture channels	24
4.3.6	Chemical analyses	24
4.4	Modelling	24
4.4.1	Mathematical model	25
4.4.2	Initial model calibration and tests	26
4.4.3	Model setups	27
5.	**RESULTS**	**32**
5.1	Geological description of the 4 sites	32
5.1.1	Havdrup-Salløv	32
5.1.2	Farum	37
5.1.3	Holbæk	40
5.1.4	Tokkekøb	43
5.2	Sorption and degradation	48
5.2.1	Degradation of MCPA and bentazon	48
5.2.2	Sorption	51

5.3 LUC hydraulic experiments 54
5.3.1 Fractures and biopores in the LUC samples 54
5.3.2 Fractures and biopores as preferential flow paths 57
5.3.3 Hydraulic conductivity and fracture hydraulic apertures 59
5.3.4 Pesticide transport experiments 62
5.4 Modelling 63
5.4.1 Excavation site 63
5.4.2 LUC experiments 64
5.4.3 Investigation of the influence of different parameters 67

6. DISCUSSION 77
6.1 Parameters controlling pesticide leaching in clayey tills 77
6.2 Hydrological parameters determined by LUC 79
6.2.1 Representing field scale fracturing and flow with the LUC method 80
6.2.2 Comparison with LUC from other study sites 81
6.3 Importance of sorption and degradation 84
6.4 PM-type and vulnerability 85

7. References 88

Appendix 1.1 Soil extraction and analysis of bentazon and MCPA

Appendix 1.2 Drilling report from well situated about 600 m west of the Farum excavation

Appendix 1.3 Drilling report from well 198.342 situated about 800 m northeast of the Holbæk excavation

1. PREFACE

This study was carried out in the period 2017 - 2020 by the Geological Survey of Denmark and Greenland GEUS; project leader: Jens Aamand) in collaboration with Department of Environmental Engineering, Technical University of Denmark (DTU) and PJ-Bluetech ApS The study was funded by the Danish Ministry of Environment's Research Program for Pesticides (MST no. 667-00226).

The project work was followed by a steering and review committee with the participants:

- Henrik F. Brødsgaard, PhD Danish Environmental Protection Agency, (Chairman),
- Anne Louise Gimsing, PhD Danish Environmental Protection Agency. From November 2019 Danish Agriculture and Food Council
- Philip Grinder Pedersen, PhD Danish Environmental Protection Agency
- Steen Marcher, Danish Environmental Protection Agency
- Professor Merete Styczen, Dept. of Plant and Environmental Sciences, University of Copenhagen
- Head of Department Niels Lindemark, Danish Plant Protection
- Advisor Walter Brüsch, Danish Society for Nature Conservation
- Senior scientist Vibeke Ernstsen, PhD The National Geological Survey for Denmark and Greenland, GEUS
- Professor Poul L. Bjerg, PhD Department of Environmental Engineering, Technical University of Denmark (DTU)
- Professor Hans Christian Bruun Hansen, Department of Plant and Environmental Sciences, University of Copenhagen
- Professor Carsten Suhr Jacobsen, Environmental Science, Aarhus University.

The project group wishes to thank Anne Louise Gimsing, Professor Merete Styczen, Senior Researcher Vibeke Ernstsen, GEUS, Steen Marcher, Philip Grinder Pedersen, Jakob Lanstorp, Danish Environmental Protection Agency, Associate Professor Bjarne W. Strobel University of Copenhagen, and Jacob Gudbjerg University of Copenhagen for reviewing and providing suggestions for improvement of the report. We would further like to thank the master students Chloe Lanters, Una Péturesdóttir, Rasmus Thalund-Hansen all from Department of Environmental Engineering, DTU, and Luca Modesti, GEUS for their scientific contribution during their research connected to their theses. We also want to thank Associate Professor Majken Caroline Looms Zibar, and PhD student Esben Bing Svendsen both from Department of Geosciences and Natural Resource management, University of Copenhagen for good suggestions and fruitful discussions at project meetings. Finally, we wish to thank technicians Hans Jørgen Lorentzen, Spire Maja Kiersgaard, Pia Bach Jakobsen, and Christina Rosenberg Lynge all from GEUS for their support during sampling and in the laboratory and Niels Eskildsen for allowing field work and excavations on the Havdrup-Salløv site.

2. SUMMARY AND CONCLUSION

This report describes results from the CLAYFRAC project investigating possibilities to map or rank clay localities according to their vulnerability to pesticide leaching. The project entailed a combined and multiscale experimental and modelling approach starting from the polymorphological (PM) concept for ranking the heterogeneity of clay-till deposits. The PM concept separate clay-till deposits in landforms differing by their pattern of superimposed geomorphological units. Four large excavations have been established representing different PM landforms. The Havdrup-Salløv excavation was established in a PM landform named MML meaning a landform where basement marine clay (L) is overlaid by a moraine plain (M), overlaid by another moraine plain (M). MML landforms have previously been studied in detail why the other excavations were carried out at less studied landforms. The Farum excavation was on the PM-landform DMS being an outwash plain (S), overlaid by a moraine plain, overlaid by a hummocky moraine (D); the Holbæk excavation was on the PM-form DM being a moraine plain overlaid by a hummocky moraine, and finally the Tokkekøb excavation was on the PM-form DR being a marginal moraine (R), overlaid by a hummocky moraine. The lithology and presence of preferential flow paths, including macropores (wormholes, root channels, burrows etc), tectonic and desiccation fractures, and sand lenses were characterized at each excavation. All sites were geologically highly heterogeneous with different clay units being mixed with sand lenses and sand layers. This was most pronounced at Holbæk where half of the excavation showed exposure of sandy deposits.

The Havdrup-Salløv excavation was characterized by having three till units separated by sand layers. Macropores dominated in the upper till with many wormholes present down to one m depth. Grey fractures were present to a depth of 1-3 meter below surface (mbs), below which the fracture surface linings became red due to iron precipitation. Macropores suggested to be relic root channels were observed to more than 5.9 m depth. At Farum the excavation revealed two till units separated by sand layers. Macropores, but not fractures were present in the upper till and there were many sand layers and sand lenses that may as well serve as preferential water transport routes. In contrast, in the lower till many large connected vertical and horizontal fractures with iron precipitation were present. At Holbæk one part of the excavation was dominated by sandy lake deposits, while the other part was primarily clayey, but with dispersed sand lenses. Wormholes were present in large numbers penetrating to greatest depth at the sand deposits (2 mbs). Furthermore, the Holbæk LUC-middle (2.6-3.1 mbs) revealed macropores probably being relic root channels. Fractures were present from about one mbs being first grey and at below 3 mbs red. The Tokkekøb excavation was characterized by two till units above sandy lake deposits present at 3-4.5 mbs. No fractures were seen in the upper till, but instead this had the highest number of wormholes (up to 1048 per m^2). Fractures with iron precipitates were present in the lower till, some being slanted and more than 6 m long, but their density decreased with depth.

Overall, all the sites were very heterogeneous with many geological units scattered among each other, implying that it may be difficult to attribute defined geological characteristics to PM types. The geological characterization, though, showed the following general trends: 1) Macropores, including wormholes were present in all upper tills where they probably are the most dominant preferential waterflow routes, 2) fractures changed colour from grey to red due to iron precipitation at greater depths, and 3) sand deposits were present at all locations in the form of sand layers and sand lenses of different thicknesses.

Six large undisturbed columns (LUCs) were sampled at different depths of the excavations; three in Havdrup and three in Holbæk. The LUC is a unique setup to determine preferential flow properties of clayey tills, including hydraulic conductivities, fracture apertures, water flow, and pesticide transport. Hydraulic characterization and transport experiments were performed in the LUC setups. Solute transport was investigated using tracers (e.g., bromide and the colour dye brilliant blue) as well as a mixture of pesticides (MCPA, bentazon and tebuconazole) with different properties. The LUC experiments showed that the hydraulic conductivity in the upper tills with grey fractures were significantly higher than observed in the deeper layers dominated by fractures with iron precipitations. The highest conductivity was measured in the Holbæk LUC-top (2.0-2.4 mbs) where macropores in the form of root channels were also present (> 200/m^2). The root channel density then decreased to 5/m^2 at Holbæk LUC-middle and no root channels were observed in the deepest LUC. The hydraulic conductivity was several orders of magnitude lower in the other LUCs that all had fractures with iron precipitates at their surfaces and except for the Holbæk LUC-top and middle and Havdrup LUC-bottom (5.4-5.9 mbs) there were no open macropores present. The lower overall hydraulic conductivity at increasing depth was attributed the fracture aperture also decreasing with depth. This was also reflected in the transport of MCPA and bentazon as very rapid breakthrough of these pesticides, following the added bromide tracer was observed in the Holbæk LUC-top. Breakthrough of tebuconazole was retarded compared to the tracer in accordance with the higher sorption coefficient of this pesticide. In contrast, the breakthrough concentrations of MCPA and bentazon were about 50 % lower in the Havdrup LUC-bottom than Holbæk LUC-top probably due to the longer residence time and higher amounts of the pesticides being accumulated in the LUC due to diffusion into the matrix. This retardation was even higher for tebuconazole where only trace concentrations were measured in the outlet.

The influence of different geological features on the waterflow, observed either by field observations or in the LUC experiments was simulated using process-based numerical modelling. These features included fracture aperture, spacing (fracture density), and orientation as well as presence of sand layers. The fracture aperture was shown to be a strong determinant of pesticide leaching as the water flux through fractures scales with the third power of the hydraulic fracture aperture according to the cubic law. This may be even more important for the cylindrical macropores as their cross-sectional area scales with the fourth power of the hydraulic pore radius. Decreased fracture density and appearance of dead-end fractures were also shown to limit waterflow. Partially iron oxide filled root cannels were present in Havdrup LUC-bottom, shown to be prehistoric tees (Jørgensen et al., 2020). Simulations of such root cannels in a fracture plane were also modelled and shown to strongly influence the breakthrough time, reducing it from decades to a few days. Sand lenses and sand layers were present at all sites contributing to their high heterogeneity. Model simulations showed that if e.g. macropores are connected to such sand layers they may have a huge effect on waterflow. This indicates that when the macropores and fractures lose significance with depth, then sand layers may take over becoming the preferential water transport routes.

In conclusion, although we know that fractures and biopores are important pathways for pesticide transport through clayey tills, our understanding of how and where this occurs is still fragmented. We need a more solid understanding of the hydraulic properties of the deeper anoxic clay-tills, and why different clay locations apparently have different capacities to retain pesticides. The inherent properties of microbiological processes in clay-tills at depths below the plough zone must be understood if we are to provide realistic simulations of transport of pesticides at a larger scale in both oxidised and anoxic environments. The experimental and modelling investigation of CLAYFRAC illuminated the combined role of fractures and macropores as key preferential flow paths in clayey tills at depths covered by the performed investigation. It is suggested that below the depths of current or ancient root channels, waterflow and pesticide migration in the glacial tills are to a high degree controlled by textual heterogeneities e.g. embedded sand lenses, sand layers, micro-layers together with textural variation in clay matrix. The multi-scale investigations performed in CLAYFRAC highlighted different features of four field sites with different PM types. All four sites showed a strong local variability of the properties of the clayey tills and were ranked as potentially vulnerable. We showed that the Holbæk side had a high sedimentological variability with sandy units and fractures/macropores in the upper clayey tills, which suggests a high potential vulnerability for this PM type. However, in order to develop comprehensive vulnerability mapping methods knowledge about heterogeneities at greater depths below the ‘fracture zone’ investigated in CLAYFRAC is needed as well as a systematic verification with pesticides contamination of groundwater aquifers underlying the clayey till aquitards.

3. INTRODUCTION

The intensive use of pesticides not only in agriculture, but also in urban areas has led to increased finding of pesticides and their degradation products in groundwater resources. Although approval of new pesticides requires documentation that they do not leach to the groundwater, even approved pesticides can be found in groundwater aquifers. It has previously been assumed that clay-till deposits protect groundwater from pollution, but today we know that clay-tills are vulnerable to pesticide leaching because they contain biopores and fractures which serve as rapid transport routes for water and dissolved pesticides. To improve pesticide approval practice and to assess the impact of agriculture on groundwater quality it is urgent that we develop tools to identify which clay-till deposits are most vulnerable to pesticide leaching.

Clay deposits often forms low permeable compacted layers along aquifers, so called aquitards, formations that are widespread in the northern hemisphere including Northern Europe, Russia, and Central Europe. In Denmark aquifers overlaid by clay-till aquitards covers about 40 % of the country (Gravesen et al., 2014). Clay-till deposits typically have a low matrix permeability, which has been thought to protect underlying groundwater resources by preventing anthropogenic chemical substances to be transported though the clay. However, the frequent occurrence of contaminants in aquifers confined beneath clay-till has shown that they are not safe barriers to contaminant transport (Jørgensen and Frederica 1992; Beven and Germann, 2013; Rosenbom *et al*., 2015; Badawi *et al*., 2015), and we must rethink our understanding of water and pesticide transport processes in clay-tills.

Near surface clay-till deposits are commonly divided into an upper oxidised and a lower anoxic zone (figure 1). The reddish, oxidised zone is characterised by an oxidation of ferric iron in the clay minerals, whereas the anoxic zone is greyish due to reduced sedimentary iron. The upper oxidised zone is highly bioturbated, and wormholes and root structures control the hydraulic properties of the clay (Chambon et al., 2010; Klint and Gravesen, 1999). The density of hydraulically active biopores in the oxidised zone can be very high, e.g. in an agricultural soil 800 to 1200 biopores per square meter have been found in the top 50 cm land surface (Nielsen et al., 2010; Bockhorn et al., 2015). The upper oxidised zone is here defined as the depth of the drainage pipes, which normally are situated 100 to 110 cm below the surface. The lower oxidised zone extends from the drainage depth to the anoxic zone, and this zone is dominated by desiccation and glaciotectonic fractures and root-casts, which often follow existing fractures. In the anoxic zone, fractures are less frequent and are typically of glacio-tectonic origin. All clay layers can contain horizontal sand lenses, and these are important for contaminant transport as they interconnect the hydraulically active fracture network (Klint and Gravesen, 1999; Klint 2001; figure 1). There is also a carbonate leaching front controlled by infiltration of atmospheric CO_2 dissolving bound calcite ($CaCO_3$). This front is important as it changes the porosity and hydraulic conductivity and thereby transport of water through the clay-till.

The nature of the glacial clay-till sediments, the geometry of fractures and biopores, and the presence of sand lenses affects the hydraulic connectivity in the clay-till and consequently flow paths, which in turn also determine biogeochemical and microbial processes including sorption and degradation (Åkeson et al., 2014; Kitchen et al., 2015). The natural recharge of groundwater through the aquitard to the groundwater is pivotal for assessment of aquifer vulnerability to pesticide contamination (Cuthberth et al., 2010; Gates et al., 2014). In Danish clayey tills more than 90 % of the groundwater recharge and pesticide leaching occur in fractures, biopores, and sand lenses (Rosenbom et al., 2015). These preferential flow paths are only a fraction of the soil volume, so rapidly leaching pesticides have only limited contact with the surrounding matrix sediments. Experimental data describing the migration of pesticides in fractured clay deposits and their diffusion into the low permeability matrix is very limited. Sorption and degradation processes which may occur both at the fracture wall and in the sediment matrix add to the complexity, as these processes determine the ultimate fate of the pesticides and thereby their risk of leaching to the underlying aquifer.

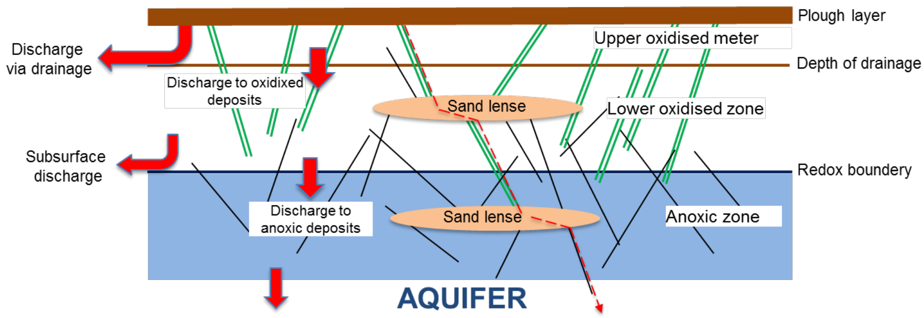

FIGURE 1. Clay-till aquitard with fractures (black lines), biopores (green double lines) and sand lenses. The red dashed line shows a typical pesticide transport route through permeable sand lenses, interconnecting biopores and glacio-tectonic fractures.

Sorption and microbial activity are some of the most important processes controlling the flux of pesticides on agricultural fields to underlying groundwater resources (Sørensen et al. 2003). These processes depend on factors such as the geochemistry and hydrology under the plough layer (Meckenstock et al. 2015), and these interlinked processes must be understood to construct precise models of the environmental fate of pesticides. The factors acting on pesticides in fractured clay are not well understood, and knowledge of individual processes such as degradation and sorption (Badawi *et al*., 2015) and the local hydrogeological settings (Rosenbom *et al*., 2015) is needed. The mineralisation potential of pesticides in loamy agricultural soil is known to decrease dramatically at the interface between the plough layer and the oxic zone (Badawi *et al.* 2013a, 2013b). The distribution of the pesticide mineralisation potential is heterogeneous below the plough layer and appears to be linked to the hydraulically active flow paths (Badawi *et al.* 2013b).

Another important source uncertainty in pesticide transport in clay-till is due to a lack of knowledge on the hydraulic characteristics of the anoxic clays (figure 1). The hydraulics influence the speed and transport path of pesticides through clays and so directly affect the vulnerability of underlying groundwater. A significant, but still not well understood, difference in the leaching behaviour of pesticides to aquifers has been observed in the Danish Pesticide Leaching Assessment Programme (PLAP), where detailed monitoring of pesticides leaching has been conducted through clay-till deposits on three sites during 16 years (Brüsch et al., 2015). One of these sites is located on an ice-push hill where pesticides are transported rapidly to the under-lying aquifer. In a second PLAP field the clay-till is intensively fractured, and oxidised, and pes-ticides are transported less rapidly through the clay to the underlying aquifer. At a third PLAP field the anoxic clay-till is very impermeable and water with dissolved pesticides and degradation products is transported via drains to surface waters. This network of drains therefore protects underlying aquifers. Jørgensen et al. (2015) showed in another recent field study that anoxic clay-tills can form hydraulic barriers when they lack fractures or when mineral precipitates have sealed fractures. The widespread occurrence of pesticides in groundwater below clay-till depos-its, however, shows that anoxic clay does not always protect underlying groundwater aquifers, and therefore our basic knowledge on the transport of pesticides through clays-tills is still incom-plete.

Recently Klint, et al., (2013) proposed a poly-morphological (PM) landform approach as a tool to assess geological heterogeneities of glacial clay-till sediments. The approach separate clay tills in different landforms based on clay-till thicknesses and layering of different clay landforms, including hummocky moraine, dead ice landscapes, marginal moraines, and meltwater plains. It is suggested that the layering of these landforms determine the heterogeneity of the clay till formation including frequencies of fractures and sand lenses. This poly-morphological concept may serve as a first step towards the development of vulnerability mapping ranking clay-tills according to pesticide leaching. However, many PM-types are still poorly investigated particularly with respect to their hydrologic and microbiologic characteristics. Pesticide specific parameters, including sorption, diffusion and degradation behaviours along preferential flow paths are poorly understood, but are necessary to rank the protective capacity of clay-till deposits.

Models have frequently been used to investigate pesticide leaching from soils and have the strength that they can integrate data types so that they can be used to provide an overall assessment of vulnerability. Model geologies or geotypes have been employed to reach generic conclusions on pesticide transport, but often neglect degradation processes (Miljøstyrelsen 2002), or are focussed on deeper groundwater and not on surface leaching processes (Tuxen et al., 2013). The interaction between degradation processes and geologic features has been considered in models by Rosenbom et al. (2014) and Chambon et al. (2009), who showed that it is critical to understand the relationship between degradation and transport processes when assessing the leaching of contaminants from clays. In particular, the spatial distribution of microbes and their relationship to fast transport routes through fractures and macropores can completely change leaching behaviours.

In conclusion, although we know that fractures and biopores are important pathways for pesticide transport through clay-tills, our understanding of how and where this occurs is still fragmented. We need a more solid understanding of the hydraulic properties of the anoxic clay-tills, and why different clay types apparently have different capacities to retain pesticides. The inherent properties of microbiological processes in clay-tills at depths below the plough zone must be understood if we are to provide realistic simulations of transport of pesticides at a larger scale in both oxidised and anoxic environments. Finally, proper pesticide vulnerability mapping methods are still to be developed for Quaternary deposits and these must be verified against observed pesticide contamination of aquifers.

The overall aim of CLAYFRAC was to develop methodologies to identify the clay-till areas most vulnerable to leaching of pesticides to groundwater resources. It was hypothesised that the PM-approach for ranking the heterogeneity of clay-till deposits can be extended, by including hydrological, geochemical, microbial and specific pesticide relevant parameters, to also rank the vulnerability of clay-till deposits to pesticide leaching to groundwater aquifers.

3.1 Selection of Field sites

A thorough description of fracture architecture and presence of sand lenses is only possible from larger excavations where visual inspection is possible. Figure 2 shows a poly-morphological map of Zealand with former larger excavations indicated. It can be seen that most studies have been carried out on the PM-forms MMS (8 studies) and MMK (8 studies) where MMS characterise a formation where a outwash plain (S) is overlaid by a moraine plain (M) overlaid by another moraine plain and MMK characterise a formation, where a basement limestone (K) is overlaid by a moraine plain overlaid by another moraine plain. Four excavations at MML locations being basement marine clay overlaid by a moraine plain overlaid by another moraine plain have been studied previously.

Four excavations were made in CLAYFRAC of which the Havdrup-Salløv location being an MML was made in collaboration with the PESTPORE2 project. The other locations were made at PM-forms less studied. The Farum excavation was on a PM-form DMS being an outwash plain overlaid by a moraine plain overlaid by a hummocky moraine. The Holbæk excavation was on a PM-form DM being a moraine plain overlaid by a hummocky moraine. The Tokkekøb excavation was on a PM-form DR being a marginal moraine overlaid by a hummocky moraine.

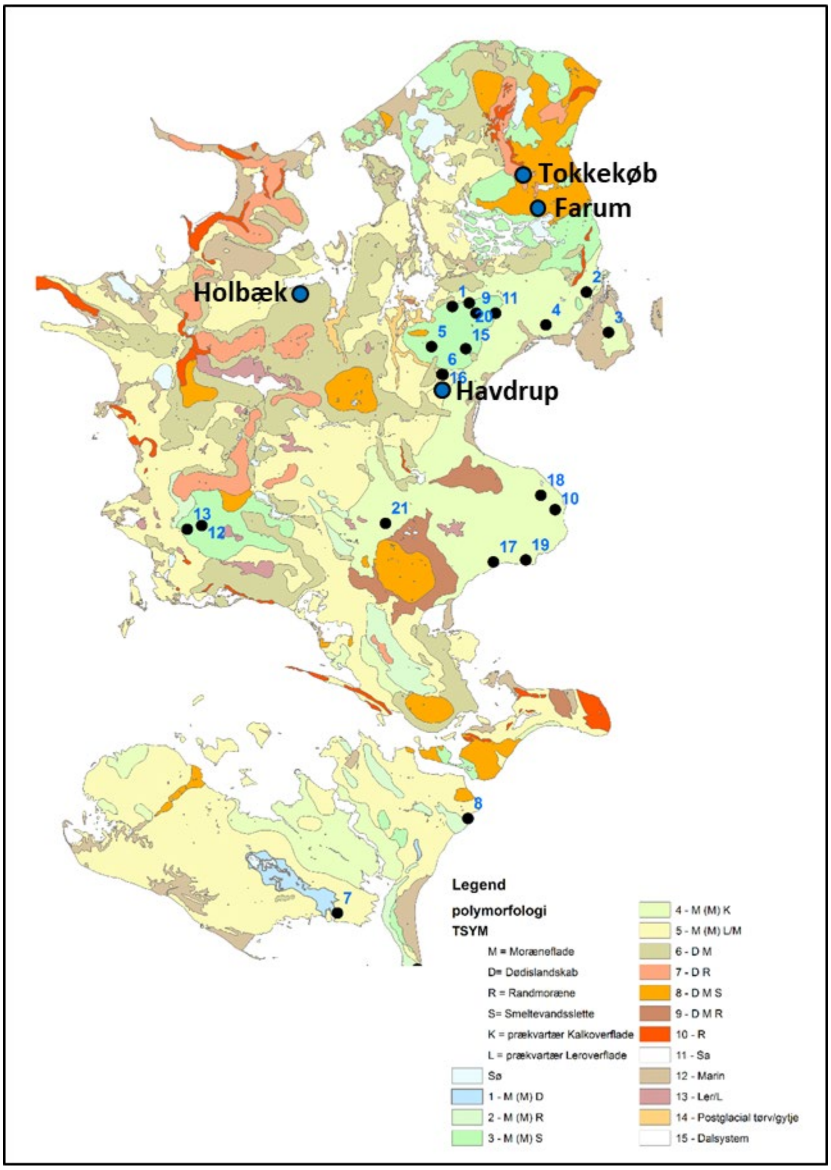

FIGURE 2. Poly morphological map of Zealand, Lolland and Falster showing the four CLAY-FRAC excavations: Havdrup-Salløv (MML), Farum (DMS), Holbæk (DM), and Tokkekøb (DR). Previous larger excavations used for geological characterization are shown as black circles with a number: Slæggerup (1, MMS); Rantzausgade (2, MMK); Englandsvej (3, MMK); Avedøre (4, MMK); Kamstrup (5, MMS); Havdrup (6, MML); Nysted (7, MML); Polmenakke (8, MML); Kallerup (a,b) (9, MMS); Sigerslev (10, MMK); Høje Taastrup (11, MMS); Flakkebjerg (12, MMS); Fårdrup (13, MMS); Gedserodde (14, MMR); Tune (a,b) (15, MMS); Havdrup-pestpore2 (16, MML); Vemmetofte-pestpore2 (17, MMK); Gjorslev (18, MMK); Højstrup (19, MMK); Vasby (20, MMS); Haslev (a,b) (21, MMK).

4. METHODS

4.1 The excavations and characterization methods

The fieldwork was performed in excavations that were dug out by an excavator (figure 3) The general concept is that the excavation is formed as an inverted pyramid, with 1 m deep and 1 m broad steps, in order to comply safety regulations and to get both vertical and horizontal profiles. The size of the excavations was typically 10x10 m and 5 m deep. At Havdrup-Salløv and Holbæk the excavations were larger, as more space was needed for collection of the Large Undisturbed Column (LUC) samples.

FIGURE 3. The excavation at Tokkekøb Hegn. Top: the digging of the excavation. Bottom: The final excavation

The lithology of the excavated units was described in accordance with Larsen et al. (2009). The till and diamicton (poorly sorted sediments, with grain sizes from clay to boulders) is interpreted according to table 1.

TABLE 1. Classification of Fine-grained Diamict Deposits (modified from Klint et al. 2013)

Till type	Depositional process	Special characteristics
Basal till **Type-A** **Type-B**	Basal tills are formed as a result of two processes: by plastering and deformation of glacial debris from the sliding base of a moving glacier (lodgement process), and as a result of incorporation into the till of the substratum under the sliding base of a moving glacier (pure deformation). Most basal tills are formed by a combination of these two processes. They may be separated by the mode of deformation as: A-type (ductile) and B-type (brittle) basal tills.	Generally massive, ice scoured stoss-lee side blocks. Boulder pavements. Consist of exotic material mixed with locally derived sediment. A-type (ductile deformation). Generally low to medium strength till, massive matrix with occasional water-escape structures and intrusion of hydro-fractures into the subsurface. Medium/strong fabric. Often drag folding or slump structures along base (Poorly drained till). B-type (brittle deformation): High strength till, massive matrix, generally strong clast fabric. Often low dipping fissile shear zones, systematic fractured or faulted (well-drained till).
Sub-glacial melt-out till	Melt-out till is deposited by a slow release of glacial debris from the sole of a stagnant glacier by subglacial melting without being redeposited	Low strength. Very strong clast fabric, layers draped over clasts. Clasts are less rounded than in the lodgement till. Often embedded rafts of substratum. Occasional isoclinal folds of sandy/silty bands.
Supra-glacial flow till	Flow-tills derived from any glacial material that is released from glacier ice or from freshly deposited till and which is redeposited by gravitational processes.	Low strength. Varied clast fabric, sometimes layered with inclusions of glaciofluvial sediments. Random orientation of fold-axes fractures and faults. Sometimes stacked sequences of debris-flows.
Supra-glacial melt-out till	Derived from any glacial material that is slowly released from glacier-ice often directly on a basal till.	Low strength, sorted and unsorted sediments. Small basins with primary sedimentary structures, sometimes with small-scale faulting from collapse after melting of buried ice.

The fine gravel composition is dependent on the provenance of the ice-transported material and might be used to establish the ice movement direction. The fine gravel analysis (2.8-4.8 mm) was performed in accordance to Ehlers (1979). The fine gravel was divided into quarts, flint, crystalline rock, and sedimentary rock. Calcareous fine gravel was divided into limestone/chalk and Paleocene limestone.

Elongated pebbles are oriented almost parallel to the ice movement direction in a basal till. Clast fabric measurements, in order to determine ice-movement direction, was performed in accordance to Krüger (1979).

Wormholes were counted in 50x50 cm horizontal grids, at different depths, and recalculated to number of wormholes/m^2.

Vertical fractures were measured along a scanline of two vertical profiles perpendicular to each other, to ensure all directions are detected. Furthermore, fracture traces of vertical fractures were measured on horizontal surfaces. Horizontal and slightly dipping fractures were measured along the vertical scanlines.

4.2 Sorption and degradation

The degradation and sorption capacity studies of MCPA and bentazon was done at the Havdrup-Salløv and Holbæk sites. Sampling, experimental set-up and analyses was done the same way at both sites.

4.2.1 Sampling

Sediments were sampled from Havdrup-Salløv and Holbæk over a two-week period after the excavations were established. The multi-bench excavation was covered by tarpaulins during sampling days to prevent dry-out and wetting from precipitation. Samples were obtained from three sides of the excavation. At both sites' samples were taken from the west, north and east sides. All samples were kept in coolers and transferred to 4°C at the end of each sampling day. The degradation studies were setup immediately after the sampling campaign, while sediments for sorption studies were stored in the freezer (-20°C) until analysis.

The sediments were sampled at different depths and compartments representing potential preferential flow paths and adjacent matrix sediments. The biopores and fractures were identified by visual inspection of their distinct colours separating them from the matrix sediments. No biopores were visible in the topsoil due to agricultural tillage or presence of heavy root systems. In the clayey sediments, biopores were identified as rounded vertically oriented channels (diam. 3-8 mm) often containing fine roots and/or earth worm excrements. In the sandy sediments (Holbæk), the biopores were identified as red/black vertical channel systems.

At the Havdrup-Salløv site, sediments were sampled from the topsoil (0 - 30 cmbs), biopores and matrix sediment (50 to 100 cmbs), reduced grey fractures and oxidized matrix sediments (100 to 200 cmbs), and oxidized iron-rich red fractures and oxidized matrix sediments (200-400 cmbs) (table 2).

At the Holbæk site, the north-east/east sides of the excavation were dominated by clay till layers, whereas the west/north west sides were dominated by sandy layers (see chapter 5.1.3). At the clayey part, sediments were sampled from the topsoil (0 - 20 cmbs), biopores and matrix sediments (20 - 70 cmbs), reduced grey fractures (100 – 200 cmbs), oxidized iron-rich red fractures (200-400 cmbs), and oxidized matrix sediments (200-400 cmbs). From the sandy part of the excavation sediments were sampled from the topsoil (0 - 20 cmbs), iron-rich oxidised red biopores and matrix sediment (100 - 200 cmbs), iron-rich oxidised red horizontal layers (200-300 cmbs), and silt-rich horizontal layers subjacent to the oxidized red layers (200 to 300 cmbs) (table 3).

Before sampling, the outermost layer of each sampling compartment was removed with a knife to expose undisturbed biopores, fractures and complementary matrix sediments and thus prevent cross contamination. The inside surface lining of both biopores and fractures were then carefully sampled, using a small spoon, and transferred to 50 ml Eppendorf tubes.

All samples were collected as triplicate composite samples, i.e., for each compartment several small subsamples were combined into three composite samples. One composite sample equalled approximately 15-30 fractures/matrix subsamples, except for the biopore, which consisted of approximately 70 subsamples. The subsampling and subsequent pooling into composite samples were done to ensure enough biopore- and fracture sediments for analysis of pesticide degradation and sorption. Before the set-up of experiments, each composite sample was homogenised by sieving (2 mm) and further mass reduction was performed by bed blending, as described in the representative sampling standard "Representative Sampling - Horizontal Standard" (DS3077, 2013) and by Kardanpour et al., (2015).

TABLE 2. Sampling compartments and depths at the Havdrup-Salløv site.

Compartment	Depth (cmbs)	Compartment	Depth (cmbs)
Topsoil	0-30		
Biopores	50-100	Matrix next to biopores	50-100
Grey fractures	100-200	Matrix next to grey fractures	100-200
Red fractures	200-400	Matrix next to red fractures	200-400

TABLE 3. Sampling compartments and sampling depths at the Holbæk site.

Compartment	Depth (cmbs)	Compartment	Depth (cmbs)
Topsoil	0-20		
Clay			
Biopores	30-70	Matrix next to biopores	30-70
Grey fractures	200-300		
Red fractures	200-400	Matrix next to red/grey fractures.	200-400
Sand			
Red biopores	100-200	Matrix next to red biopores	100-200
Red horizontal layer	200-300	Silt layer	200-300

4.2.2 Degradation

Aerobic degradation of MCPA and bentazon (table 4) was studied in 12 ml Pyrex glass tubes added 2-g homogenised sediment (wet weight) and 100 µL of a stock solution containing MCPA and bentazon (400 µg/L each) in autoclaved milli Q water giving final pesticide concentrations in the tubes of 20 µg/kg (wet weight). All sediments were then added 200 µl autoclaved Milli Q water giving a final water content of ~10 % (vol/weight) and sealed with PTFE sealed screw caps. The tubes were placed in the dark at 10°C. At each sampling point three tubes were harvested, and the pesticides were extracted and analysed as described in appendix 1.1 The incubation period was 85 days and included eight sample points. No abiotic controls were included as previous studies had shown that neither MCPA nor bentazon were degraded abiotically.

TABLE 4. Compounds included in the experiments. Pure MCPA and bentazon are used for all degradation experiments. ^{14}C-labelled MCPA and bentazon are used for method development

and sorption experiments. Deuterated MCPA and bentazon are added to all samples prior to the extraction procedure in the degradation experiment as internal standards.

Compounds	Chemical name	CAS RN	M_w ($g\ mol^{-1}$)	Purity (%)
Bentazon (BTZ)	3-Isopropyl-1*H*-2,1,3-benzothiadiazin-4(3*H*)-one 2,2-dioxide	25057-89-0	240,28	99.9
MCPA	(4-chloro-2-methylphenoxy) acetic acid	94-74-6	200,62	98.5
^{14}C-labelled				
Bentazon	Bentazon, [benzene ring-U-14C]	-	1.85 MBq[a]	99.02/98.54*
MCPA	MCPA, [benzene ring-U-14C]	-	9.25 MBq[a]	99.79/100*
Deuterium labelled standards (internal)				
Bentazon-d7	3-Isopropyl-d7-1H-2,1,3-benzothiadiazin-4(3H)-one 2,2-dioxide	131842-77-8	247.32	98.0
MCPP-d6	2-(4-Chloro-2-methyl-d3-phenoxy-d3) propionic acid; Mecoprop-d6	1705649-54-2	220.68	99.9/98.5*

*Radiochemical purity, [a]Radiochemical activity

4.2.3 Sorption

Sorption capacities of MCPA and bentazon to all soil compartments was done using the batch equilibrium technique described in OECD guideline 106 (OECD 2000), with slight modifications. The temperature (10°C) and units used in this study (µg/kg and µg/L) deviate from the OECD guideline (20-25°C and mg/kg), but were chosen since the lower soil temperature and pesticide concentrations in the microgram per litre or kg range are much more realistic for subsoil environments and additionally relates to the conditions used for the degradation experiments.

Sorption was studied at four concentration levels and data were fitted to the Freundlich isotherm:

$$C_s = K_F \times C_w^n$$

where C_s is the concentration of MCPA or bentazon in the soil (µg/kg), C_w is the concentration in the aqueous solution (µg/L), K_F is the Freundlich coefficient in L/kg and n describes the non-linearity of the isotherm. The exponent, n will be < 1, when sorption increases with decreasing pesticide concentration. The model was fitted to the experimental data by power function regression in Microsoft Excel.

Assuming all pesticide removed from the solution was sorbed to the soil, the concentration of MCPA and bentazon Cs was calculated as:

$$C_s = \frac{(V(C_i - C_w)}{m_s}$$

where V (mL) is the volume of solution in the suspension and m_s is the mass of soil (g) and C_i is the concentration in the solution with no added soil.

2-g samples (prepared as described in 4.2.1) were transferred to 11 mL Pyrex tubes and added 3870 µL10mM $CaCl_2$ and 30 µL10% NaN_3 (for inhibition of microbial degradation). The liquid-soil slurries were then equilibrated at 10°C for 24 h by vertical head-to-bottom rotation (7 revolutions per min) before spiking with 100 µL MCPA or bentazon. The bentazon and MCPA spike solutions were prepared in 10 mM $CaCl_2$ with added traces of ^{14}C-labeled MCPA and ^{14}C-labeled bentazon, respectively. Sorption of MCPA and bentazon was tested at four concentration levels: 1, 5, 25 and 125 µg/kg and a final soil:CaCl-ratio of 1:2 (w/v).

After addition of the pesticides, tubes were rotated at 10°C for another 24 h to reach equilibrium between concentration in solution and in the fraction sorbed to the soil. Then the tubes were centrifuged at 3000×g for 15 min and the MCPA and bentazon concentration in the aqueous phase was determined by liquid scintillation counting (Tri-Carb 2810 TR, PerkinElmer) of the ^{14}C activity in duplicate 1-mL aliquots.

4.3 Hydrology and LUC columns

Flow and pesticide transport were investigated in laboratory studies using LUCs collected from the Havdrup-Salløv and Holbæk study sites. The LUC method is recognized to solve the normal shortcomings of column studies such as lack of column intactness, small column size, and column rim flow (Cherry et al. 2006, Jørgensen et al. 2019). It offers advantages over field experiments from well-defined boundary conditions and the ability of mimicking *in situ* conditions including effective stress and temperature (Jørgensen et al. 2019). This allows for providing unique data of sub-surface flow and transport processes, which are difficult or impossible to achieve otherwise in field and lab experiments.

4.3.1 LUC samples acquisition and laboratory setup

Holes were excavated to depths of 3.6 and 6 m at the Holbæk and Havdrup-Salløv sites, respectively, from where the LUC samples were collected (figure 4).

Initially in the sampling procedure, blocks for collection of the LUC with dimensions 2 by 2 by 1 m high was left undisturbed on the floor of the excavation. To avoid disturbance, mechanical excavation was halted 2 m from the sample location. The block was then excavated by pick and shovel to within 0.5 m of the actual sample, after which hand trowels, scrapers, and knives were used to carefully carve out the column. A 0.5 m inside diameter steel cylinder fitted with a bottom-cutting edge was gradually lowered over the sample to minimize sample disturbance as the column was trimmed to its final dimensions of 0.5 m diameter and 0.5 m height (figure 5a-d). On completion of sample carving the cutting tool, which also served as a temporary casing, was removed and a precast, flexible polymer membrane was placed around the sample. Liquid polymer was poured between the clay sample and the membrane to bind them together. A steel casing was then placed around the membrane, and the polymer could solidify overnight. The base of the sample was detached from the underlying clay, and fitted with temporary PVC end caps, transported back to the lab, and stored in a 5 °C cold room until it was prepared for installation into the sample apparatus triaxial cell (figure 5).

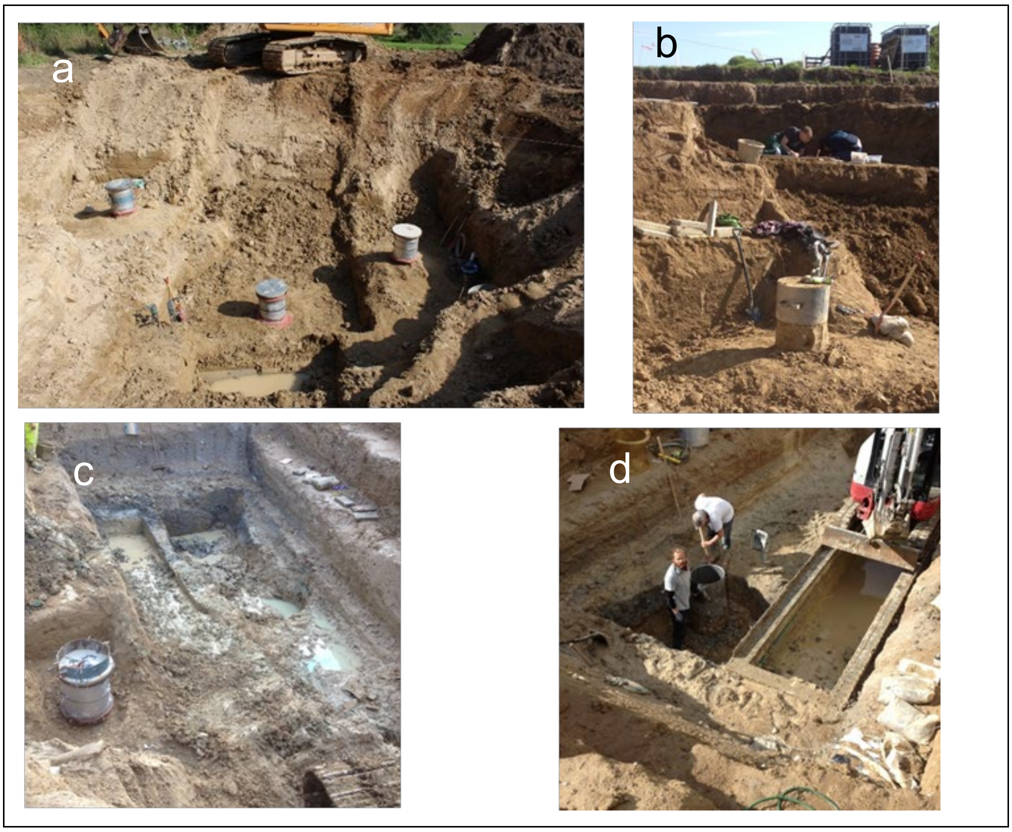

FIGURE 4. LUC sampling at the Holbæk and Havdrup-Salløv sites. a: Holbæk excavation with Holbæk LUC-top (1.95-2.4 mbs), Holbæk LUC-middle (2.6-3.1 mbs), Holbæk LUC-bottom (3.1-3.6 mbs). b-d: Havdrup-Salløv excavation with b: Havdrup-Salløv LUC-top (3.4-3.9 mbs), c: Havdrup-Salløv LUC-middle (4.4-4.9 mbs), and d: Havdrup-Salløv LUC-bottom (5,4-5.9 mbs).

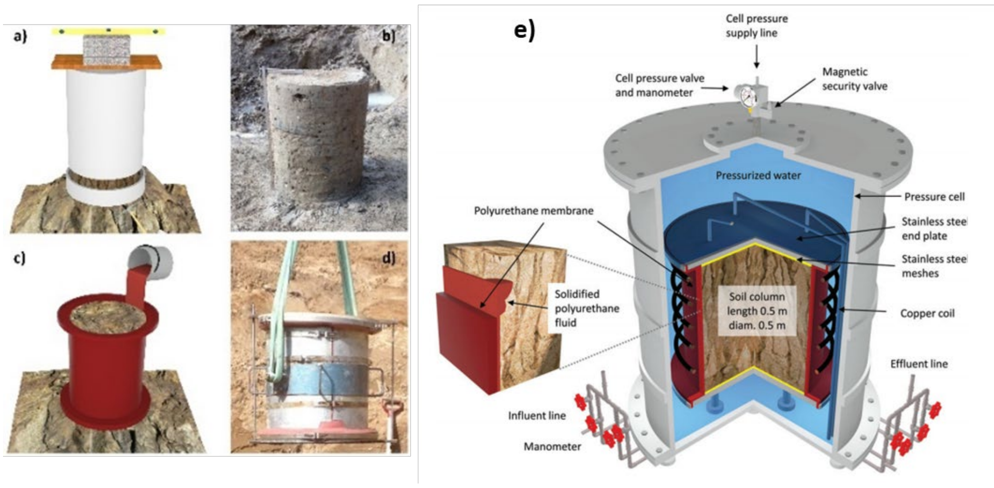

FIGURE 5. LUC sample collection. a): Gently lowering of cutting cylinder after hand excavation of the column to give the final LUC cylindrical shape; b): The final shape of the LUC after removal of the cutting cylinder; c): Prefabricated flexible membrane in place around the LUC and sealing of column rim with polyurethane. d): Lifting of the fixed LUC in a transport casing. e): The flexible wall permeameter with the LUC installed. Insert show interface between the LUC flexible membrane and the LUC to prevent rim flow (From Jørgensen et al., 2019).

Before placing the sample in the triaxial apparatus, the ends of the sample were vacuumed to remove fine particles infilling the natural fractures. To ensure good hydraulic connection between the end plates and the sample, 1 cm deep by 1 cm wide V notch grooves were carefully chipped along the visible fracture traces on both ends of the sample and then filled with clean, coarse-grained silica sand. Two stainless steel screens, 250 x 250 wires per 2.5 cm and 24 x 24 wires per 2.53 cm mesh, were placed on each end of the sample prior to clamping the stainless-steel end plates to the flexible polymer membrane, completely enclosing the sample. The four ports in each end plate were equipped with Swagelock TM fittings and stainless-steel tubing (0.42 cm OD, 0.1 cm wall thickness). Tubing connecting to influent and effluent bottles were Teflon. The steel casing was removed from around the sample, and the column was installed top down in the water-filled containment cell to avoid entrapped air to block water flow in the columns during the experiments. The cell was pressurized to near the calculated in situ effective stress to mimic *in situ* field temperature and stress conditions. Further details about the method and the use of the LUC method to describe flow and transport in clayey till and other low-permeability media in general is described by O´Hara et al. (2000) and Jørgensen et al. (2019).

4.3.2 Laboratory procedures and experiments

After installation in the triaxial cell, the LUC samples were slowly restored by injection of simulated groundwater through the four bottom inlet ports (figure 5). Because the column was installed in an inverted position, this was analogous to vertical downward flow in the natural fracture setting and facilitate displacement of entrapped air out of the top of the column. Water with similar chemical composition as the groundwater *in situ* was pumped into the bottom of the column using the falling head method, or by using a peristaltic pump. Build-up of gas generated by microbial activity caused pressure fluctuations during the initial stages of the hydraulic testing and was removed by flushing the column ends. After removing accumulated gas, flow rates in the LUC were monitored in response to different applied hydraulic gradients and two levels of effective stresses to determine hydraulic conductivity under different simulated depositional overburden. After the hydraulic experiments, selected columns were infiltrated with a pesticide solution of bentazon, MCPA and tebuconazole. Thereafter the columns were infiltrated with a conservative tracer (KBr) and the dye tracer Brilliant Blue FCF (BB), which is only weakly adsorbed in the columns (Flury and Flühler 1995). Applied concentrations are given in table 5. After the flow and transport experiments, the LUC samples were removed from the triaxial cell and cut up. The distribution of fractures, macropores, and the dye tracer was mapped on transparent plastic sheets and photographed before and after the experiments to document the active flow paths in the columns. Also using the distribution of the dye tracer, it was checked whether rim flow had occurred along the column rim. This revealed that minor flow had occurred, but only along the rim of the Havdrup-Salløv LUC-bottom. This was caused by a defect in a LUC membrane, which was not possible to repair. Such artefact might have enhanced both water and pesticide fluxes in this LUC. Rim flow was not observed to have occurred in any of the other LUCs.

Water saturated bulk hydraulic conductivity (Ksb) of the LUC samples were determined from flow experiments (Jørgensen et al. 2019) using Darcys law:

$$\mathrm{Q}_{LUC} = -K_{LUC}\left(\frac{dh}{dl}\right)A_{LUC}$$

where Q_{LUC} is the flow (m^3/s), K_{LUC} is the saturated bulk hydraulic conductivity (Ksb), $\left(\frac{dh}{dl}\right)$ is the hydraulic gradient across the LUC, and A_{LUC} is the cross sectional area of the LUC. The flow experiments were generally producing linear flow vs applied gradients and thereby following Darcy law (figure 6). Small variations between the flow measurements were caused by accumulation of gas in the columns and small changes in LUC effective stresses caused by the different applied hydraulic gradients. Based on the variations r^2 = 0.95-1.00 was calculated, which describes the uncertainty of the Ksb values determined from the LUC samples.

TABLE 5. Pesticides and solute tracers infiltrated in the LUC experiments. Target concentrations of pesticides were 20 µg/L.

Sample	**Solute/tracer**				
	Bentazon	MCPA	Tebuconazole	Bromide	Brilliant Blue
	µg/L*	µg/L*	µg/L*	mg/L	g/L
Havdrup-Salløv LUC-top (3.4-3.9 mbs)	-	-	-	-	2
Havdrup-Salløv, LUC-middle (4.4-4.9 mbs)	-	-	-	80	2
Havdrup-Salløv, LUV-bottom (5,4-5.9 mbs).	23	19	6	80	2
Holbæk, LUC-top (1.95-2.4 mbs)	20	20	20	80	2
Holbæk, LUC-middle (3.1-3.6 mbs)	-	-	-	80	2
Holbæk, LUC-bottom (4.4-4.9 mbs)	-	-	.	80	2

**Table shows measured concentrations in influent solutions.*

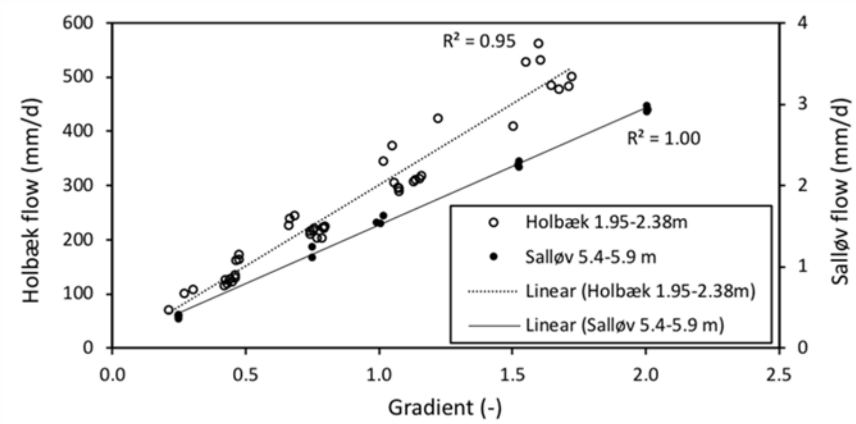

FIGURE 6. Examples of flow measurements showing linear relation between applied gradient and resulting flow rate for two Holbæk and Havdrup-Salløv LUC samples.

Additional flow experiments were carried out in campaigns of different soil effect stresses (σ') to investigate responses of LUC hydraulic conductivity to different levels of simulated depositional overburden. Effective stress is defined as the difference between the total soil stress (σ) (which is determined by the overlying weight of soil (saturated) and the pore fluid pressure (u) (Freeze and Cherry 1979),

$$\sigma' = \sigma - u$$

The effective stress acting on the columns in the LUC permeameter setup was estimated as:

$$\sigma' = P_{cell} + \rho_b g H_s - \left(H_s + \frac{\Delta h}{2}\right)\rho_w g$$

where P_{cell} is the confining cell pressure, ρ_b is the bulk density, ρ_w is the density of water, g is the acceleration due to gravity, H_s is the height of the overburden measured from the centre of the column and Δh is the hydraulic head difference between top and bottom of the column. LUC response of hydraulic conductivity to effective stress was tested for the LUC samples in order to evaluate the effect of depositional overburden on fracture apertures and thereby the ability of fractures to stay open at greater depths than the actual sampling depth of the columns.

4.3.3 Matrix permeability, porosity, and texture

Intact 70 mm cores of the unfractured matrix were collected from the LUC samples to determine hydraulic conductivity (Ksm), texture and porosity (n) of the non-macroporous and unfractured clayey material of the LUC samples (table 6). Like the LUC, additional flow experiments were carried out to determine the response of Ks for the matrix (Ksm) to the same soil effect stress (σ') values applied for the LUC samples. From the difference in response between the LUC and the 70 mm cores the closure of fracture apertures in the LUC samples due to depositional overburden were estimated. The hydraulic measurement for the 70 mm cores were carried out by the consulting company GEO (table 6).

TABLE 6. Saturated hydraulic conductivity (Ks), porosity and texture of unfractured 70 mm intact cores collected form the LUC samples.

Sample	Depth	Hydraulic conductivity, Ks,	Porosity	Texture %			
				Clay	Silt	Sand	Gravel
	m	m/s		0.001-0.002 mm	>0.002-0.06 mm	>0.06-2 mm	>2 mm
Havdrup-Salløv, CT (P_{eff}.low)[a]	2.8-2.9	3.2E-9	0,30	15	35	46	4
Havdrup-Salløv, CT (Peff.high)[a]	2.8-2.9	2.2E-9	-	15	35	46	4
Havdrup-Salløv LUC-top	3.4-3.9	2.5E-9	0,30	17	31	42	10
Havdrup-Salløv LUC-middle	4.4-4.9	2.8E-9	0,27	17	32	49	2
Havdrup-Salløv LUC-bottom	5.45-5.5	1.7E-9	0,23	19	33	46	2
Havdrup-Salløv LUC-bottom	5.8-5.9	4.9E-9	0,21	16	29	52	3
Havdrup-Salløv, LUC-bottom	5.8-5.9	2.3E-8	0,31	13	32	43	12
Holbæk LUC-top	1,95-2.4	1.5E-9	0,30	21	41	31	7
Holbæk LUC-middle	2.6-3.1	8.8E-9	0.28	18	35	45	2
Holbæk LUC-bottom	3.1-3.6	1,9e-9	0,28	20	45	33	2

[a]*Intact core to characterize the effect of confining stress on matrix hydraulic conductivity. The core was collected from CT-XRT column 1 in the PESTPORE2 project (Jørgensen et al. 2020).*

4.3.4 Identification and mapping of preferential flow in fractures and macropores

Before installation of the LUC samples in the permeameter, fractures and macropores in each end of the prepared LUC samples were mapped and drawn on transparent plastic sheets. After the experiments, the LUC samples were cut up and the distribution of BB dye tracer along the fractures and macropores were mapped to identify active preferential flow channels. For each LUC, plastic sheets were drawn from 4 horizontal sections.

4.3.5 Calculation of apertures for fracture and fracture channels

Mean hydraulic fracture apertures (2b) in the columns were calculated from the hydraulic measurements using the cubic law (Snow, 1968, Witherspoon 1980):

$$2b = [((Ksb-Ksm)A12\mu)/(W\rho g)]^{1/3}$$

where *2b* is the fracture aperture*, Ksb* is the bulk hydraulic conductivity, Ksm is the hydraulic conductivity of the unfractured matrix, *A* is the cross sectional area of the column, *μ* is the viscosity of water at 10 °C*, ρ* is the density of water at 10°C*, g* is the gravitational constant*,* and *W* is the fracture trace length in the cross section of the column.

The widths of the fractures and fracture channels were measured in the bottom of the LUC as the total horizontal length of the fractures and horizontal length of dyed fractures. For columns with completely dyed fractures or completely lack of dyed fractures, the hydraulic aperture was calculated as the mean values for the total observed lengths of the fractures. For cases where only segments of the total fracture length were dyed (channelled flow) the mean hydraulic aperture of the dyed fracture segments were calculated by using the approach of O´Hara et al. (2000), which assumes that the contribution of flow from non-dyed fracture sections was negligible. This assumption was justified by experiments and model simulations by Thalund-Hansen (2018), who showed that 10-15 cm visible penetration of BB tracer into fractures would occur for fracture apertures of 10 µm meaning that even small contributions of flow along the fractures would be revealed from occurrence of the BB dye.

4.3.6 Chemical analyses

Bromide in effluent LUC water was analysed by the certified analytical laboratory Eurofins (Roskilde, Denmark) using ion chromatography, except for the Holbæk LUC-top where the analysis was performed by DTU using a bromide selective electrode. Brilliant Blue was determined spectrophotometrically by GEUS, while pesticides where analysed by Eurofins. As the pesticide results from the Holbæk LUC-top showed high uncertainties these samples were reanalysed by GEUS. Soil samples from Havdrup-Salløv LUC-bottom were also analysed by GEUS (se appendix 1.1).

4.4 Modelling

The focus of this chapter is on the modelling of water flow and pesticide transport at the field sites and in the laboratory experiments on the LUCs described in chapter 4.3.and 5.3. A major goal was to identify the most important parameters and processes influencing pesticide leaching through fractured (macroporous) clayey till. Therefore, we developed 2D and 3D discrete-fracture-matrix (DFM) models, integrated data from the other CLAYFRAC work packages and employed them on different setups. DFMs, which explicitly resolve fractures and matrix, represent the most accurate framework to describe the physics of fractured clayey-till aquitards. They allow for a detailed investigation of the influence of fractures/biopores and matrix on pesticide leaching. Furthermore, DFM models are applicable to dynamic flow conditions without the need of extensive model recalibration, as for example dual-continuum models or equivalent porous media models require (Blessent et al., 2014). Dominant processes that have to be considered when investigating the vulnerability of clayey tills to pesticide leaching were analysed and assessed with the help of DFMs, with a focus on the influence of fractures and macropores on solute transport and on the risk of pesticide leaching through clayey tills.

4.4.1 Mathematical model

The DFM models were implemented in the finite-element code COMSOL Multiphysics. The models consist of equations for flow and transport in the matrix and in the lower-dimensional fractures (e.g., 2D fractures in a 3D clayey-till matrix). Flow was described by Darcy's law combined with the continuity equation, $\nabla \cdot \ (-\mathbf{K}\nabla h) = 0$, where **K** is the hydraulic conductivity tensor and *h* is the hydraulic head. We considered steady-state flow fields and fully water-saturated conditions, focusing on the saturated clayey tills below the plough layer.

Pesticide transport was described by the following differential equation, which accounts for advection, diffusion/dispersion, sorption, and degradation of a pesticide species:

$$\phi \frac{\partial c}{\partial t} + \rho_b \frac{\partial c_s}{\partial t} + \nabla \cdot (\phi c \boldsymbol{v}) - \nabla \cdot (\phi \mathbf{D}_{\mathrm{eff}} \nabla c) + (\phi \lambda c) = 0$$

with the porosity ϕ, the solute concentration c, the bulk density ρ_b, the fluid velocity $\boldsymbol{v}$, the effective hydrodynamic dispersion tensor $\boldsymbol{D}_{\mathrm{eff}}$, the sorbed concentration $c_s = cK_d$ (assuming linear equilibrium sorption), where K_d is the distribution coefficient, and the degradation rate λ.

Fracture flow was described with the well-established cubic law ((Snow, 1968, Witherspoon 1980), which relates the fracture flux to the fracture width (aperture) cubed. This approximates fractures as the void spaces between parallel plates with a distance d_{f} (also called the hydraulic fracture aperture and often denoted as twice the fracture half-width, d_{f} = *2b*):

$$q_{\mathrm{f}} = -d_{\mathrm{f}} K_{\mathrm{f}} \nabla_{\mathrm{T}} h = -{d_{\mathrm{f}}}^3 \frac{\rho_{\mathrm{w}} g}{12 \mu_{\mathrm{w}}} \nabla_{\mathrm{T}} h$$

where ∇_{T} is the gradient in the directions tangential (along) to the fractures and $\mathrm{K_f} = \mathrm{d_f}^2 \rho_{\mathrm{w}} \mathrm{g}/(12\mu_{\mathrm{w}})$ is the fracture hydraulic conductivity, with the water density ρ_{w}, the gravity constant *g*, and the dynamic viscosity of water μ_{w}. Further, a transport equation is solved on the fractures. The transport equation for a solute through an open fracture (no filling in the fracture, fracture porosity of 1) was defined as

$$d_{\mathrm{f}} R_{\mathrm{f}} \frac{\partial c}{\partial t} + \nabla \cdot (d_{\mathrm{f}} q_{\mathrm{f}} c) - \nabla \cdot (d_{\mathrm{f}} D_{\mathrm{f}} \nabla_{\mathrm{T}} c) = 0$$

where $R_{\mathrm{f}} = 1 + K_d \rho_b$ is the retardation factor to account for equilibrium sorption on fracture walls, D_{f} is the longitudinal hydrodynamic dispersion coefficient along the fracture, which can be approximated as $D_{\mathrm{f}} = D_{\mathrm{aq}} + (v_{\mathrm{f}} b)^2 (210 D_{aq})^{-1}$ (Wang et al., 2012), and q_{f} is quantified by the cubic law defined above. The cubic law implies that the fracture fluxes are proportional to the aperture cubed, i.e., larger apertures lead to considerably higher flow velocities and much stronger water fluxes and thus potentially stronger pesticide fluxes.

The exchange of water and solutes across fracture-matrix interfaces is realized by establishing the continuity of water and solute mass fluxes and by the continuity of hydraulic heads and concentrations at the fracture-matrix interfaces. Fractures were identified in LUC or field experiments and implemented as representative fractures (parallel plate model) with a comparable trace length and an average hydraulic aperture. Small-scale variabilities of the fracture aperture (fracture roughness) were not considered.

Some pesticides like tebuconazole can exhibit a non-equilibrium sorption behaviour with different sorption and desorption kinetics. To capture this in the model, a kinetic sorption model was implemented (Brusseau et al., 1989; Zheng and Bennett, 2002). Therefore, an additional equation for the sorbed substance was solved and coupled to the transport equation via the source/sink term. The additional equation with the coupling term facilitates the kinetic exchange of mass between fluid (dissolved pesticide) and bulk material (sorbed pesticide):

$$\rho_b \frac{\partial c_s}{\partial t} = \beta \left(c - \frac{c_s}{K_d} \right)$$

The kinetic sorption parameters $\beta_1$and β_2 can be defined to account for a different sorption and desorption behaviour from and to the matrix:

Sorption: $(c - c_s/K_d) \geq 0: \beta = \beta_1$

Desorption: $(c - c_s/K_d) < 0: \beta = \beta_2$

4.4.2 Initial model calibration and tests

In a first step, we tested the developed DFM model against existing experimental data from previous LUC experiments (Jørgensen et al., 2004a, 2019). The DFM model could successfully reproduce breakthrough curves from tracer experiments in large undisturbed columns from fractured clayey tills under a constant flow rate (figure 7a) and variable flow rates (figure 7b). This demonstrated the usability of the model to investigate pesticide leaching through clayey tills.

DFM models usually require a very fine mesh resolution close to fractures to capture gradients correctly and to avoid unphysical oscillations and grid-dependent solutions. The meshes used in the 3D models had usually several million mesh elements and the models were run on a high-performance computer to allow for the usage of such memory-intense fine meshes in a limited computational time.

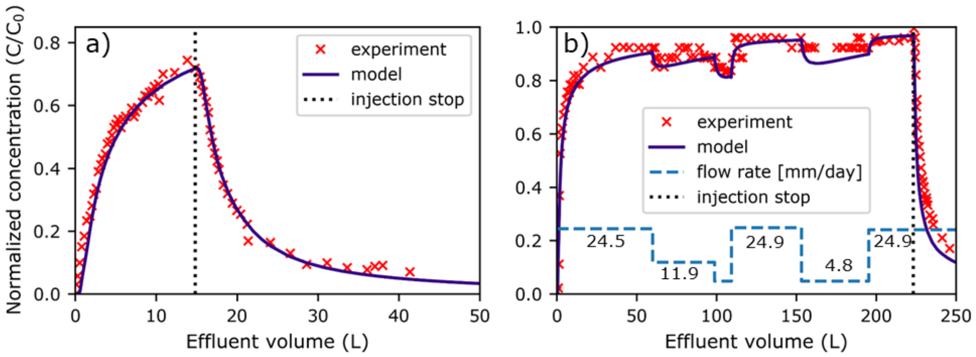

FIGURE 7. Model testing with tracer test data (breakthrough concentrations) from large undisturbed columns under (a) static flow conditions and (b) variable inflow rates. After Jørgensen et al. (2019).

After the initial model tests, we used the calibrated model with a constant flow rate (figure 7a) to investigate the competition between fracture advection and matrix diffusion by running simulations of solute infiltration into a vertical fractured clayey-till profile (see Jørgensen et al. (2019) for details about the model setup). This setup involved relatively large hydraulic fracture apertures of 94.6 µm on three continuous fractures through an LUC with the typical height and diameter of 0.5 m. Pulse injections of 20 L solute were simulated, followed by flushing with clean water at constant flow rates ranging from 0.2 to 50 mm/day. The resulting breakthrough concentrations were plotted over the effluent volume (figure 8Figure 8). The simulations showed that advection through the fractures dominates the transport at high flow rates, which results in fast solute transport and high peak concentrations. Lower flow rates lead to a longer residence time of the tracer in the fractures and is accompanied by more matrix diffusion. This results in later peak arrival times, lower peak concentrations and a longer tailing of the breakthrough curve. Note that the peak arrival times for the simulated flow rates differs strongly; the breakthrough time at a flow rate of 50 mm/day is much shorter than, e.g., with 2 mm/day and the differences in the concentrations over time would be even more pronounced than over the effluent volume.

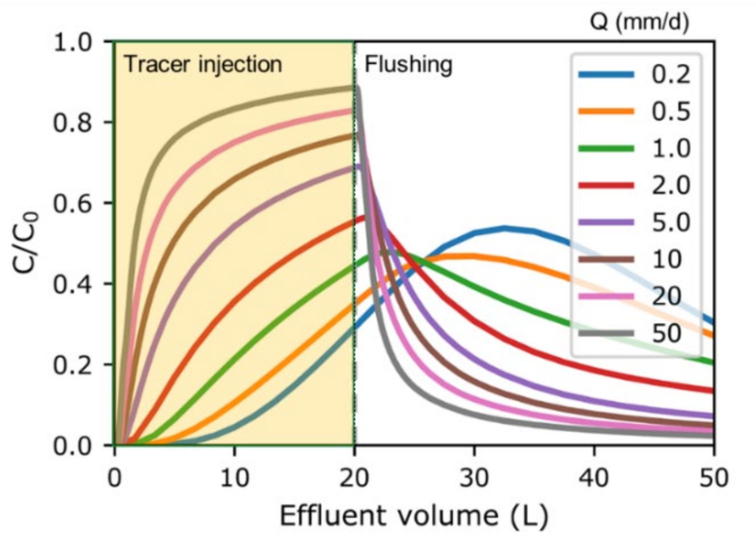

FIGURE 8. Simulated breakthrough curves for an LUC flow through experiment with different flow rates Q and a pulse injection of 20 L tracer solution, followed by flushing with clean water (Jørgensen et al., 2019).

4.4.3 Model setups

After the initial model testing, different setups were considered to investigate the effects of various parameters on the transport behaviour of pesticides. They included the following setups:

1. Tracer infiltration experiment at the excavation site at Havdrup-Salløv
2. Large undisturbed column (LUC) experiments
3. Generic setups to study the influence of specific parameters and processes on pesticide transport
4. Geological cross sections with typical hydrogeological features of the investigated field sites

Flow and transport simulations were run with the parameter values of the pesticides and tracers employed in the CLAYFRAC project. The three considered pesticides bentazon, MCPA, and tebuconazole have similar diffusion coefficients (about $3 \cdot 10^{-10}$ to $4 \cdot 10^{-10}$ m^2/s), but different sorption and degradation characteristics, which were quantified in the investigations described in chapter 4.2 and 5.2 and in previous investigations in similar clayey tills (Albers et al., 2019). Furthermore, the tracers bromide (high diffusion coefficient of $2 \cdot 10^{-9}$ m^2/s and minimal sorption to clayey till) and Brilliant Blue FCF (sorbing food dye) were employed to produce breakthrough curves and to dye preferential flow paths. Flow-through tracer tests in LUC columns and a tracer infiltration test at the field site Havdrup-Salløv were conducted with these substances to investigate the leaching behaviour of pesticides. The experiments are described in chapter 4.3 and 4.4 (and partly in Jørgensen et al 2021 (in review). Numerical modelling was an integral part of the experimental investigations. Preliminary simulations based on estimated parameter values and values obtained from literature and previous experiments assisted with the planning and design of new experiments. After the field and laboratory experiments were finished, we included the measurements from the other work packages (hydraulic parameters, sorption coefficients, geological characterization), and simulated and interpreted the experimental data. The degradation tests (see chapter 4.2.2) showed hardly any degradation in the depth below the plough layer (below 1 m, being the focus of this study) for the considered pesticides. Hence, degradation was not considered in the modelling.

Excavation site

At the Havdrup-Salløv excavation site, a tracer infiltration test was carried out in the framework of the PESTPORE2 project in collaboration with CLAYFRAC. The infiltration basin was situated directly below the location, where the Havdrup-Salløv LUC-bottom was excavated (below 5.9

mbs). A relatively constant water table was maintained throughout the experiment. 386 L of Brilliant Blue FCF (BB) solution with a concentration of 2 g/L were infiltrated into the infiltration basin (with a 6 m x 1 m surface) at a depth of ca. 5 mbs over approximately 15 days. Then, the surface of the infiltration basin was removed layer by layer to map the fracture pattern and other hydrogeological features at different depths and to determine the infiltration depth of the BB tracer (figure 9). This served as basis for the generation of a detailed 3D DFM model of a section of the tracer infiltration basin. The model incorporated the 3D fracture pattern (figure 9e) that was mapped at the field site (figure 9a-c) and digitized in a CAD program (figure 9d). Hydraulic fracture apertures were varied until the model reproduced the observed infiltration depths of the BB. A retardation factor of 3 was estimated for Brilliant Blue based on previous investigations. More details about the infiltration experiment can be found in the master thesis work of Thalund-Hansen (2018).

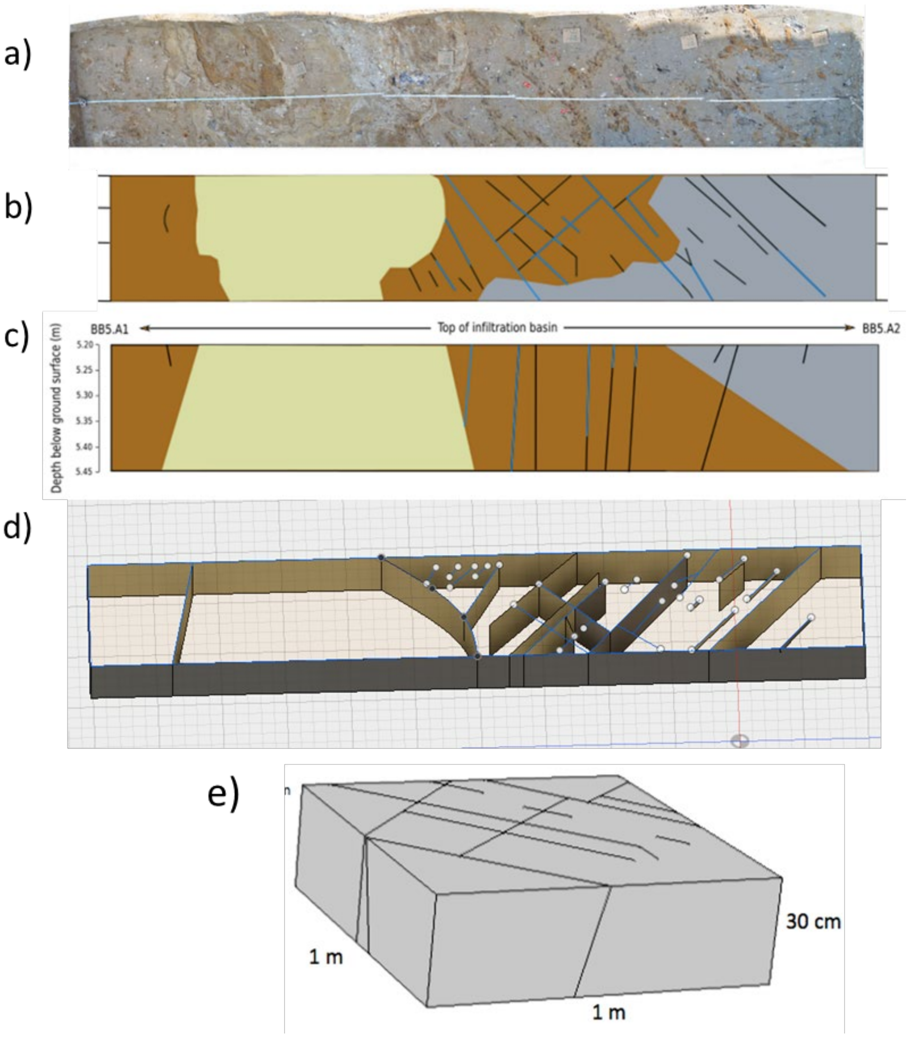

FIGURE 9. (a) Photo of the excavation basin (top view) before the tracer infiltration test. Conceptualization and observed infiltration depth of the Brilliant Blue tracer, (b) top view and (c) side view. (d) 3D CAD model of the fracture system in the infiltration basin. (e) Geometry of the modelled part of the infiltration basin.

LUC experiments

Six LUCs were excavated at the field sites Havdrup-Salløv (3 LUCs) and Holbæk (3 LUCs), as described in chapter 4.3 and 5.3. Hydraulic tests yielded information about bulk hydraulic properties and gave approximate values for hydraulic fracture apertures based on hand calculations. One LUC from each field site was used for more extensive testing in the GEUS laboratory, including tracer and pesticide flow-through tests and the determination of tracer breakthrough curves and sorption parameters. After the flow-through transport tests were conducted, the LUC monoliths were segmented, and fractures were mapped at different horizontal planes of the LUCs. This mapping served as basis for the setup of the 3D model, however with a simplified fracture geometry based on the fracture trace length. We tested more detailed fracture geometries in the model including a varying hydraulic aperture within the fractures; however, they did not substantially improve the model results compared to the simplified setups.

The large undisturbed column (LUC) tests in Holbæk LUC-top (from ca. 2 mbs) and Havdrup-Salløv LUC-bottom (from ca. 5.5 mbs) were analysed with 2D and 3D numerical models. The general LUC setup (0.5 m diameter and 0.5 m column height) was according to the experimental LUC setup, which is further described in chapter 4.3 and in Jørgensen et al. (2019). Water was injected from the bottom of the column towards the top, with the clayey-till column installed upside-down. In Holbæk LUC-top, the flow rate was lowered after 29.6 hours from initially 81 mm/day, mimicking a heavy rainfall event, to 9.8 mm/day. In Havdrup-Salløv LUC-bottom, a constant flow rate of 2.44 mm/day was applied. Tracers and pesticides were injected with the influent water as pulse injection, followed by a flushing period with tap water. In Holbæk LUC-top, the tracers and pesticides were injected over a period of 221.6 hours, while in Havdrup-Salløv LUC-bottom, the injection happened over 359.2 hours. A detailed description of the Holbæk LUC-top experiment and modelling interpretation can be found in the master thesis of Pétursdóttir (2019).

Holbæk LUC-top and Havdrup-Salløv LUC-bottom were conceptualized based on the flow-through tests and the information gained from dismantling and slicing the LUCs after the flow-through experiments were conducted. Cross sections of the model setups for Holbæk LUC-top and Havdrup-Salløv LUC-bottom are shown in figure 10 and the hydraulic parameters are listed in table 7. Holbæk LUC-top was conceptualized as a column with three continuous fractures (two parallel fractures and one perpendicular to the cross section shown in figure 10) and 7 cm gravel infill on top of the clayey-till column. The conceptualization of Havdrup-Salløv LUC-bottom was more complex, including one vertical fracture with changing aperture due to observed precipitate in the fracture in the upper part of the column. Furthermore, a domain with different hydraulic properties for a more conductive yellow sandy clayey till, and two horizontal sand layers connecting the main fracture with the more conductive clayey till were included.

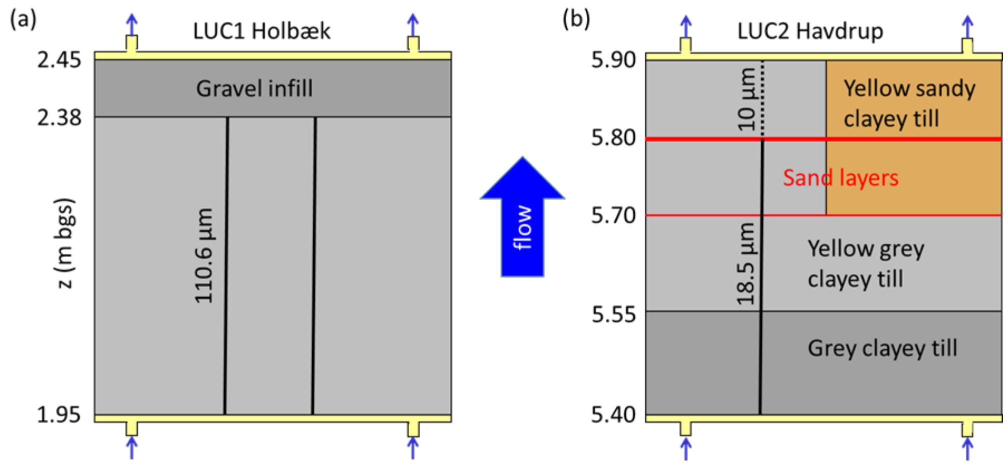

FIGURE 10. Conceptualization and schematic model setup for (a) Holbæk LUC-top and (b) Havdrup-Salløv LUC-bottom. Vertical 2D cross-sections through the cylindrical domains are shown. Red lines indicate sand layers Modified after Mosthaf et al. (2020).

The models were setup with the same orientation as the laboratory experiments (upside down with flow from the bottom to the top). They included a distribution layer that distributes the flow at the inflow and outflow sides of the LUC according to the hydraulic conductivity in the clayey-till column. The distribution layer also mimics the effect of the steel meshes on the top and bottom of the clayey-till column in the physical experiment. The flow model was calibrated to observed hydraulic head gradients along the LUC for given flow rates by varying the hydraulic fracture aperture until the flow rates and the hydraulic head difference between LUC inflow and outflow observed in the experiment could be matched. The fracture trace lengths were chosen based on the measured active fracture traces observed on the slices from the LUCs: 0.95 m for Holbæk LUC-top and 0.43 m for Havdrup-Salløv LUC-bottom. The matrix hydraulic conductivities, porosities and dry bulk densities were kept constant at the values determined on the matrix sub-cores from different clays as described in chapter 4.3. Then, the transport model was run using different diffusion and sorption parameters for the different tracers and pesticides.

TABLE 7. Matrix hydraulic conductivities, dry bulk densities and porosities determined on sub-cores with constant head flow tests in a triaxial cell. Average hydraulic fracture apertures as determined by the models.

Clay and depth below ground surface (mbs)	Hydraulic conductivity (m/s)	Matrix porosity (-)	Dry bulk density (kg/m^3)	Average hydraulic fracture aperture (µm)
Holbæk LUC-top – bulk	$4.1 \cdot 10^{-6}$			
Yellowish brown clay – 2 m	$1.5 \cdot 10^{-9}$	0.30	1870	110.6
Havdrup-Salløv LUC-bottom – bulk	$9.4 \cdot 10^{-9}$			
Grey clay - 5.5 m	$1.7 \cdot 10^{-9}$	0.23	2070	18.5**
Brownish sandy clay - 5.8 m	$2.3 \cdot 10^{-8}$	0.31	1850	-
Brownish grey clay - 5.8 m	$4.9 \cdot 10^{-9}$	0.21	2130	10*

* assumed due to no visible trace of Brilliant Blue in this fracture segment
** value that might be affected by rim flow

Cross-sectional setups

Three cross-sectional setups were employed for the investigation of the influence of a multitude of parameters on the pesticide leaching behaviour. One setup was a 2D cross section with a depth of 1 m, one with a depth of 4 m and one with a depth of 5 m. Water and solutes (tracers/pesticides) continuously enter the model domain from the top. The standard setup used the following parameters (Table 8):

TABLE 8. Model parameters for the base cases of the generic setups.

Name	Value	Unit	Description
d_f	10/50/100	µm	mean fracture aperture
Φ	0.25/0.33	-	matrix porosity
ρ_b	1900	kg/m^3	bulk density
K_m	10^{-8}	m/s	matrix hydraulic conductivity
K_s	10^{-4}	m/s	sand lens hydraulic conductivity
D_w	$2 \cdot 10^{-9}/3.7 \cdot 10^{-10}$	m^2/s	molecular diffusion coefficient bromide/tebuconazole

At the inflow side (top boundary), either the water flux and solute flux were fixed, or a constant head boundary condition was combined with a constant concentration boundary condition for transport. The boundary conditions on the outflow side were usually specified as fixed hydraulic head and outflow for transport.

Geological cross section

The geologic characterization of the Havdrup-Salløv site (see chapter 5.1.1) and from the LUCs was used as basis for a model setup of a geological cross section, as shown in figure 11. The characteristic fracture spacing (distance between fractures, a larger spacing lead to a lower fracture density), fracture orientations and inclined sand lenses were incorporated in the model. Then, solute was injected with a water flux from the top boundary. The simulation results show that the solute is spreading along the fractures first, but also migrates through the matrix due to diffusion and advection. The inclined sand lenses do not show a strong influence on the solute leaching, mainly because they are oriented almost perpendicular to the main flow direction.

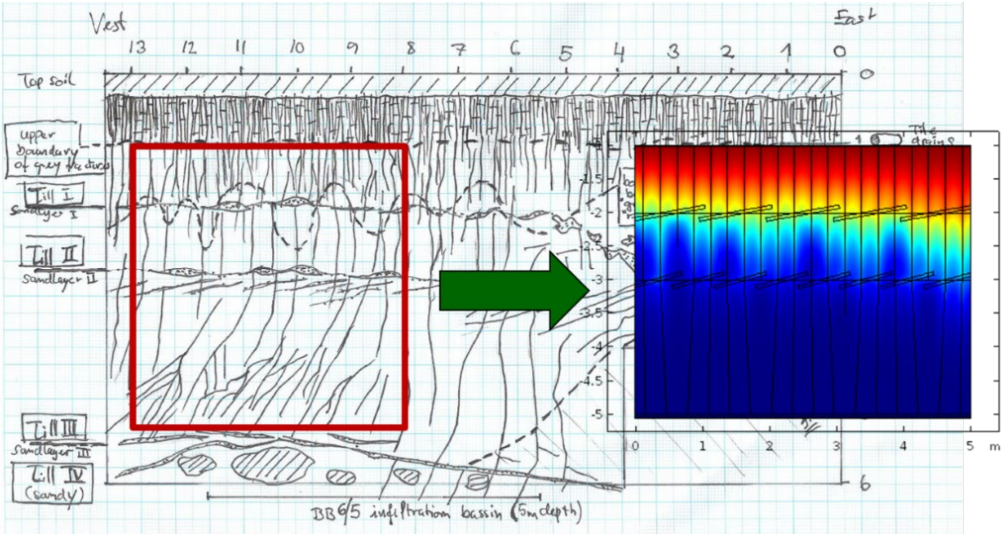

FIGURE 11. Geologic characterization of a cross section at the Havdrup-Salløv excavation and simulation example with fractures of different length/orientation and inclined sand lenses. The red rectangle indicates the simulation domain and the coloured picture on the right shows a simulated concentration distribution on the cross section (solutes infiltrating from the top).

5. RESULTS

5.1 Geological description of the 4 sites

In general, the four investigated sites all correspond with the PM types expected as defined in Klint et al. 2013. However, for Farum (DS), Holbæk (DM) and Tokkekøb (DR) the PM-types were solely determined based on the dead ice deposits exposed at the excavations.

5.1.1 Havdrup-Salløv

The Havdrup-Salløv site is situated in a ground moraine terrain, formed subglacial during the latest ice-advance; the Bælthav Re-advance about 17.000 years ago (figure 12).

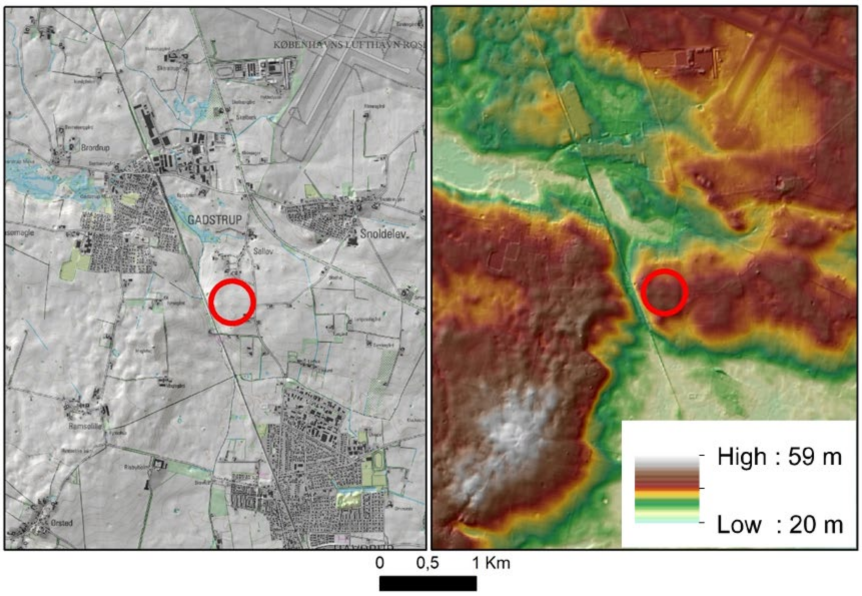

FIGURE 12. Location of the Havdrup-Salløv site (red circle), just north of Havdrup. To the right a digital terrain model of the area.

The PM type of this site is MML according to Klint et al. (2013), and according to a geological map clayey till is covering the surface of this area.

The excavation at Havdrup-Salløv was carried out in collaboration with the PESTPORE2 project (Jørgensen et al., 2020) and it was therefore larger than the other sites (18 x 18 m).The lithology and fractures were mainly investigated along the eastern and northern excavation walls, but in the lowest part of the excavation, the southern wall was investigated as well (figure 13). Three till units separated by sand layers at 3 and 5 mbs were observed. The upper sand layer was continuous with larger sand lenses occurring in the north-eastern corner of the excavation at 2-3 mbs. The lower sand layers at 5 mbs. consisted of several 1-3 cm thick sand layers with laminated till in between. The sand layers were folded with north western – south eastern striking fold axes. Based on this, the sand layer and diamictons were interpreted as being deposited as layers formed subglacially during a decoupling of the ice and substratum.

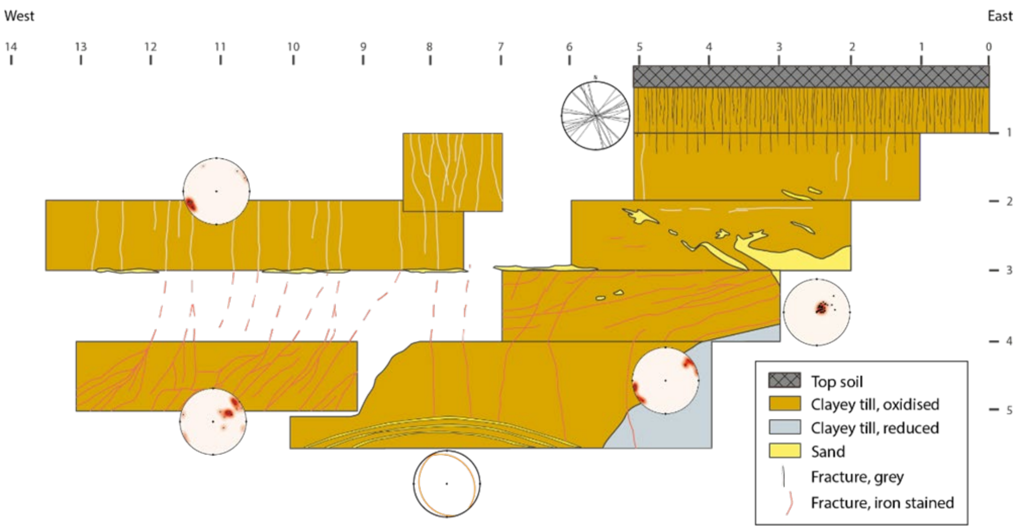

FIGURE 13. A composite profile of the excavation at Havdrup-Salløv. The uppermost Stereonet shows the orientation of desiccation fractures. The red stereonet plots show the orientation of fractures at different depth and position in the excavation. The lowermost stereo plot shows the orientation of the folded sand layers in the lowest part of the excavation. For more details see figure 14.

The upper till unit from the surface to 3 mbs. was a clayey till, silty sandy and gravely, yellow brown (oxidized), partly with sand lenses and sand layers in the lower part. The calcareous non-calcareous interface was at one mbs. Two clast fabric measurements were performed, and they indicate an ice movement direction from south to north (figure 14). The well-defined fabric, and the presence of fractures, indicate that this layer is a B-type basal till. The middle till unit below the sand layer at 3 mbs. and down to 5-6 mbs was also silty, sandy, and gravely. Most of this till was yellow brown (oxidized), but in the north eastern part of the excavation it was olive grey (reduced) (figure 13).The clast fabric showed a slightly different orientation indicating that it is indeed another unit. However, the clast fabric and the presence of fractures suggest that this till is also a B-type basal till. The lowest till unit below the sand layer at 5- 5.5 mbs was only partly exposed and not investigated further.

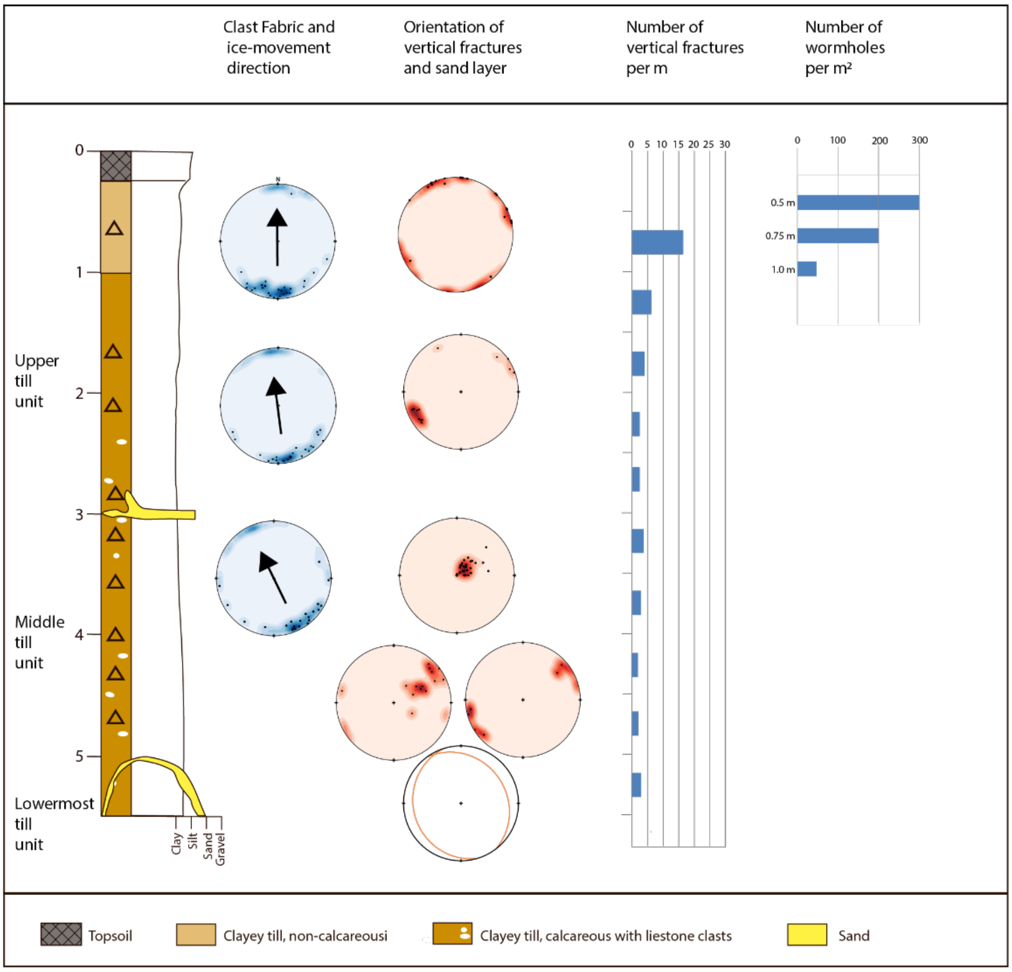

FIGURE 14. Overview of fabric data, fracture data and wormholes measured in the Havdrup-Salløv excavation. To the left is shown a lithological profile of the site. The blue stereonets shows the distribution and orientation of elongated pebbles (clast fabric) and suggested ice-movement directions (arrows). The red stereonets shows the distribution and orientation of fractures measured at the excavation. The vertical distribution of fractures and wormholes are shown to the right.

FIGURE 15. The uppermost 2 m of the excavation where desiccation fractures dominated the upper 1.5 m. The folding ruler is 1 m long.

The upper till unit was strongly dominated by macropores in form of root channels, wormholes, and desiccation fractures down to one mbs (figure 14 and figure 15). Wormholes were counted and at 0.5 mbs there were 300 wormholes pr. m^2 decreasing to 40 pr. m^2 at one mbs (figure 14). The number of desiccation fractures was up to 17 pr. m^2 having a random orientation. Vertical fractures with a grey halo surrounding the fracture occurred, from 1-3 mbs. (figure 13 and figure 16). At 2 mbs fracture traces were measured on a 5 x 6 m surface and a fracture density of 4.5 per m^2 were calculated (figure 17)

FIGURE 16. Grey fractures at 1-2 mbs.

Most of the fractures were striking in 140º while a less prominent fracture set was visible with strikes of about 40º (figure 14 and figure 17).

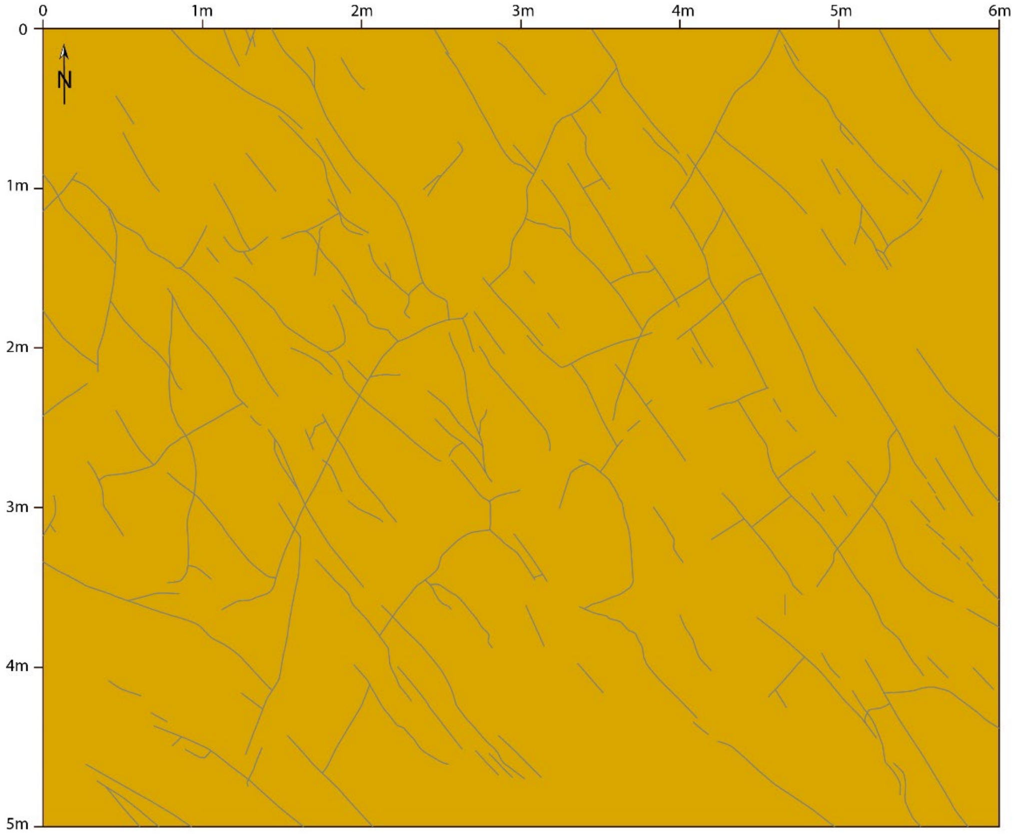

FIGURE 17. Fracture traces on the exposed surface at 2 mbs. The till in this depth was yellow brown and the fractures were grey.

In the middle till (3-5.5 mbs) the fractures had iron and manganese coatings (figure 18). Many of these fractures were inclined with an orientation of about 140º and dipping about 30º towards southwest (figure 13 and figure 14). The vertical fractures had the same strike as the inclined and some were extending into the underlying sand layers.

FIGURE 18. Fractures with iron and manganese coatings (arrows) on the fracture surfaces (4-5 mbs)

5.1.2 Farum

The Farum site was situated in a Hummocky terrain, formed from dead-ice during the melting of the latest ice-advance, the Bælthav Readvance about 17.000 years ago (figure 19).

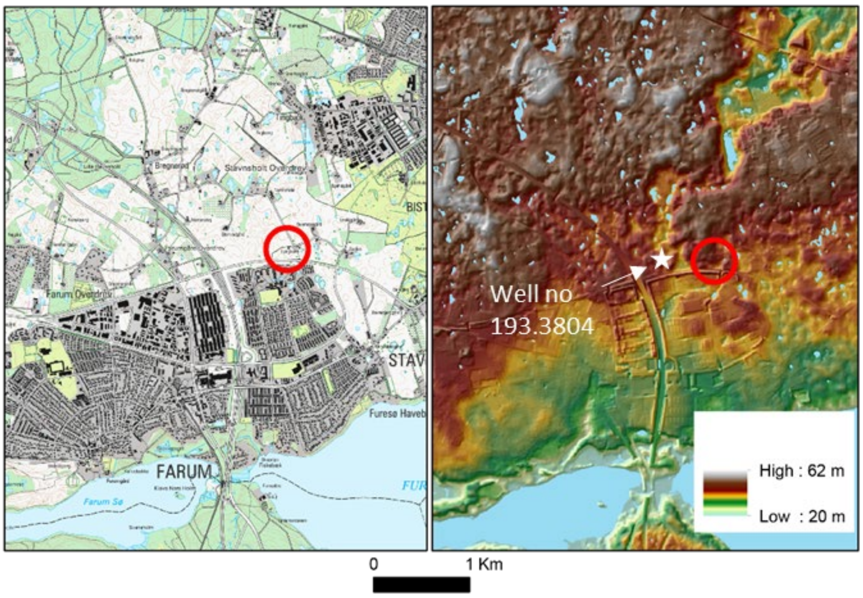

FIGURE 19. Location of the Farum site, north of Farum city. To the right a digital elevation model of the area showing the ruggedness of the terrain typical for a dead ice landscape. The location of well no. 193.3804 is shown.

A geological map of the area indicates that the surface consists of clayey till. West of the excavation raw material wells showed alternating layers of clayey till, sandy till, and meltwater sand with thicknesses of about 15 m, above meltwater sand, which form a regional aquifer (Appendix 1.2). According to Klint et al., 2013 the PM type of this till is classified as a DMS type.

The excavation revealed two till units separated by sand layers and layers of sandy diamictons (figure 20). The upper unit was 2.5-4 m thick and characterized as a clayey till, strongly mixed with sand, silt, and gravel: the sediment being yellow brown with many sand lenses and sand layers. Part of the upper unit was also characterized as a sandy till. The calcareous – non-calcareous interface was varying in depth from 1.10-2.5 mbs and often followed the sand lenses in the till. This till was interpreted as being a melt-out till which typically has many sand lenses. Data from the raw material well supports the observation that the sedimentology is with many lithological units above the underlying sand. The lower unit was a clayey till, strongly mixed with sand, silty and gravely, yellow brown, calcareous. This till was a B-type (brittle) basal till, with a strong clast fabric, indicating an ice movement direction from southeast towards northwest (figure 20).

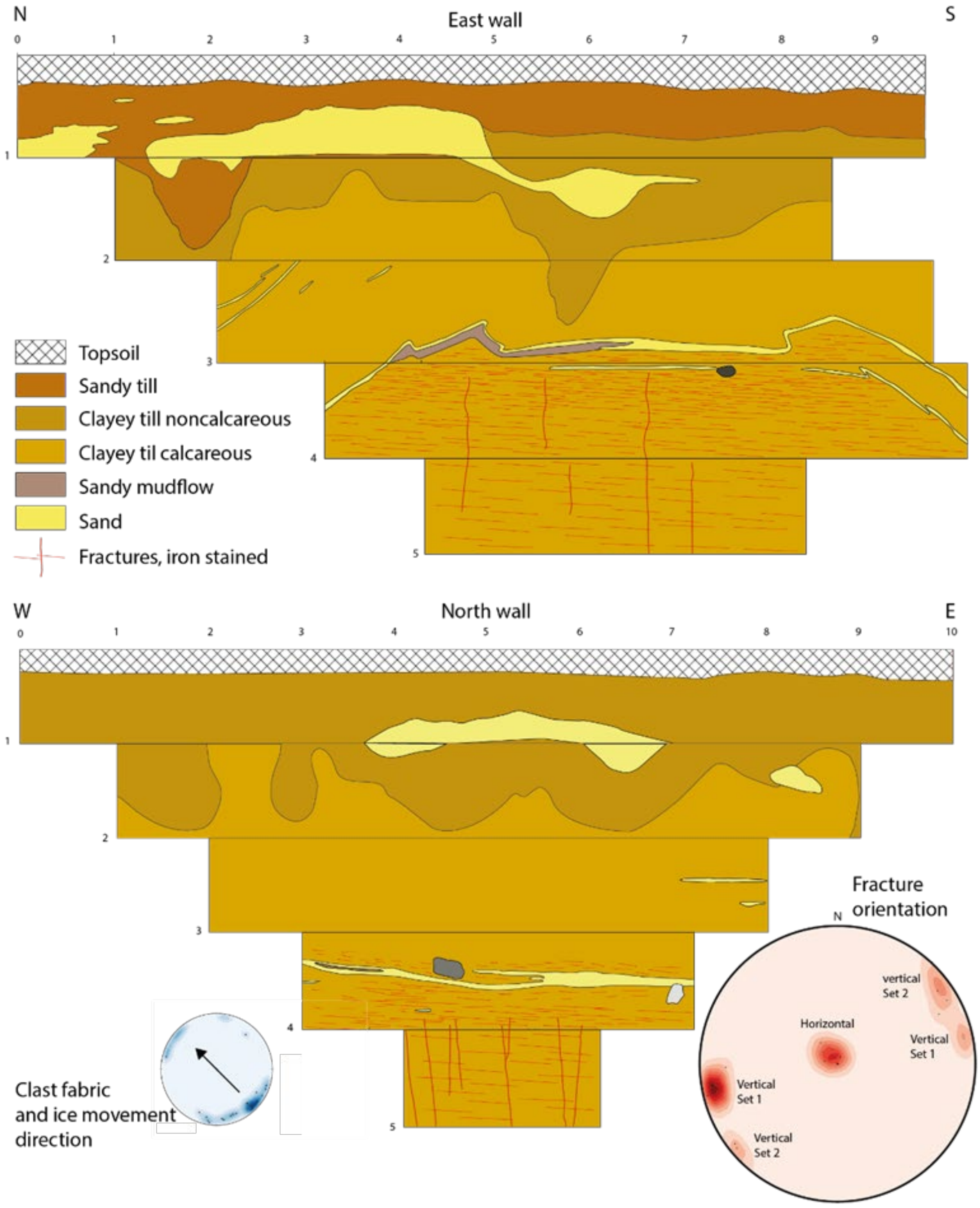

FIGURE 20. Composite profiles of the eastern and northern walls of the excavation at Farum. The red stereonet show the distribution and orientation of fractures plotted as normal to the fracture plane, with indications of the two dominant vertical fracture orientations (set 1 and set 2) as well as the horizontal fractures at 3-5 mbs. The blue stereonet shows a contour plot of the distribution and orientation of elongated pebbles and the suggested ice-movement direction (arrow).

The two till units are separated by a continuous sand layer and partly also a sandy diamict layer. The sand layer and diamicton are interpreted as being deposited as layers formed subglacial during a decoupling of the ice and substratum and is marking the change from an active flowing ice to a stagnant ice body. The layers were folded, and small-scale thrustings are seen indicating some motion of the ice before it was transformed to a dead-ice mass (figure 21).

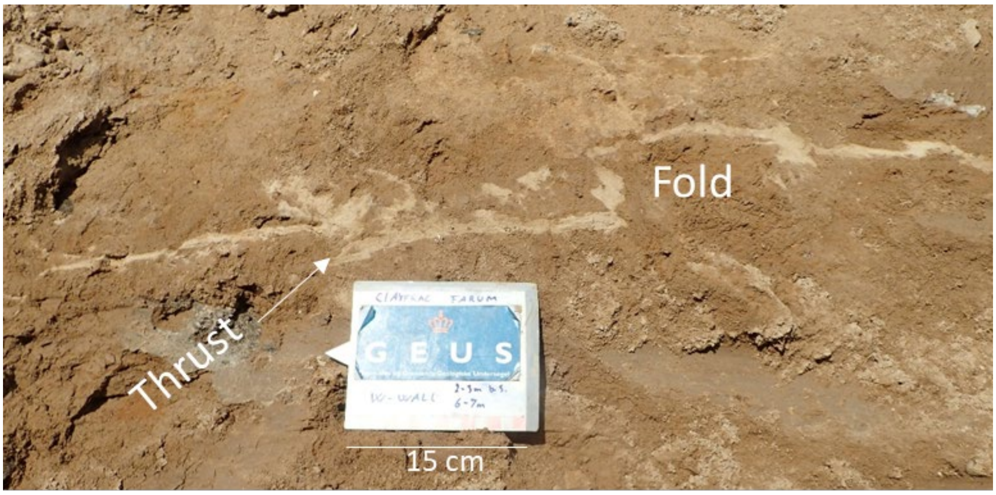

FIGURE 21. Small-scale folding and thrusting of the continuous sand layer on the west-wall at 2-3 mbs.

The number of wormholes were 224/m^2 at 0.5 mbs decreasing to 128/m^2 at 1.0 mbs. Fractures were not observed in the upper till. There were, however, many sand layers and sand lenses that may as well serve as preferential water transport routes. In contrast, there were many large connected vertical and horizontal fractures in the lower till (figure 22). The vertical fractures could be separated into two sets with different geographical orientation. Set 1 was dominant and had an orientation of 177º with an inclination of 10º towards east, while set 2 had an orientation of 155º with an inclination of 12º towards east (figure 20). The spacing between the set 1 fractures ranged from 10 to 50 cm with an average of 32.5 cm, while the spacing of the set 2 was fractures were larger ranging from 50 to 100 cm with an average of 75 cm. The horizontal fractures were dipping towards SE with an average orientation of 55º/8º SE. The length of the horizontal fractures was typically 40 to 80 cm. The average spacing of these fractures increased with depth as it was 3 cm at 3-3.5 mbs, 5.5 cm at 3.5-4 mbs and 10 cm at 4-5 mbs. Visual inspection (reddish colour) showed that all horizontal fractures contained precipitated iron. There were connections between the horizontal and vertical fractures (figure 22) and there were also connections between the sand layer that separates the two till units and the deeper vertical fractures (figure 23).

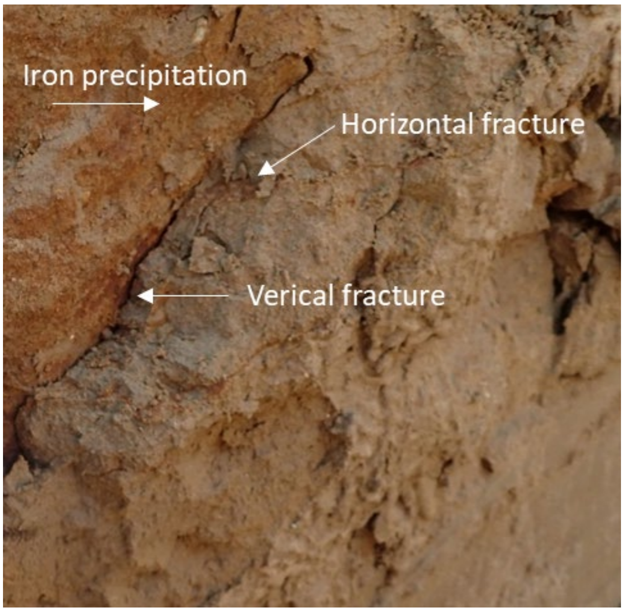

FIGURE 22. Large vertical fracture with iron staining connected to smaller horizontal fractures.

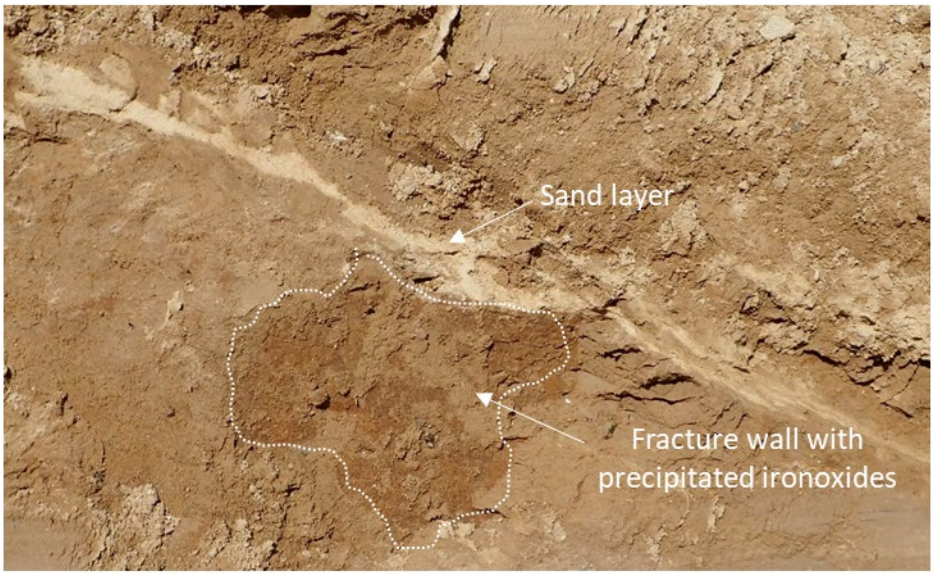

FIGURE 23. Vertical fracture with iron oxide staining intersecting sand layer at 2.5 mbs.

5.1.3 Holbæk

The Holbæk site is situated in a Hummocky terrain, formed from dead-ice during the melting of the latest ice-advance the Bælthav Readvance about 17.000 years ago (figure 24).

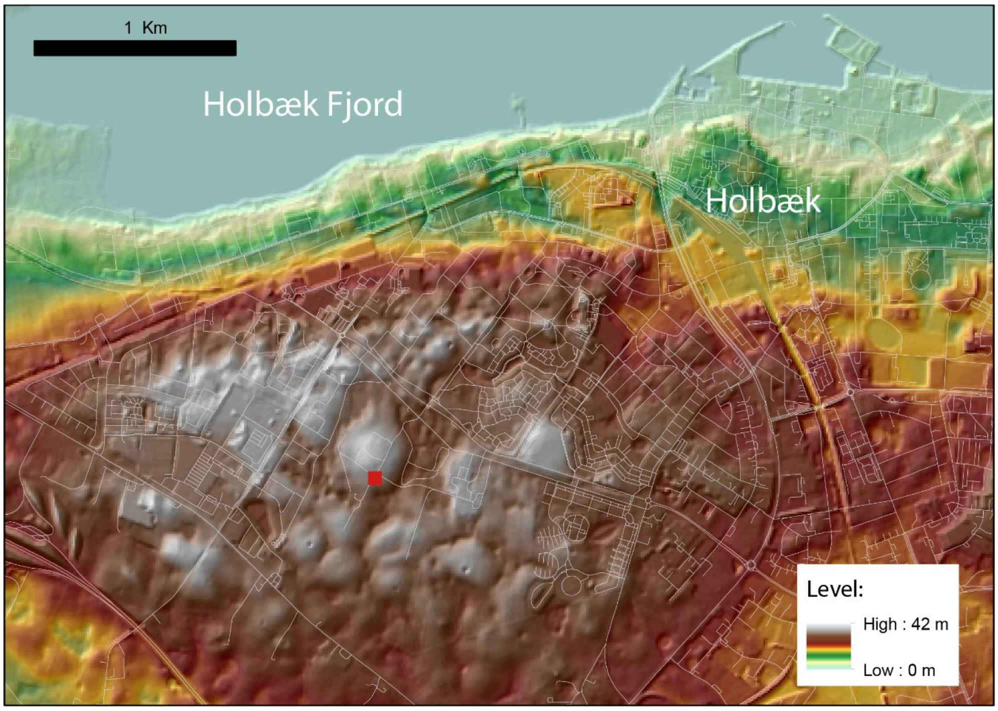

FIGURE 24. Location of the Holbæk site (red square). The site is situated on the flank of a hill in a hummocky terrain typical for a dead ice landscape.

The PM type is a DM according to Klint et al. (2013). The geological map showed dominance of clayey till in the area, and data from several geotechnical wells adjacent to the field site showed presence of clayey till in the upper 10 m.

Part of the excavation was only excavated to 3 mbs. as it consisted mainly of sand and gravel with a water table as this depth. This made the sediment unstable, and it was not possible to dig further. In the south eastern part, however, a clayey till was present, which made it possible to continue the digging to 4 mbs. Subsequently the excavation was enlarged to the east, for sampling of the LUCs.

FIGURE 25. The excavation at Holbæk showing the major lithological units. More details are shown on the composite profiles in figure 26.

A clayey till, silty, sandy, gravely, dark yellow-brown, non-calcareous overlaid all other lithological units (figure 25 and figure 26). The lowermost 20 cm of this layer was sandier characterized as a sandy till, silty sandy, gravely, brown, laminated, and non-calcareous (figure 26 and figure 27). It is interpreted as being a glacitectonite, and as such a deformation zone where the subsurface has been incorporated in the sole of the till.

Below the overlaying tills, the western and northern walls of the excavation was dominated by lake deposits consisting of 1-20 cm layers, varying in content of gravel, sand, silt, and clay. Furthermore, there were diamict layers, which were sandy with silt and gravel, interpreted as mudflow layers and coarse grained gravely and stony diamicts layers that were interpreted as debris flow layers. These diamict layers are interpreted as deposited in a lake delimited by dead ice, and possibly also till. The deposition of the sediment may have occurred as pulses from different directions into the lake, as the layers were dipping in different directions. Furthermore, the loads and flow of especially the debris have caused small-scale thrusting in the underlying sediments indicating the different in-fill directions (figure 27).

On the eastern side of the excavation, a smaller sand unit was present, consisting of layered grained sand more uniform than the lake deposits to the west. However, most of the eastern side of the excavation consisted of clayey till being silty, sandy, gravely, yellow brown, and calcareous. Within this till a lens of sandy till, striking 50º and dipping towards southeast was present. The till seems consolidated, but the clast fabric was quite random, suggesting that it could be a flow till deposited in a dead-ice environment.

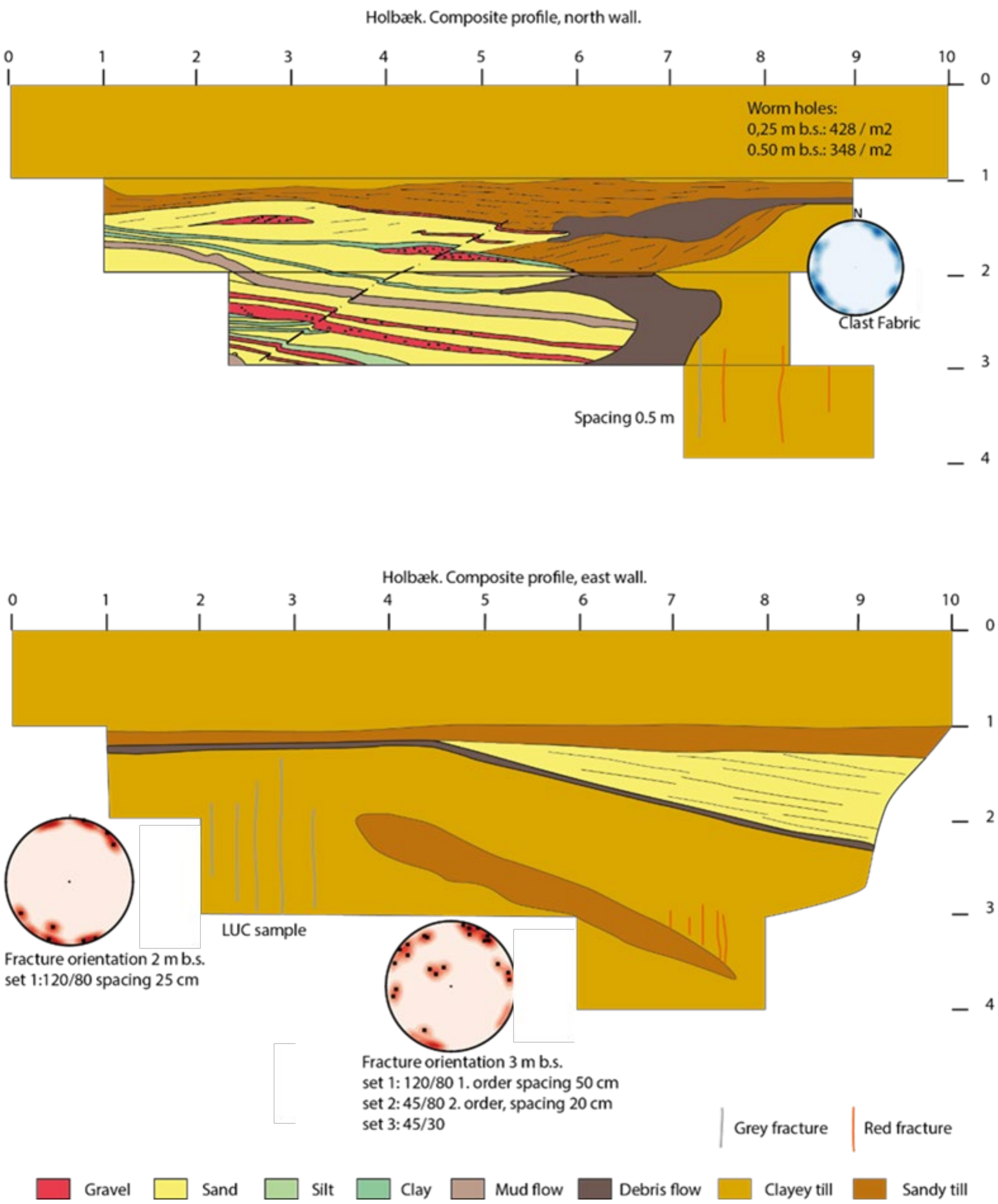

FIGURE 26. Composite profiles of the northern and eastern walls of the excavation at Holbæk. The red stereonets show the distribution and orientation of fractures with indications of dominant fracture orientations (set 1, set 2, and set 3.). The blue stereonet shows the distribution and orientation of elongated pebbles. No distinct orientation is seen indicating that the till is a flow till rather than a basal till.

Trike

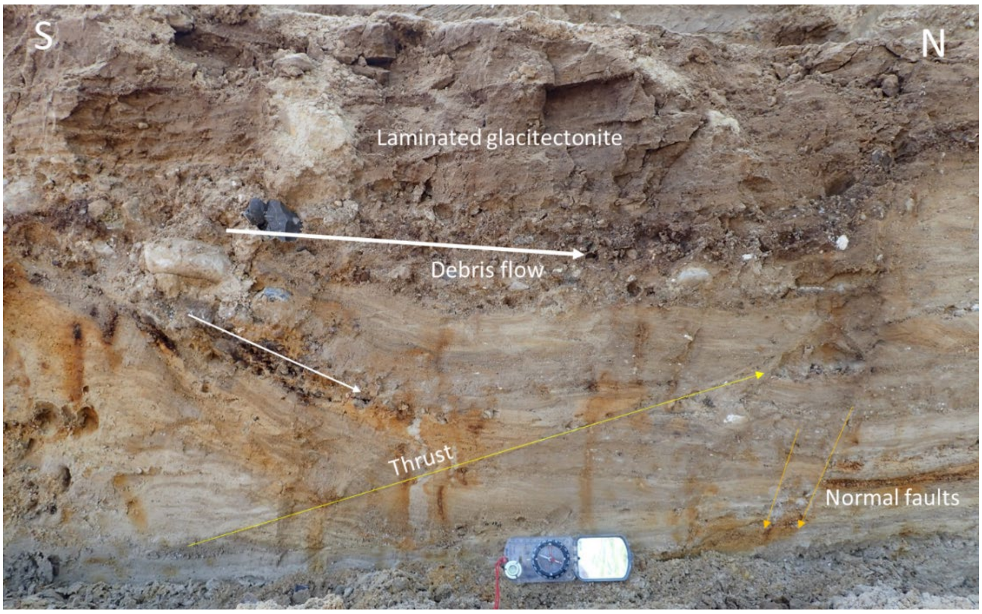

FIGURE 27. Part of the western wall from 1 to 2 mbs. Coarse grained debris flows sliding into the glacial lake have caused small scale thrusting and faulting in the underlying sediments. The infill direction is in this case from south to north.

The number of wormholes at the north wall were 428/m^2 at 0.25 mbs decreasing to 348/m^2 at 0.5 mbs. At the western wall, in the sand deposit at one mbs, the number of wormholes were 332/ m^2 and they continued down to 2 mbs.

In the clayey till of the eastern part of the excavation fractures were present from about one mbs and downwards. They had a grey halo until about 3 mbs. below which they had iron and manganese coatings. The grey fractures from 2-3 mbs. had an average orientation of 120º /80º with an average spacing of 25 cm and often they had root marks on the surfaces. From 3-4 mbs the fractures had a more random orientation, but 3 set were recognized with orientations of 120º /80º, 45º/80º; and 45º/30º and spacings of 50, 20 and 66 cm. Horizontal fractures also occur with an average spacing of 10 cm.

The groundwater head was measured within the lake deposits and in the till giving heads of 3.0 and 4.9 mbs respectively. This means that the hydraulic variability is large, even with a few meters distance.

The sedimentological heterogeneity was very high, as sandy lake deposits were found next to clayey tills, with a rather abrupt delineation. Even the lake deposits had a high sedimentological variability with alternating layers of sand, silt, clay and diamict layers. In a well 800 m northeast of the excavation, in a similar hilly landscape, a comparable sediments and variability was seen (Appendix 1.3) supporting that such smaller lake deposits are frequently occurring within dead-ice environments where they creates a high degree of geological variability.

5.1.4 Tokkekøb

The Tokkekøb site was situated in a Hummocky terrain, formed from dead-ice during the melting of the latest ice-advance the Bælthav Readvance about 17.000 years ago (figure 28).

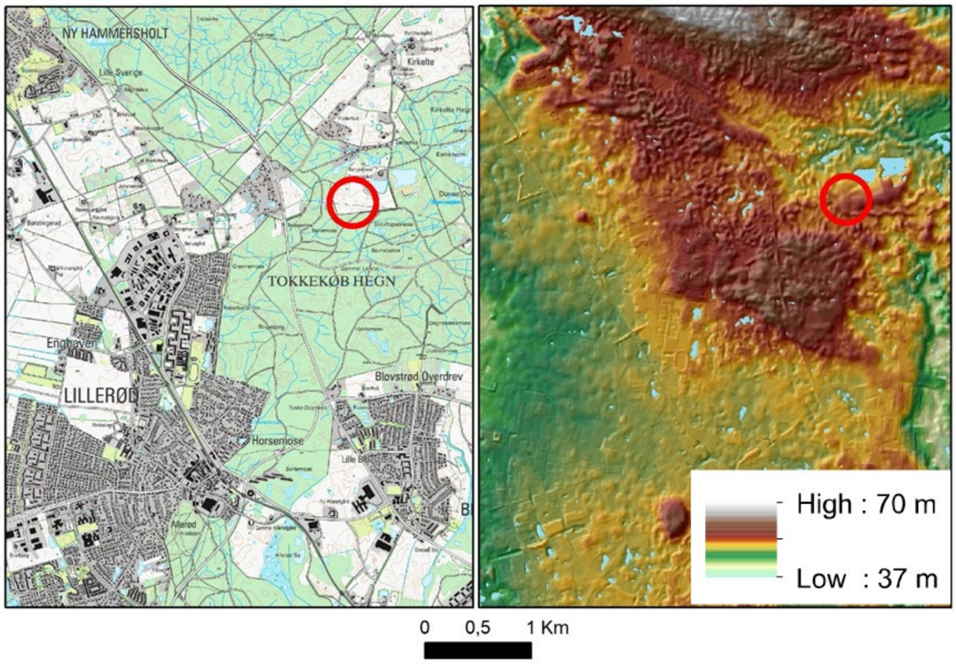

FIGURE 28. Location of the Tokkekøb site northeast of Lillerød. To the left is a map of the area; to the right is a topographic map of the area showing the ruggedness of the terrain indicating a dead ice landscape. The site was located in a clearing of Tokkekøb Hegn marked with a red circle.

According to Klint et al., (2013) this till is classified as a D(M)S type. It could, however, also be interpreted as being a P(M)S type. The geological map of the area indicated presence at clayey till and data from the closest wells in the area showed presence of tills to depths of about 15 m, above meltwater sand, which creates a regional aquifer.

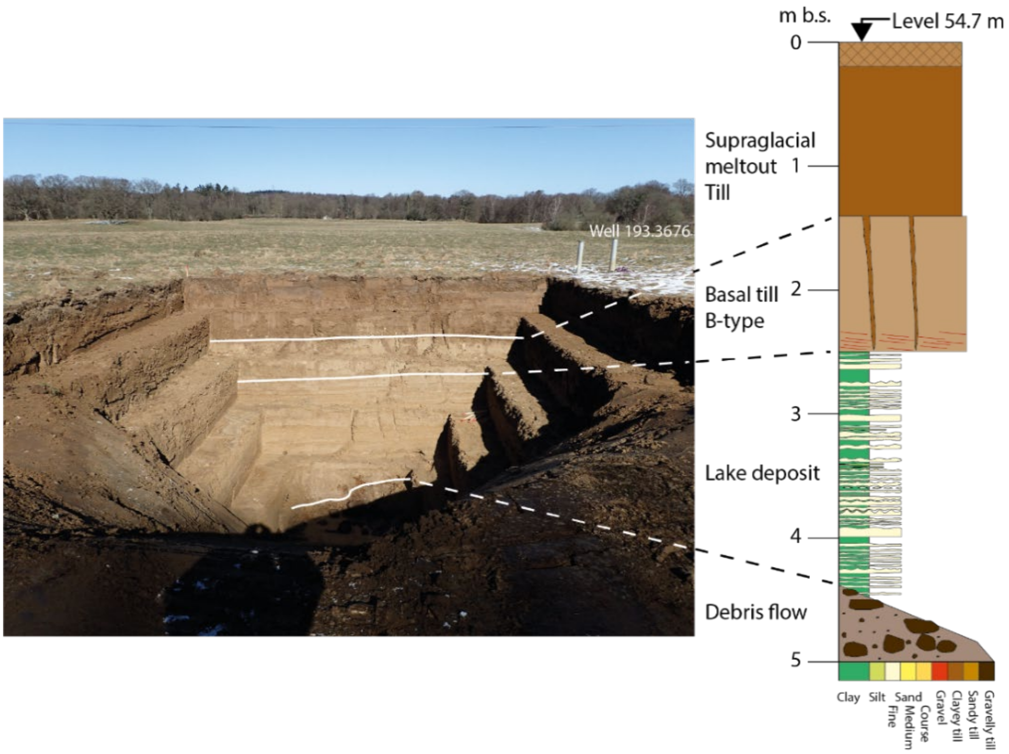

FIGURE 29. The excavation at Tokkekøb. To the right I shown a log of the lithological characteristics of the units seen in the excavation.

There were two till units down to about 2.5 m below which lake deposits were observed. From about 4.5-5 mbs a gravely and stony till was seen (figure 29).

The upper till was a clayey till, sandy, silty, and gravely, dark yellow brown, and non-calcareous. It was soft, had a very low strength, when tested with a pocket penetrometer, and the fabric was very diffuse. Based on this the till was interpreted as being a melt-out till, which has not been compressed by the weight of the ice. The lower till from 1.4 - 2.5 mbs was a clayey till, sandy, silty, and gravely, yellow brown and calcareous and the strength was higher than the overlying till. It was fractured and there was a non-calcareous dark yellow-brown zone, about 3 cm wide, along the fractures which was as soft as the till above. There were only few wormholes and rootholes in this till. From 2.5 - 4.5 mbs lake deposits were observed, with alternating laminated clay and sand layers. The sand layers were up to 4 cm in thickness, and wave ripples occurred in most sand layers (figure 30 and figure 31). The lake deposits rested on a stony and gravely diamicton, interpreted as a debris-flow deposit related to a lake environment within a dead ice body.

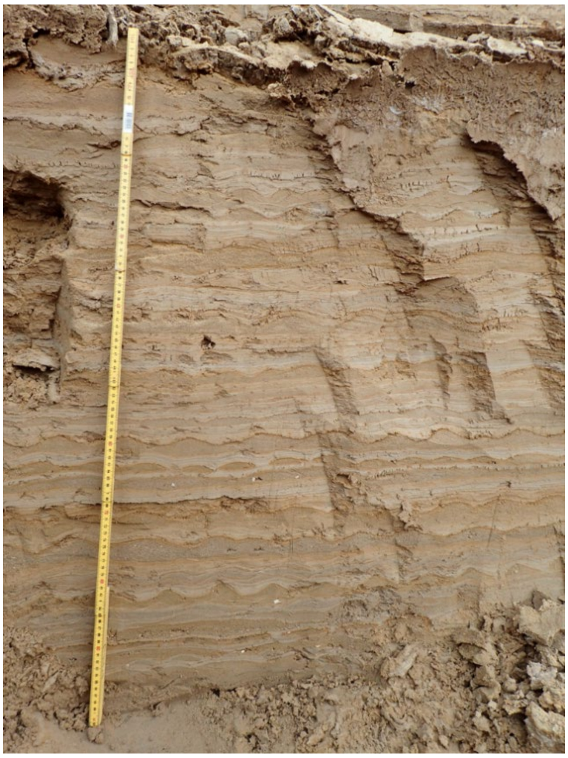

FIGURE 30. Layered lake deposits with alternating sand and clay layers

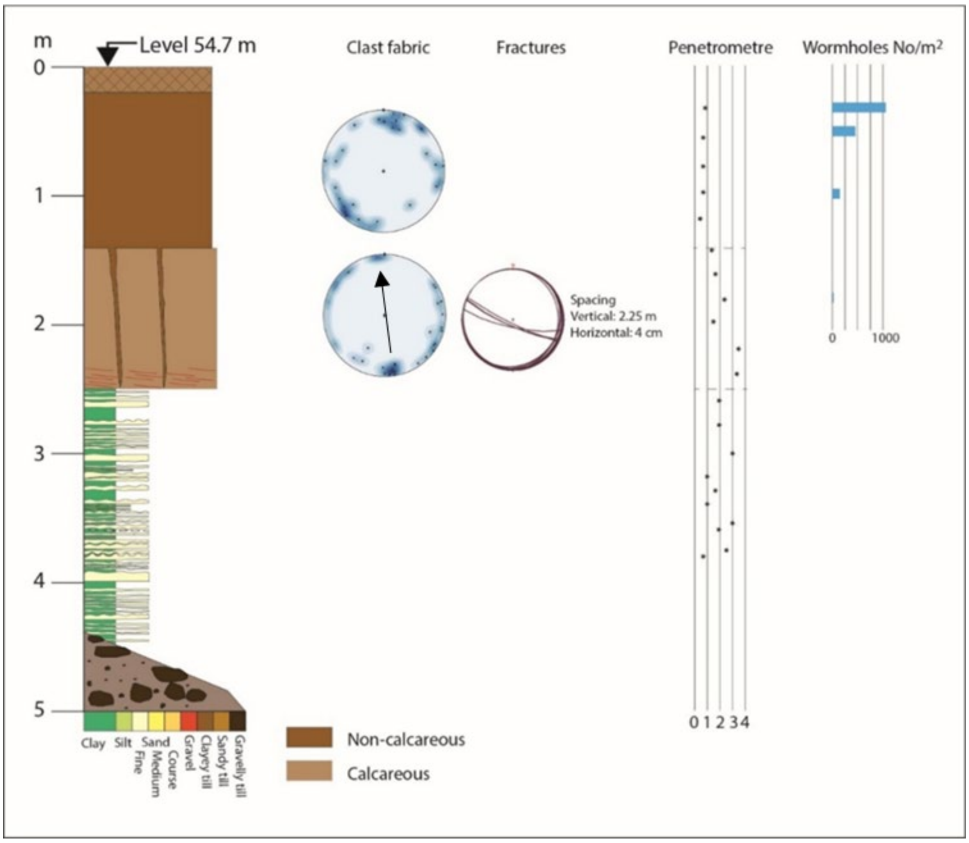

FIGURE 31. Overview of fabric data, fracture data, penetrometer data (soil compressive strength kg/cm^2) and wormholes measured in the excavation at Tokkekøb. To the left is shown a lithological profile of the site. The blue stereonets to the left show the distribution and orientation of elongated pebbles. The upper blue stereonet shows no distinct orientation, indicating that the till is a flow till rather than a basal till. The lower blue stereonet has a week maximum from the south suggesting an ice-movement direction from south to north (arrow). The white stereonet show the distribution and orientation of fractures. The vertical distribution of penetrometer data and wormholes are shown to the right.

The number of wormholes decreased with depth as 1048/m^2, 428/m^2 and 184/m^2 were counted at depths of 0.3, 0.5 and 1.0 mbs. There were no wormholes at 2 mbs in the calcareous clayey till, but in the non-calcareous till some wormholes and rootholes were observed along the fractures.

Fractures were only observed in the calcareous clayey till between 1.4 and 2.5 mbs (figure 32). In this unit large vertical fractures were seen striking 106º on average with an average spacing of 2.25 m. Laterally some of these fractures were more than 6 m long with iron coatings. Along the fractures there were a dark yellow brown, non-calcareous zone softer than the surrounding calcareous till. In the lower 25 cm of the calcareous till, horizontal fractures were present. They dip slightly easterly, in the strike direction of the vertical fractures. They have spacing of 4 cm and were iron coated. This lower zone was also slightly more compact than the rest of the till, with higher penetrometer values.

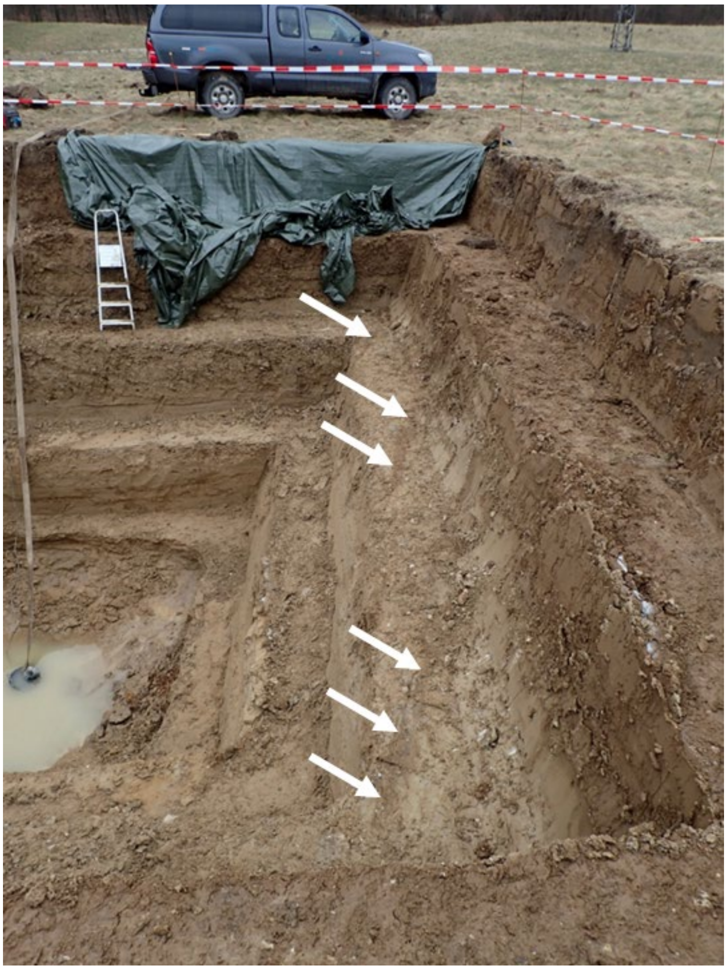

FIGURE 32. Northern part of the excavation (north to the right). The fractures are outlined by the dark yellow-brown zones that are present along the fractures. Arrows point at the vertical fractures seen 2 mbs on the lighter-brown till surface.

The presence of both lake deposits and two different till types in a dead-ice environment created a high degree of sedimentological variability. About 4 m northeast of the excavation, a well was drilled showing similar sedimentological units as the excavation, but it was very difficult to correlate the units observed in the well to the excavation, despite the short distance (figure 33). This indicates that the lake deposits must have an abrupt change in thickness and distribution. In the well, there were also more units that could be interpreted as debris-flow and in general a higher sedimentological variability.

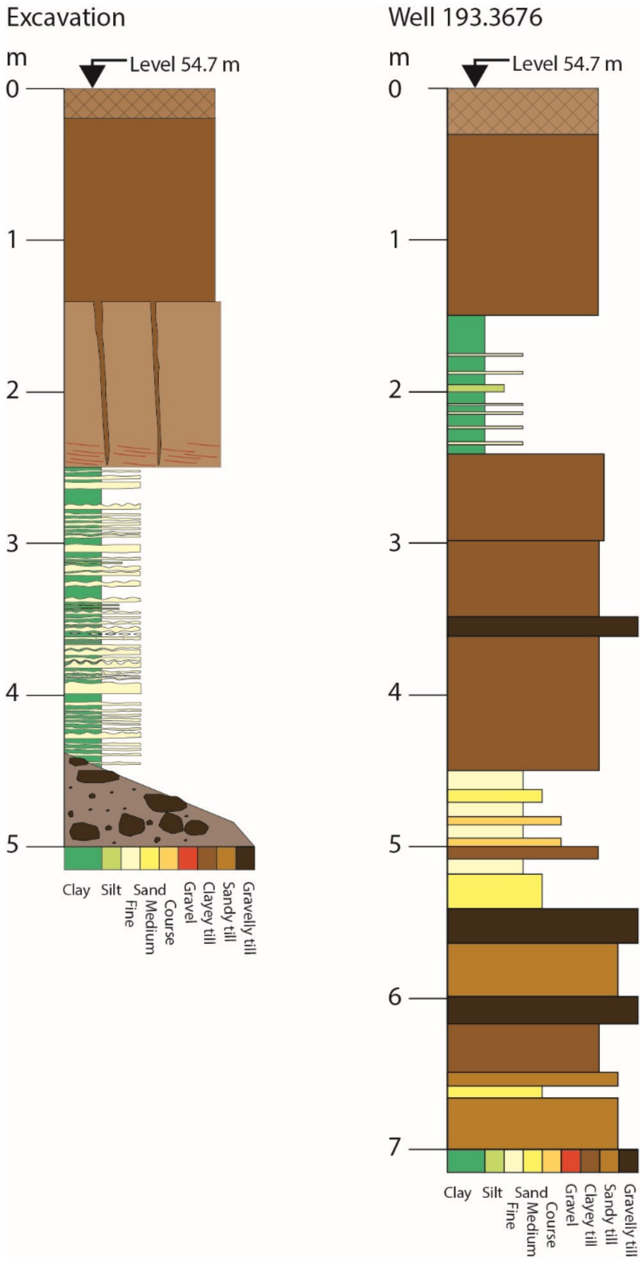

FIGURE 33. Sedimentological logs of the excavation at Tokkekøb and well 193.3676 four m northeast of the excavation.

5.2 Sorption and degradation

Degradation and sorption were studied in samples obtained from the plough layer and down to a depth of 3-4 mbs. The subsoil was sampled to differentiate the preferential flow paths and their corresponding matrix soil and thus representing both different flow regimes and microbiological settings. The degradation experiments from Havdrup-Salløv and Holbæk are presented in figure 34 and the calculated DT_{50}-values and sorption data are summarized in table 9 and table 10.

5.2.1 Degradation of MCPA and bentazon

MCPA was rapidly degraded in all topsoil and biopore samples following first order degradation kinetics to concentrations below the limit of quantification (0.05 µg/kg). DT_{50} values were calculated ranging from 1.4 to 1.8 days in the topsoil and 2.5 to 3.8 days in the biopores, with slightly lower DT_{50} values at Holbæk (figure 34A and C; table 9). In contrast, much slower degradation was observed in the matrix sediment next to the biopores. Some degradation was observed at

Holbæk with a calculated DT_{50} value of 20 days (clayey part), while no degradation was observed at Havdrup-Salløv until day 66 and it was not possible to calculate a DT_{50} value.

In general degradation was much slower below the biopore zone with only small differences between samples from the preferential flow paths and the adjacent matrix sediments. At Havdrup-Salløv the calculated half-life's (time to 50% degradation) was 57 days in the grey fractures while degradation was a little slower in the corresponding matrix sediments with half-life's of 87 days. No degradation was observed at even greater depths either in the red fractures or the matrix sediments.

At Holbæk, deeper at the clayey part of the excavation (figure 34C), degradation was very slow or absent. In the red and grey fractures DT_{50} were 35 and 144 days respectively while no degradation was seen in adjacent matrix sediments. At the sandy part of the excavation red to black coloured biopores and distinct sandy horizontal layers probably serving as preferential flow paths were observed. However, MCPA degradation in these biopores and sandy layers was much slower than seen for the biopores in the clayey part of the excavation with DT_{50} values of 66 and half-life's larger than 87days, respectively. In a silt layer, subjacent to the red horizontal sandy layer, only minor and slow degradation was observed with calculated half-life of 153 days (table 9).

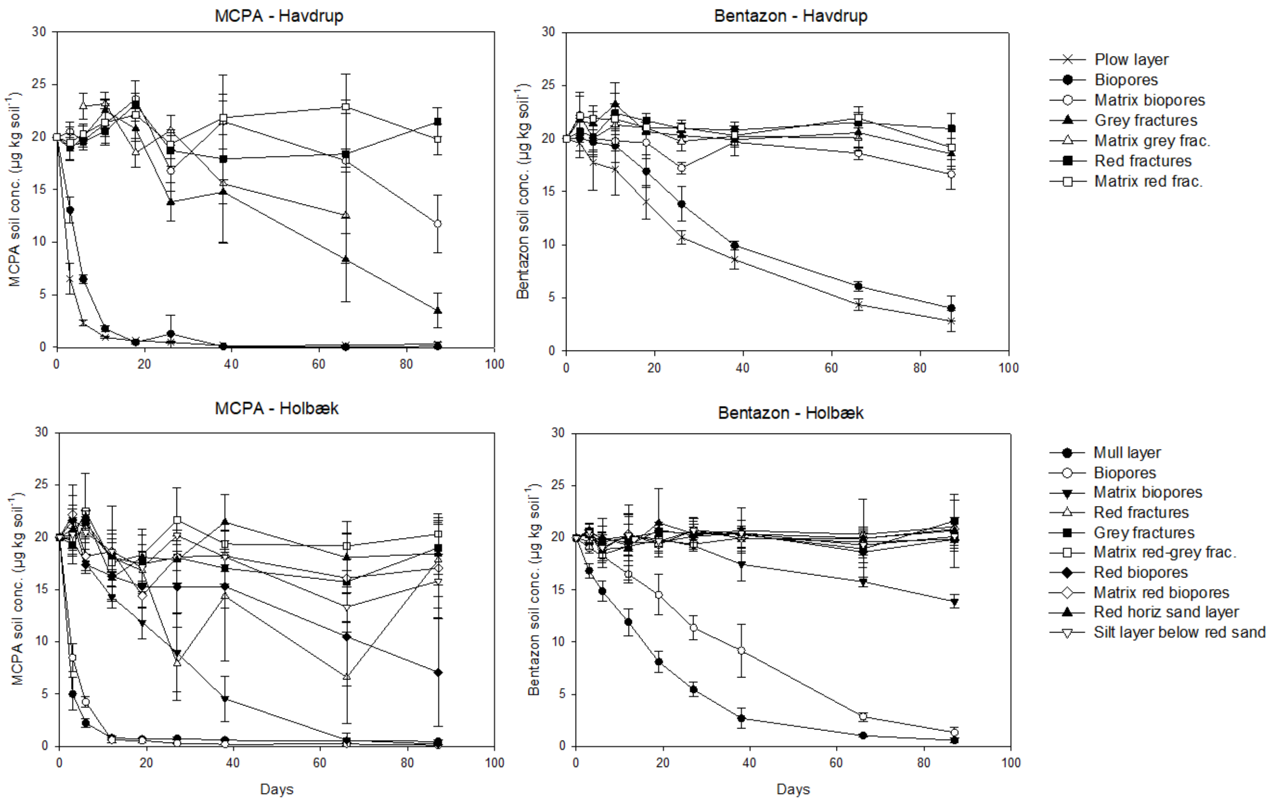

FIGURE 34. Degradation of MCPA and bentazon in soil from the seven soil compartments at the Havdrup-Salløv site (A and B) and the ten soil compartments at the Holbæk site (C and D).

TABLE 9. Calculated degradation rate constants (k) and DT_{50} values for MCPA and bentazon in sediments from the Havdrup-Salløv and Holbæk sites.

	MCPA		**Bentazon**	
Field site/ Compartment	*k*	DT_{50} (days)	*k*	DT_{50} (days)
Havdrup-Salløv				
Topsoil (0-30 cmbs)	0.385[a]	1.8	0.023[a]	30
Biopores (50-100 cmbs)	0.184[a]	3.8	0.018[a]	38
Matrix sediment (50-100 cmbs)		> 87		> 87
Grey fractures (100-200 cmbs)	-0.201[b]	57		>87
Matrix sediment (100-200 cmbs)	-0.139[b]	87	no	no
Red fractures (300-400 cmbs)	no	no	no	no
Matrix sediment (300-400 cmbs)	no	no	no	no
Holbæk				
Topsoil (0-30 cmbs)	0.481[a]	1.4	0.048	14[a]
Biopores (30-70 cmbs)	0.281[a]	2.5	0.024	29[a]
Matrix sediment (30-70 cmbs)	0.035[a]	20	0.004	161[a]
Red fractures (200-400 cmbs)	0.021[a]	35	no	no
Grey fractures (200-300 cmbs)	-0.069[b]	144	no	no
Matrix sediment (200-400 cmbs)	no	no	no	no
Red biopores in sand (100-200 cmbs)	0.010[a]	66	no	no
Matrix sandy sediment (100-200 cmbs)		>87	no	no
Red horizontal sand layer (200-300 cmbs)		>87	no	no
Silt layer (200-300 cmbs)	-0.066[b]	153	no	no

[a)] k and DT_{50} calculated based on 1. order degradation kinetics: [b)] k and DT_{50} calculated by linear regression of data. >) degradation was observed, but data could not be fitted with 1. order or linear regression and half-life to 50% degraded was noted as larger than 87 days; no: no degradation observed.

As the degradation experiment was done with independent samples and at each time point three samples were extracted, the large standard deviations, especially in the matrix soils and deeper soil layers shows that even though the initial samples have been thoroughly homogenized and that each replicate is thus a composite sample of many subsamples, the degradation potentials are very heterogeneously distributed. This is probably due to a low number of specific degrader bacteria present in the soil as previously described for MCPA degraders in subsoil (Batioglu-Pazarbasi et al. 2012, Badawi et al. 2013a, 2013b).

The degradation experiments of MCPA at the two fields sites clearly shows the difference in degradation potentials, both regarding sediment depth and compartments. The degradation is as expected much faster in the top soils and underlying biopores - rich in organic material and large bacterial diversity and density (Bak et al. 2019), but if MCPA bypasses the upper one meter, no degradation and sorption is likely to occur and thus MCPA is prone to leach to underlying subsoil layers and ultimately groundwater reservoirs.

Bentazon degradation was generally slower compared to MCPA at both sites. The degradation of bentazon in the topsoil of Havdrup-Salløv, (figure 34B) and Holbæk (figure 34D) followed 1. order kinetics, but with more than 10 times higher DT_{50} values (30 and 14 days, respectively; table 9) compared to MCPA (1.8 and 1.4 days), and bentazon was still present in the topsoil at the end of the experimental period (87 days), both at Havdrup-Salløv (0.3 µg/kg soil) and at Holbæk (0.6 µg/kg soil).

At the Havdrup-Salløv site (figure 34B), bentazon was degraded in the biopores following first order kinetics similar to the topsoil, but with a slightly higher DT_{50} value of 38 days and the degradation in the adjacent matrix soil was very slow with predicted half-life larger than 87 days. Only minor degradation of bentazon (half-life > 87 days) was observed in the underlying grey fractures and no degradation of bentazon was observed in the adjacent matrix or underlying red fractures and matrix soil.

At the Holbæk site (figure 34D), bentazon was degraded in the biopores following first order kinetics (DT_{50} – 29 days), similar to the Havdrup-Salløv site, but the degradation was slower than in the topsoil. A much slower degradation was observed in the matrix adjacent to the biopores. The degradation followed 1. order kinetics and the DT_{50} value was calculated to be 161 days. No degradation of bentazon was observed at even greater depths either in the red and grey fractures and adjacent matrix from the clayey part of the excavation or in any of the red sandy biopores, red horizontal layer or the silt layer of the sandy part of the excavation.

Generally, bentazon was more persistent than MCPA, having higher DT_{50} values (ranging from 14 days in topsoil to > 153 days in sub-sediments) and more compartments with no degradation. Additionally, bentazon is not fully degraded in topsoil during the experimental period of 87 days and in combination with the lack of degradation potential in sub-sediments, bentazon is of high risk of leaching to underlying groundwater reservoirs.

5.2.2 Sorption

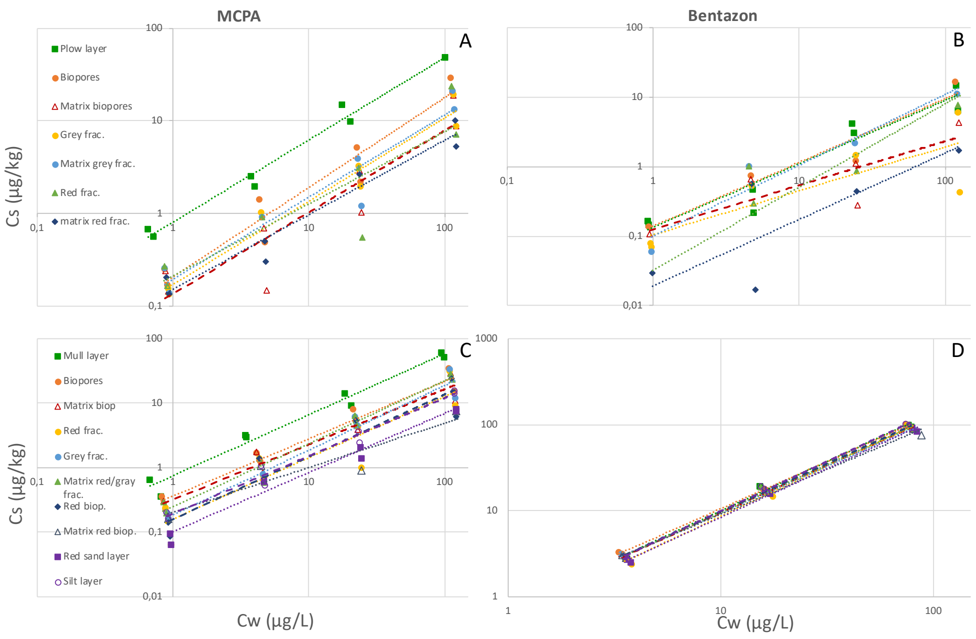

FIGURE 35. Sorption isotherms for MCPA (A) and bentazon (B) in the seven soil compartments from the Havdrup-Salløv site, and MCPA (C) and bentazon (D) from ten compartments at the Holbæk site. C_w is the pesticide concentration in the aqueous phase and C_s is the pesticide concentration in the soil phase. Sorption isotherms for bentazon in the topsoil at Havdrup-Salløv (B) are fitted to duplicate samples, but the other sediment compartments are represented by single samples per concentration level due to no sorption.

Sorption of MCPA was well determined at the Havdrup-Salløv site and followed the Freundlich model (R^2 > 93), except in the matrix to biopores (R^2 > 0.85) and in the red fractures (R^2 > 0.81) (figure 35A, table 10), which may be due to the large deviations in the duplicate samples as shown in figure 35A. The MCPA sorption was in general independent of the concentration in the sediment compartments (0.9 < *n* < 1.1), except in the red fractures (n = 0.78) and adjacent matrix sediment (*n* = 0.80). At this depth, the sorption seemed to be slightly dependent on concentration (0.69 < *n* < 0.90), indicating that sorption of MCPA decreases with increasing concentration, presumably due to saturation of the sorption sites. Sorption of MCPA in the topsoil was four-fold higher compared to all soil domains and K_F values decreased from K_F = 0.81 in the topsoil to K_F = 0.21 in the red fractures and 0.15 in the matrix sediments at the deepest compartments. There was a tendency of slightly lower sorption in the matrix sediments compared to both the biopores and the red fractures. Though this compartment dependency was not present in the grey fractures and corresponding matrix sediment.

TABLE 10. Freundlich parameters for MCPA sorption to seven soil compartments from the Havdrup-Salløv site and 10 compartments from the Holbæk site.

	K_F	n	R^2
Havdrup-Salløv			
Topsoil (0-30 cmbs)	0.81	0.89	0.99
Biopores (50-100 cmbs)	0.21	0.97	0.94
Matrix sediment (50-100 cmbs)	0.14	0.88	0.85
Grey fractures (100-200 cmbs)	0.17	0.90	0.97
Matrix sediment (100-200 cmbs)	0.19	0.89	0.93
Red fractures (300-400 cmbs)	0.21	0.78	0.81
Matrix sediment (300-400 cmbs)	0.15	0.80	0.95
Holbæk			
Topsoil (0-30 cmbs)	0.75	0.95	0.97
Biopores (30-70 cmbs)	0.36	0.89	0.96
Matrix sediment (30-70 cmbs)	0.32	0.86	0.95
Red fractures (200-400 cmbs)	0.16	0.95	0.85
Grey fractures (200-300 cmbs)	0.19	1.00	0.96
Matrix sediment (200-400 cmbs)	0.25	0.98	0.97
Red biopores in sand (100-200 cmbs)	0.16	0.96	0.91
Matrix sandy sediment (100-200 cmbs)	0.20	0.69	0.86
Red horizontal sand layer (200-300 cmbs)	0.10	0.92	0.97
Silt layer (200-300 cmbs)	0.19	0.90	0.98

At the Holbæk site, MCPA sorption followed the Freundlich model (R^2 > 0.95) in seven out of the ten compartments (figure 35C; table 10). In the red fractures and the red biopores and adjacent matrix sediments, the Freundlich model fitted less well (R^2 was 85 to 91), which can be explained by relatively large differences (and also no sorption in several replicates) between the duplicate samples from these compartments. The MCPA sorption was in general independent of concentration in the sediment compartments (0.9 < *n* < 1.1), except in the matrix sediments adjacent to the red biopores (*n* = 0.69), having a slight concentration dependence (0.69 < *n* <

0.90). This could indicate decreasing MCPA sorption with increasing concentration, presumably due to saturation of the sorption sites, but sorption at this compartment was very low and the model was fitted to single samples due to no measured sorption and results should therefore be considered tentative. Similar to sorption of MCPA in the Havdrup-Salløv site, MCPA was slightly more sorbing in the topsoil (K_F = 0.75), and sorption was also decreasing with depth with a factor of three to four in the clayey compartments (grey fractures/matrix, K_F = 0.19/0.25) and a factor of eight in the sandy compartments (silt layer, K_F = 0.19).

TABLE 11. Freundlich parameters for bentazon sorption to seven soil compartments from the Havdrup-Salløv site and 10 compartments from the Holbæk site.

	K_F	*n*	R^2
Havdrup-Salløv			
Topsoil (0-30 cmbs)	0.14	0.91	0.92
Biopores (50-100 cmbs)	0.14	0.92	0.93
Matrix sediment (50-100 cmbs)	0.13	0.63	0.71
Grey fractures (100-200 cmbs)	0.11	0.63	0.68
Matrix sediment (100-200 cmbs)	0.10	1.02	0.94
Red fractures (300-400 cmbs)	0.03	1.20	0.81
Matrix sediment (300-400 cmbs)	0.02	0.96	0.70
Holbæk			
Topsoil (0-30 cmbs)	0.72	1.14	0.99
Biopores (30-70 cmbs)	0.85	1.10	1.00
Matrix sediment (30-70 cmbs)	0.74	1.11	1.00
Red fractures (200-400 cmbs)	0.59	1.16	0.99
Grey fractures (200-300 cmbs)	0.77	1.10	1.00
Matrix sediment (200-400 cmbs)	0.73	1.11	1.00
Red biopores in sand (100-200 cmbs)	0.75	1.12	1.00
Matrix sandy sediment (100-200 cmbs)	0.82	1.05	1.00
Red horizontal sand layer (200-300 cmbs)	0.62	1.13	1.00
Silt layer (200-300 cmbs)	0.69	1.16	1.00

Bentazon sorption at the Havdrup-Salløv site was very low even in topsoil (figure 35B, table 11) and except from this compartment, all other compartments, had several replicates with no sorption or large differences between duplicate samples. Consequently, the isotherms for these compartments are based on single data points at most of the concentration levels, resulting in poor fits (R^2 = 0.68-0.71) and thus the calculated K_F and *n* values will be subject to great uncertainty. However, the sorption experiment clearly shows that bentazon sorption in general was very low in all compartments and decreased with increasing depth. At the Holbæk site, bentazon sorption followed the Freundlich model in all ten compartments ($R^2 \geq 0.99$; figure 35D and table 11). The sorption was in general independent of the concentration in the compartments ($0.9 < n < 1.1$) and there was no significant difference in bentazon sorption between the different compartments, depth or whether it was in the sandy or clayey part of the excavation. Bentazon sorption was at least a factor of four higher in all soil domains (K_F = 0.59 – 0.85) in the clayey part of the excavation compared to the corresponding compartments at the Havdrup-Salløv site (K_F = 0.02 – 0.14).

Sorption of MCPA and bentazon was in general very low in all compartments with K_F values < 0.9 even in the topsoils. Both MCPA and bentazon are registered in the Pesticide properties database (PPDB 2019) as non-persistent, with DT_{50} values of 24 and 20 days, respectively, and both mobile in soil with K_F values of 0.94 for MCPA and 0.97 for bentazon (PPDB 2019). These values are usually determined from standardized degradation and sorption studies with bulk topsoil samples. In relation to the present study, these values only resemble the topsoil data and not the combination of very low sorption and no or very slow degradation observed in sub-sediments for both compounds at both field sites. These results clearly strengthen and underline the necessity for depth dependent parametrization in pesticide leaching assessments as also suggested in FOCUS groundwater scenarios (FOCUS, 2014).

5.3 LUC hydraulic experiments

The focus of the LUC experiments was to quantitatively characterize types of preferential flow paths and pesticide transport in the sub-soil below 1 m depth at the Havdrup-Salløv and Holbæk sites. Special attention was given to documentation of flow in Fe/Mn-oxide stained fractures (red fractures) because the common view among scientists is that these are determinants of rapid preferential flow and pesticide transport in glacial tills (Cherry et al. 2006), while some recent investigations of flow in fractures suggest they are largely closed and, hence, have minor importance for groundwater vulnerability (e.g. Jørgensen et al. 2017, and 2020).

5.3.1 Fractures and biopores in the LUC samples

The types of investigated fractures, fracture redox conditions, and macropore structures in clayey tills are shown in figure 60. Fracture spacings in the LUCs from Havdrup-Salløv and Holbæk and all other previously investigated LUC´s are shown in figure 60 and compared with the fracture spacings mapped in field investigations. The LUCs represents reasonably well the maximum fracture densities in the field investigations and therefore can be expected to reflect the maximum hydrologic influence of fractures at field scale.

Root channels occurred predominantly along the fractures, however, occasionally also as solitary root channels in the matrix (figure 37 and figure 38). In the upper LUC from the Holbæk site (1.95-2.4 mbs; figure 37 a-b) the fractures with root channels had grey rims (grey fractures) caused by dissolution of Fe/Mn oxides under anaerobic decay of root material (e.g. Jørgensen et al. 2017). In the columns from greater depth, the fractures were reddish-brown (red fractures) due to Fe/Mn oxide precipitation and infilling along the fractures (figure 37c).

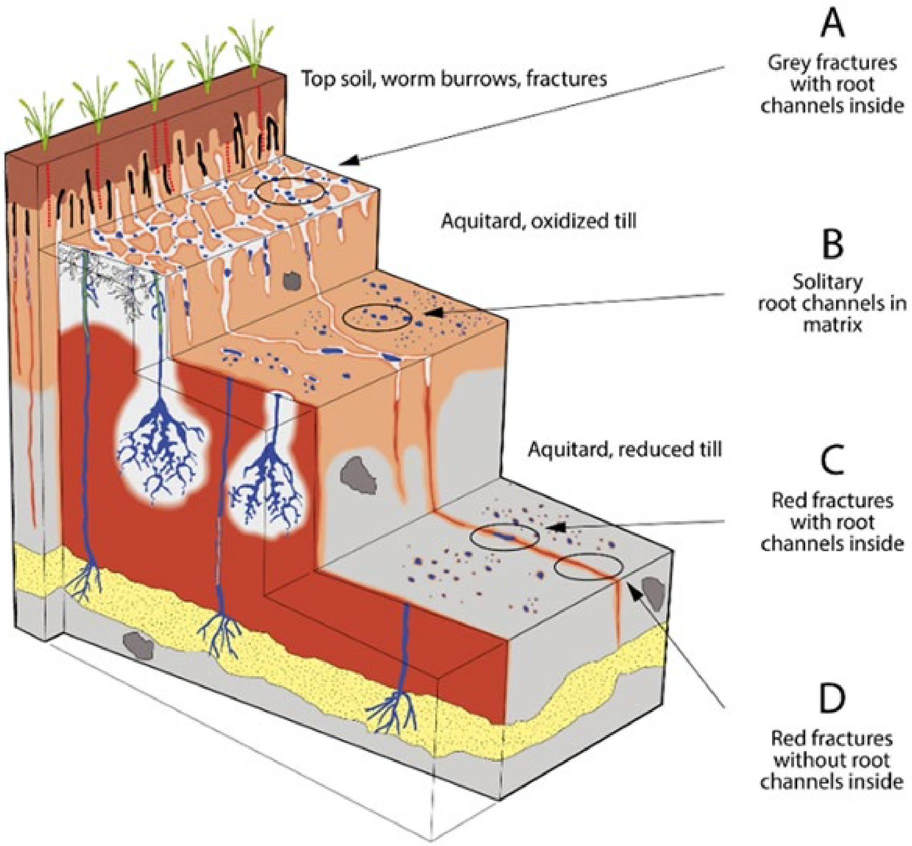

FIGURE 36. Conceptual model of clayey till showing types of fractures, biopores and associated redox conditions together with preferential flow paths (blue) and their representation in the LUC experiments. The fracture and macropore redox conditions represented in the subsoil were Fe-oxide reduced (grey fractures) and Fe-oxide stained (red fractures). The geochemical development of the fractures and biopores is described in Jørgensen et al. (2017).

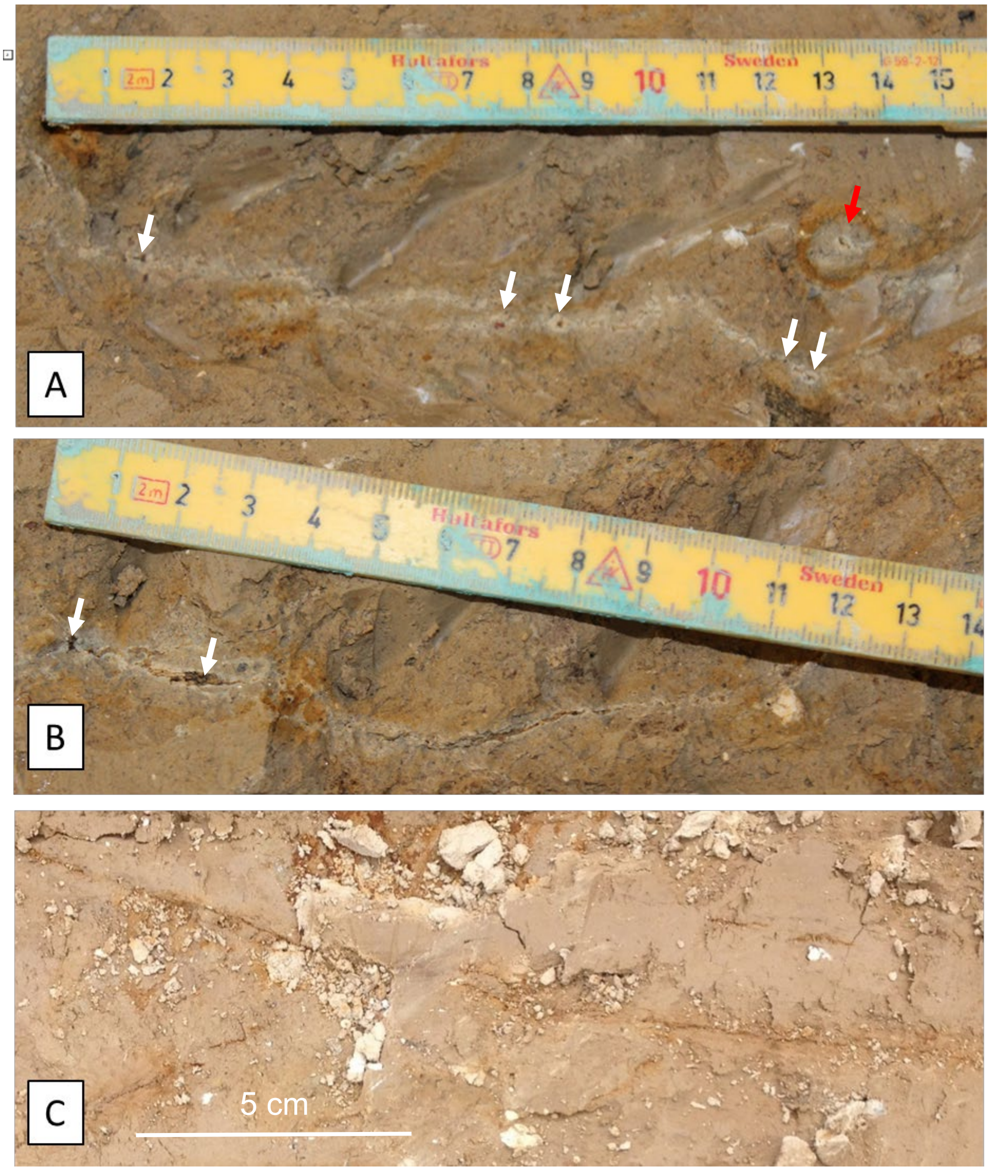

FIGURE 37. Sub-vertical fractures and root channels in Holbæk and Havdrup-Salløv viewed from above. A and B: Grey fractures with root channels (white arrows) embedded in a matrix of oxidised till (from Holbæk LUC-top: 1.95-2.4 m). A single solitary root channel is also seen (red arrow). C: Red fractures in oxidized till in 4 m depth at the Havdrup-Salløv field site.

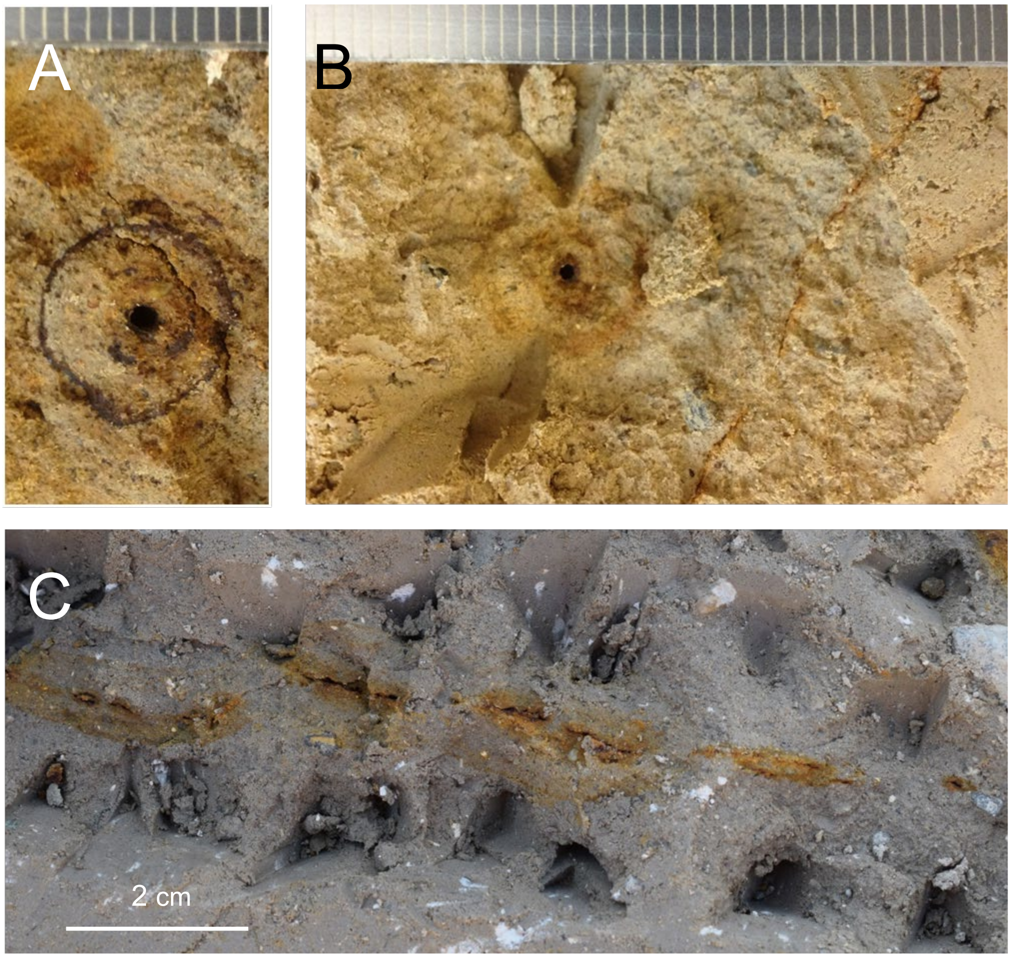

FIGURE 38. Sub-vertical root channels and fractures at Holbæk and Havdrup-Salløv viewed from above. A-B: Solitary 0.5 - 1 mm root channels in oxidized till at 2.6 m depth in Holbæk (1 mm scale shown in top). C; Red fracture in grey unweathered till matrix in 5.2 m depth in Havdrup-Salløv. Notice subdivision of the fracture in 1-2 cm long fracture segments of enhanced aperture resembling root channels. Ancient DNA (aDNA) sequencing suggests these to originate from ancient Willow trees (Seljepil, Gråpil, Sortpil), (Jørgensen et al. 2021 in review).

The root channels occurred as tubular pores 0.5-2 mm in diameter (figure 38 a-b) or few cm long channel segments along fractures, which are likely created by shrinkage of the matrix near the roots (figure 38c). Similar relic root channels and root channel casts inside fractures have been described previously by e.g. Cherry (1989), Ruland et al. (1991), McKay and Fredericia (1995), Klint and Gravesen (1999), Jørgensen et al. (2002, 2017).

5.3.2 Fractures and biopores as preferential flow paths

Figure 39 and figure 40 show the observed distribution of geological structures visualised by the infiltrated Brilliant Blue (BB) in the columns when they were opened and cut in horizontal slices after the hydraulic experiments. Figure 39A-C show the uppermost LUC column from the Holbæk site (1.95-2.4 mbs) in which the BB dye tracer revealed that flow had occurred in closely spaced dyed root channels along the total horizontal length of the grey fractures. In the column collected immediately below this depth (2.6-3.1 m depth), the grey fracture had disappeared leaving only red fractures in which there was no indication of dye tracer flow. Instead the column contained dyed solitary root channels in the matrix (figure 39D-F). Most of these solitary root channels terminated within the upper 15 cm of the column (corresponding to 2.8 m depth) except for 1 root channel in which the dye tracer had penetrated the full length of the column (figure 39F). Hence, there was only very minor flow of the dye tracer in the red fractures in this column despite flow had been forced by application of an unnaturally high hydraulic gradient to identify any preferential flow. The same minor occurrence of preferential flow along the red fractures was also observed in all the other 4 columns (Holbæk 3.1-3.6, Havdrup-Salløv 3.4-3.9m, and Havdrup-Salløv 4.4-4.9m) in which the dye tracer only penetrated 2-15 cm into the red fractures after 1-3 month of forced flow with high hydraulic gradients (figure 39G-I).

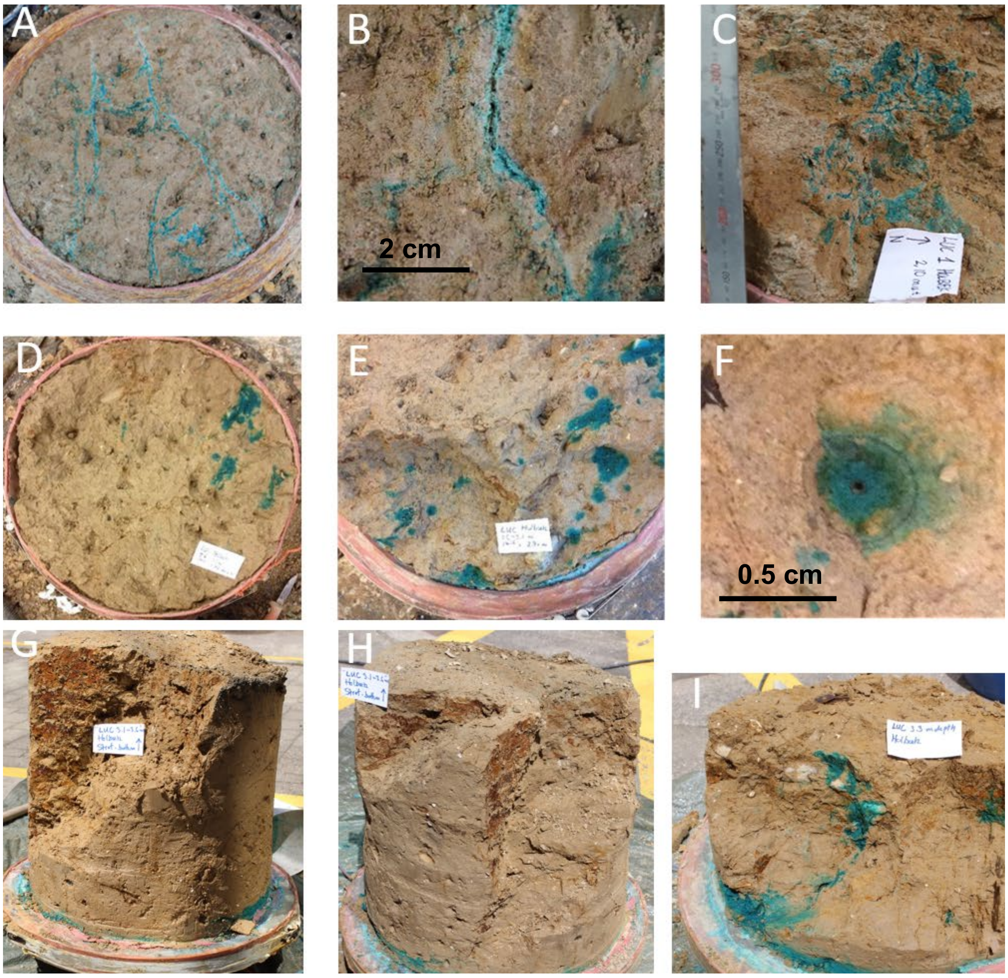

FIGURE 39. Cutting up the LUC samples from the Holbæk site after Brilliant Blue (BB) dye tracer infiltration. The infiltration was carried out as water saturated flow from the bottom and upwards to avoid retardation of flow by gas bubbles. LUCs were moreover flipped upside down for correct flow direction in the soil. A: Top surface of Holbæk LUC-top (1.95-2.3 m depth) showing transport of dye in root channels along grey fractures in 1.95 m depth (>200 channels/m^2). B: Magnification of fracture from "A". C: Root channels along an exposed fracture wall surface in the same LUC. D and E: Transport of BB tracer in solitary root channels in Holbæk LUC-middle (2.6-3.1 m depth; notice absence of dye in the exposed red fracture). F: Penetration of dye tracer in one solitary root channel through the full Holbæk LUC-middle length (root channel density decreasing from 125 to 5/m^2 from top to bottom of LUC). G and H: Absence of BB flow in exposed prominent red fractures without root channels in the Holbæk LUC-bottom, no root channels in LUC (3.1-3.6 m depth). I: Lower 0-20 cm of the same column as photo "H" showing 15-10 cm penetration of the dye tracer along the red fracture after three months dye infiltration with a forced hydraulic gradient.

Figure 40 show one exception from this pattern, which was in the deepest column from the Havdrup-Salløv site (5.4-5.9 m depth). In this LUC the dye tracer had penetrated 7.5 cm along three Fe/Mn-oxide filled root channels occurring inside the main fracture in the column after only one week of forced flow (figure 40A-E). Hence, aside from the partially filled root channels in this column, the red fractures appeared in general to be largely closed by precipitated Fe/Mn oxides. The root channels were identified by ancient DNA (aDNA) analysis as originating from the *Salix Chamaetia/Vetrix* clade of scrubs and trees (Jørgensen et al. 2021 in review). This clade includes the common Danish species *S. caprea* (seljepil) *S. cinerea* (Gråpil), and *S. myrsinifolia (Sort pil).* They were among the first shrubs and trees to spread widely in the open post glacial landscape 11,000 – 10,000 year ago (GEUS 2007).

FIGURE 40. Overview and dye tracer flow in the main fracture of Havdrup-Salløv LUC-bottom (5.4-5.9 m depth). Same experimental set-up and overall conditions as described in figure 39. A: Sampling of the LUC in the field before the dye tracer experiment showing main fracture and subdivision between upper unweathered and lower weathered part of the LUC. B: Sub-division of the main fracture in root channels in the unweathered till. C: Dye tracer in cross section of sub-vertical root channels. D: Magnification of dyed root channel in "C". E: longitudinal section of the central root channel in photo "C" viewed inside the fracture. aDNA sequencing of the root channel filings and walls suggested they originated from ancient S. caprea (seljepil), S. cinerea (Gråpil), and S. myrsinifolia (Jørgensen et al. 2021, in review), root channel density decreased from 15 to 5/m^2 from top to bottom of LUC.

5.3.3 Hydraulic conductivity and fracture hydraulic apertures

Figure 41 shows the water saturated hydraulic conductivity (Ksat) for the LUC samples from Holbæk and Havdrup-Salløv, and for 70 mm intact cores of unfractured matrix, collected from the LUCs after completion of the experiments. Table 12 summarize data from the LUC fracture and dye tracer experiments.

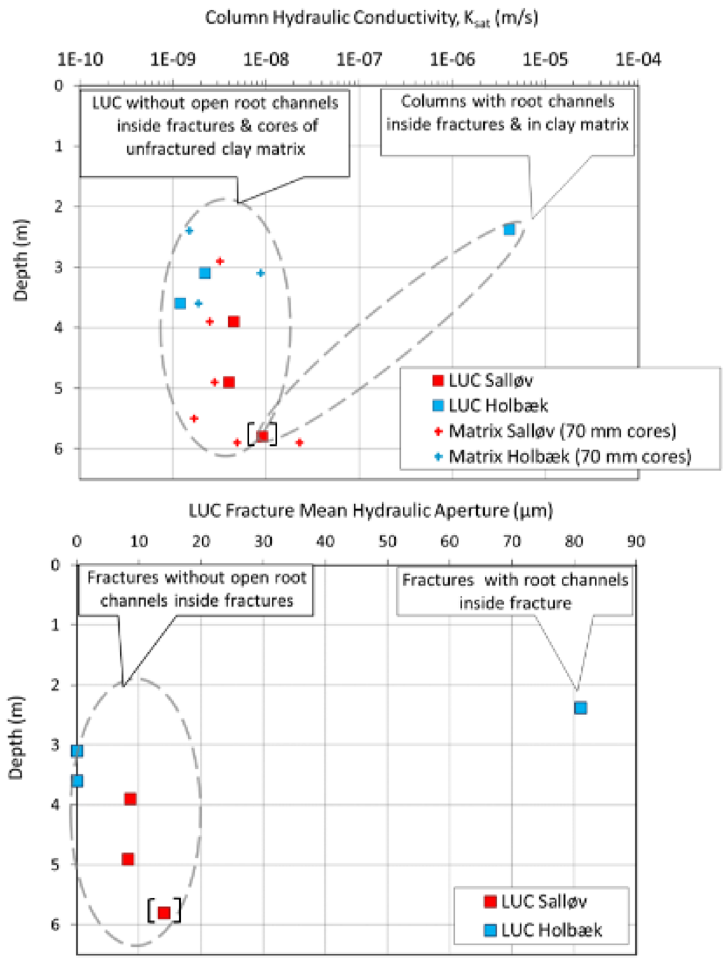

FIGURE 41. Column hydraulic conductivity and mean fracture hydraulic apertures at Havdrup-Salløv (Salløv) and Holbæk. A: Saturated hydraulic conductivity (Ksat) of LUC and 70 mm cores of unfractured matrix and B: Fracture mean hydraulic apertures (2b). Hydraulic conductivity and fracture aperture value for Havdrup-Salløv LUC-bottom is artificially exaggerated due to rim-flow along column.

Figure 41a show that the LUC bulk hydraulic conductivity (Ks) is approximately 2-3 order of magnitude higher for the Holbæk LUC-top with root channels inside the grey fractures than for the LUCs containing only red fractures without open root channels (Holbæk LUC-middle, Holbæk-LUC-bottom, Havdrup-Salløv LUC-top, and Havdrup-Salløv LUC-middle). This is despite that the hydraulic conductivity of the unfractured matrix is largely the same in all samples. Consequently, the bulk Ks values of the four LUCs with red fractures without root channels are the same or only a factor 2-3 higher than the matrix, which indicates that the increase of total flow caused by the red fractures is marginal compared to the 1000 times increase caused by the grey fractures. The appearance of the dye tracer along the root channels in the grey fractures indicates that the high hydraulic conductivity is caused by root channels being the principal agent of fracture aperture enhancement. Root channels may therefore be determinants of elevated groundwater risk where grey fractures are connected to underlying groundwater aquifers in embedded coarser layers, which were abundant in the Holbæk and Havdrup-Salløv aquitards. The relatively high Ks value of the Havdrup-Salløv LUC-bottom compared with the other LUCs with red fractures was partially influenced by the observed rim flow along this LUC, but also controlled by the combination of textural heterogeneities and flow along the partially filled root channels found along the red fractures (table 12; figure 41). Figure 41b show the mean fracture apertures calculated for the columns. This shows the same pattern as 41a, where very small apertures characterise the fractures without root channels. Figure 42 show the response of fracture hydraulic aperture to depositional overburden in the LUCs, which was simulated by increasing the cell pressure in the permeameter. The small relative decrease in hydraulic conductivity with depth in fractures with root channels has little significance to their role as rapid preferential flow paths. In contrast, for the fractures without root channels the observed decrease of already small apertures causes these fractures to lose influence further as preferential flow paths or they may potentially close completely.

TABLE 12. Hydraulic parameters for LUC (water-saturated conditions). Mean fracture hydraulic apertures are calculated using the cubic law (Snow 1968) for primary fractures assuming flow through the total fracture trace length in cases where no root channels were identified, and only through channels in cases where channels were identified. In both cases flow was identified by dye-tracer.

	Column depth	Permeameter pressure	LUC hydraulic conductivity (K_{sat})	Cumulative fracture spacing (2B)	Total fracture length, (*W*)	Dyed fracture length	Mean hydraulic aperture of dyed fracture sections *(2b)*
	mbs	kPa	m/s	m	m	%*	µm
Havdrup-Salløv	LUC-top 3.4-3.9 (ox)	42	$4.5\cdot10^{-9}$	0.125	1.4	67	8.6
	LUC-middle 4.4-4.9 (ox)	51	$4.0\cdot10^{-9}$	0.17	1.1	62	8.2
	LUC-bottom 5.4-5.9 (re/ox)	88	$9.1\cdot10^{-9}$	0.25	0.53	14 (rc)	31
Holbæk	LUC-top 2.0-2.4 (ox)	27	$4.1\cdot10^{-6}$	0.13	2.4	100 (rc)	81
	LUC-middle 2.6-3.1 (ox)	44	$2.0\cdot10^{-9}$	0.17	2.3	100	0[a]
	LUC-bottom 3.1-3.6 (ox)	60	$1.2\cdot10^{-9}$	0.25	1	100	0[a]

Ox: oxidised (weathered); re: reduced (unweathered). * % of W; rc: root channels observed; [a]: Too small to be distinguished as active flow paths.

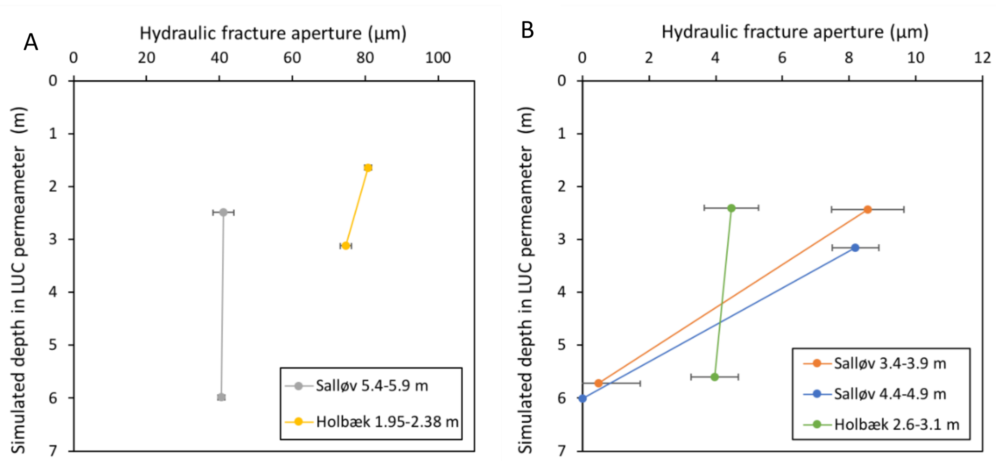

FIGURE 42. Response of fracture hydraulic apertures in the LUCs to simulated depositional overburden in the LUC permeameter of Holbæk and Havdrup-Salløv (Salløv). (a) Fractures with root channels. (b) Fractures without root channels.

5.3.4 Pesticide transport experiments

Transport of pesticides and bromide (conservative tracer) in the columns is shown in figure 43 and 44 for the Holbæk 1,95 -2.4 m and Havdrup-Salløv 5.4-5.9 m LUCs, representing grey and red fractures with root channels, respectively.

In the shallow Holbæk LUC-top, transport was initiated at a high flow rate of 600 mL/h, which was followed by 100 mL/h. The high flow rate is within possible field values in grey fractures under rain-storm conditions and was chosen to investigate possible influence of non-equilibrium sorption of the pesticides. Very rapid breakthrough of the pesticides is seen to occur at the high flow rate exhibiting similar mobility as bromide, which suggests the pesticides behaves like a conservative tracer independent of sorption properties at the rainstorm conditions. After the flow rate was lowered the relative pesticide concentrations were reduced in the order of increasing pesticide sorption, i.e. tebuconazole, which is most strongly adsorbed was reduced most. The experiment demonstrated that due to the root channels in the grey fractures, these represent pesticide flow paths with very great potential to transport both mobile and relatively strongly adsorbed pesticides into underlying groundwater aquifers.

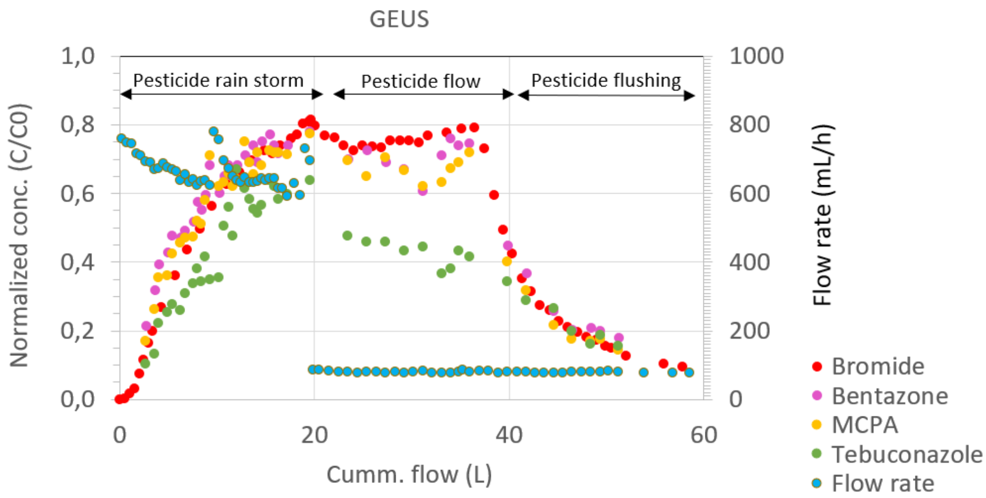

FIGURE 43. Breakthrough of infiltrated pesticides and conservative tracer bromide in Holbæk LUC-top (1.95-2.4 mbs) with grey fractures. Initial high flow rates mirrored a 24-hour rainstorm event followed by less intensive flow.

Due to much smaller fracture apertures in the Havdrup-Salløv LUC-bottom, the hydraulic conductivity was approximately 250 times lower than the Holbæk LUC-top (figure 41). The pesticide transport reveals approximately 50% lower breakthrough concentrations of the mobile pesticides (bentazon and MCPA) and bromide in the Havdrup-Salløv LUC-bottom than observed in the Holbæk LUC-top (figure 43 and figure 44). This reduction is probably due a higher amount of the solutes being accumulated in the LUC by diffusion into the matrix. For tebuconazole the retardation was even higher and only traces of the pesticide were appearing in the effluent in accordance with strong sorption of this compound. Also, rim flow was observed to have occurred with this specific LUC, which has further enhanced flow and transport compared with natural conditions. These circumstances must be considered when directly comparing figure 43 and figure 42.

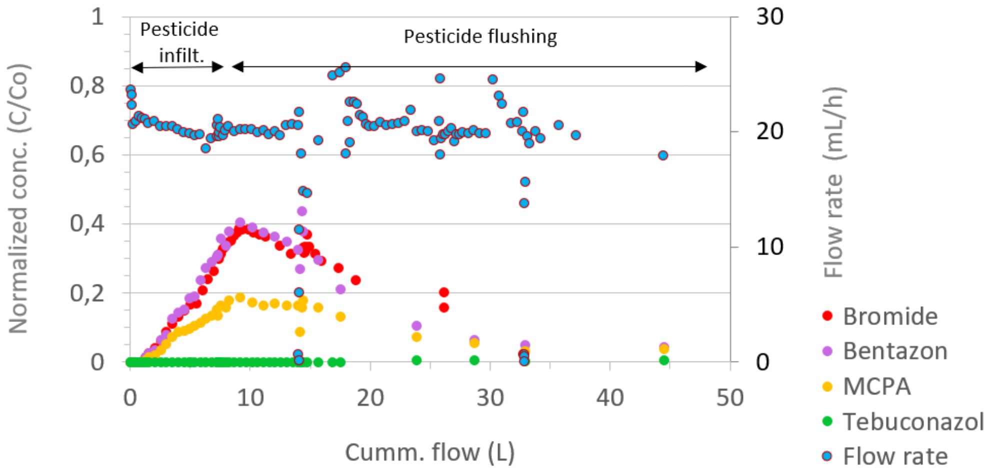

FIGURE 44. Breakthrough of infiltrated pesticides and conservative tracer bromide in heterogenous clayey till of the Havdrup-Salløv LUC-bottom (5.4.5,9 m depth). Forced flow is applied with a flow rate 3-4 higher than in the field.

Pesticide and bromide transport curves for the red fractures without root channels was not possible to obtain because flow and transport was so extremely slow in these fractures (2b = 3-14 µm; figure 44). Instead bromide and BB was injected under forced flow for more than one month to confirm that no BB or bromide transport occurred.

5.4 Modelling

The modelling served several purposes: (i) to quantitatively evaluate the water flux contributions of fractures and matrix to the total water fluxes, (ii) to plan and to interpret laboratory and field tests, (iii) to investigate the transport behaviour of pesticides and to determine main influential quantities and processes on pesticide leaching through fractured clayey tills. In the following, modelling results focusing on different aspects are presented, starting with the simulation results of the tracer infiltration test at the excavation site at Havdrup and of the LUC experiments with tracers and pesticides. Then, generic model setups are used to investigate and quantify the influence of a variety of parameters and properties of the solutes and of the clayey-till aquitards on the risk of pesticide leaching.

5.4.1 Excavation site

The Brilliant Blue infiltration experiment at the Havdrup-Salløv field site into the infiltration basin at a depth of ca. 5 mbs over a period of approximately 15 days was followed by the layer-wise removal of the clayey till revealed a pattern of vertical and subvertical fractures. The infiltration depth of the tracer dye along these fractures was mapped, as shown in figure 9b-c and figure 57a. Within the infiltration period, the dye tracer had left dyed traces down to a maximum depth of ca. 25 cm, which indicates fracture segments with the largest hydraulic fracture aperture. The fracture segments were grouped according to the observed infiltration depth into four groups: i) no infiltration, ii) 0-10 cm infiltration, iii) 10-20 cm infiltration, and iv) 20-30 cm infiltration.

A 3D discrete-fracture model of a section of the infiltration basin was setup and the mapped fracture pattern was included with help of a CAD program. The mapped infiltration pattern of Brilliant Blue (top view shown in figure 45a) could be reproduced by the 3D model by adjusting the hydraulic fracture apertures for the grouped fracture segments according to the observed tracer infiltration depth. The 3D visualization in figure 45b illustrates the simulated non-uniform infiltration pattern. Figures 45c-e show horizontal cross sections of the simulated tracer infiltration from three different depths below the infiltration basin. The model simulations yielded hydraulic fracture apertures in the order of 3-10 µm. However, the fractures in the clayey till were most likely not fully water-saturated and the entrapped air could impede the tracer infiltration. Partially unsaturated conditions would lead to a reduced tracer infiltration depth and hence to an underestimation of the hydraulic fracture aperture, i.e., the real hydraulic fracture aperture could be larger when determined under well-controlled conditions, like in the LUC experiments. The aperture values were, however, in agreement with the aperture values determined in the PESTPORE2 field experiments at the site, which were water saturated before the start of infiltration (Jørgensen et al. 2002). They also corroborate with the LUC experiments in the same geological profile immediately above.

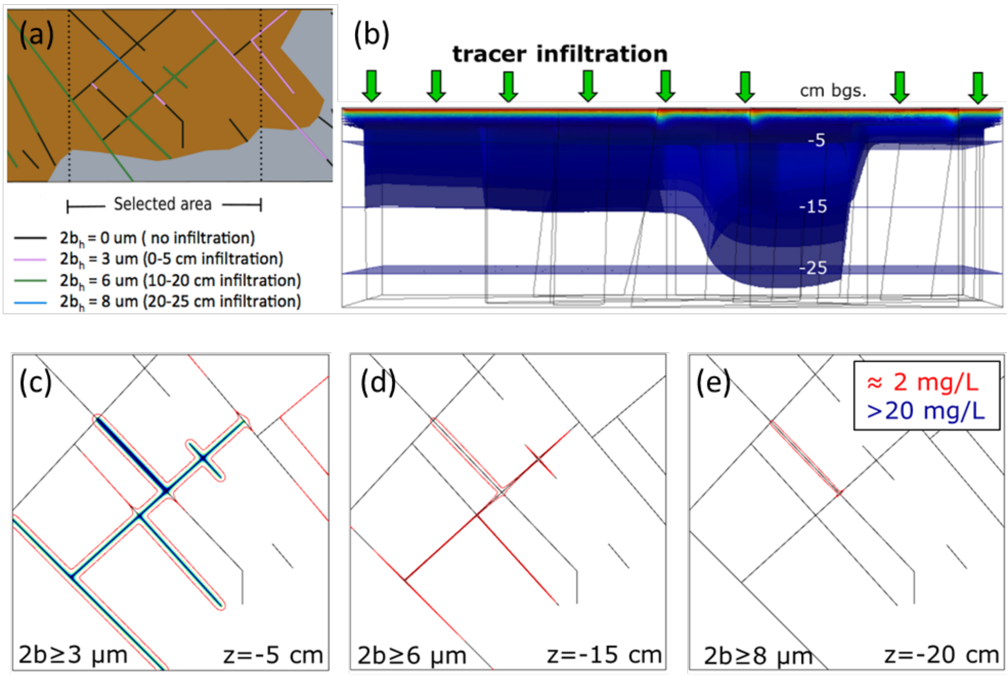

FIGURE 45. (a) Top view of the fracture mapping from the Havdrup-Salløv field site with the observed infiltration depth and the respective hydraulic fracture apertures determined with the model. (b) Tracer concentration distribution simulated with the 3D DFM model. (c)-(e) Simulated cross sections (1 m x 1 m) at 5 cm, 15 cm, and 20 cm below the infiltration basin.

5.4.2 LUC experiments

Here, we present and discuss the results of the modelling interpretation of the two long-term flow-through laboratory experiments. Despite being from relatively similar clayey-till geologies, the two LUCs revealed a very different flow and transport behaviour. The flow and transport through Holbæk LUC-top was clearly dominated by large-aperture fractures and macropores, which were found more in the shallow depth of approximately 2 mbs. The simulation results indicate that all the water flow in Holbæk LUC-top happened through fractures/macropores with a hydraulic fracture aperture of 110.6 μm determined with the model. This aperture is greater than the calculated hydraulic value in Table 12. which is based on the visualized fracture trace length at a depth of two mbs, whereas the value obtained in the modelling is an average value for the entire LUC. It was calculated by assuming uniform flow along the total fracture width and was fitted in the model to reproduce the hydraulic conditions as well as the observed bromide transport. The larger transport aperture suggests that flow was not uniformly distributed along the total fracture trace, but was channelled along larger aperture channels, which were probably the large root channels shown by the dye tracer (figure 39B and C). Havdrup-Salløv LUC-bottom was excavated from a greater depth and had only few active fracture/macropore segments, which were partially filled with precipitated iron oxides. The simulations quantified that about 83 % of the water flow happened through the main fracture with a computed hydraulic aperture of 18.5 μm. However, in the upper section of the same column (towards the outflow), the aperture was assumed smaller (10 μm) due to almost no observed staining after the Brilliant Blue injection. With the higher conductive sandy clayey till in this depth, the fracture contributed only about 18 % to the total water flux in the upper part of the LUC. This indicates a redistribution of flow and transport from the fractures to the higher conductive matrix when the fracture aperture becomes narrower and the contrast between fracture and matrix hydraulic conductivity shrinks.

Figure 46 shows the simulated evolution of the bromide distribution in Holbæk LUC-top (a-c) and Havdrup-Salløv LUC-bottom (d-f). In Holbæk LUC-top, the solute is quickly transported through the fractures and the gravel layer. It reaches the four outlet ports at the top of the LUC setup in a few hours (figure 46a). After initiating the flushing (figure 46b), the concentrations in the fractures and the matrix decrease quickly again. After 480 hours (figure 46c), there is only little solute left in the LUC.

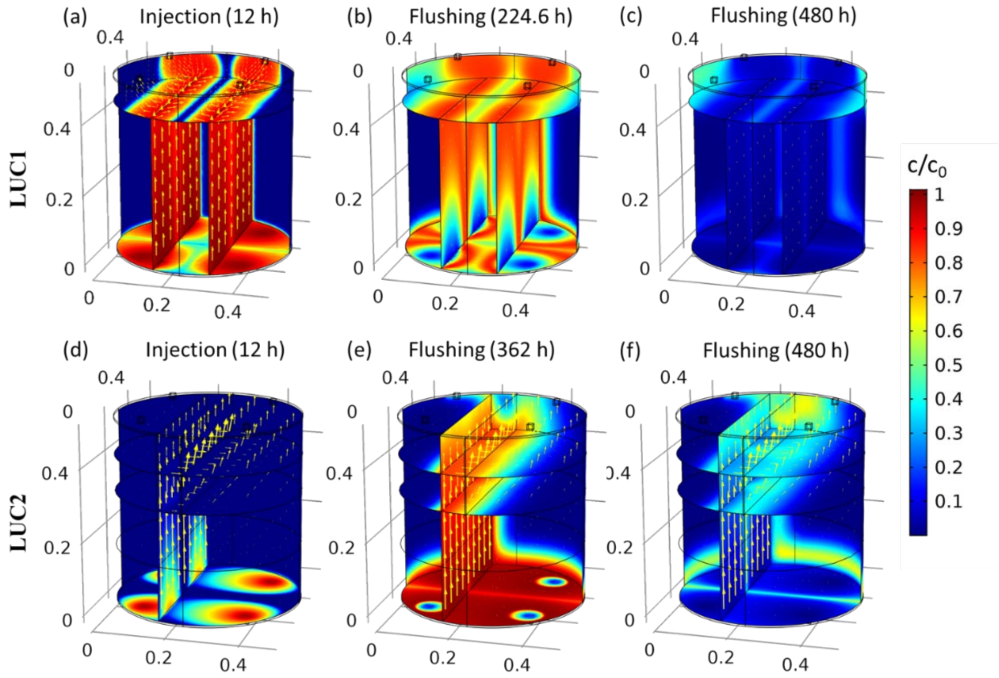

FIGURE 46. Simulated normalized bromide concentration distribution in Holbæk LUC-top (a)-(c) and Havdrup-Salløv LUC-bottom (d)-(f) during the injection (a, f), at the beginning of the flushing period (b, e), and after a longer period of flushing (c, f). The arrows indicate the flow field. Modified from Mosthaf et al. (2020).

Havdrup-Salløv LUC-bottom shows a more complex flow field (indicated by the arrows in figure 46d-f). First, most of the solute is transported through the main fracture (figure 46d). Due to the lower fracture aperture and the lower flow rate, it takes much longer time until the solute arrives at the outlet ports. When the solute arrives at the two horizontal sand layers, which provide a connection to the higher conductive sandy clayey till (upper right in the figure 46d-f, see also figure 10b), a part of the flow is redirected and leaves the column through the higher conductive sandy clayey-till part of the matrix. The outlet concentrations also decrease when starting to flush Havdrup-Salløv LUC-bottom with tap water (figure 46e). However, more solute has entered the matrix and the concentrations decrease much slower than in Holbæk LUC-top. Due to matrix diffusion and advection (mainly in the sandy clayey till), there is a larger amount of solute left in the matrix after 480 hours (figure 46f), which diffuses both deeper into the matrix, as well as back towards the fracture.

The experimentally determined breakthrough curves from the laboratory flow-through tests in Holbæk LUC-top and Havdrup-Salløv LUC-bottom can be seen in Figure 47a and Figure 47b. The solute breakthrough behaviours in the two columns were very different. For both experiments, the models were calibrated to the breakthrough curves of bromide. Then, the diffusion and sorption parameters were varied to simulate the pesticide experiments. The DFM models could reproduce the main features of the breakthrough curves. At the Holbæk site, the breakthrough of bromide and of the three pesticides happened after a few hours, while it took about

60 hours in the column from the Havdrup-Salløv site, despite a larger vertical hydraulic gradient on the LUC. This is in line with the very different fracture apertures that was determined for the main fractures of the two columns. For the Holbæk column, a hydraulic fracture aperture of 110.6 µm was determined, while the value for the main fracture in Havdrup-Salløv LUC-bottom was about 18.5 µm. According to the cubic law, the water flux through a fracture scales with the third power of the hydraulic fracture aperture (i.e., double fracture aperture leads to eight times stronger flux).

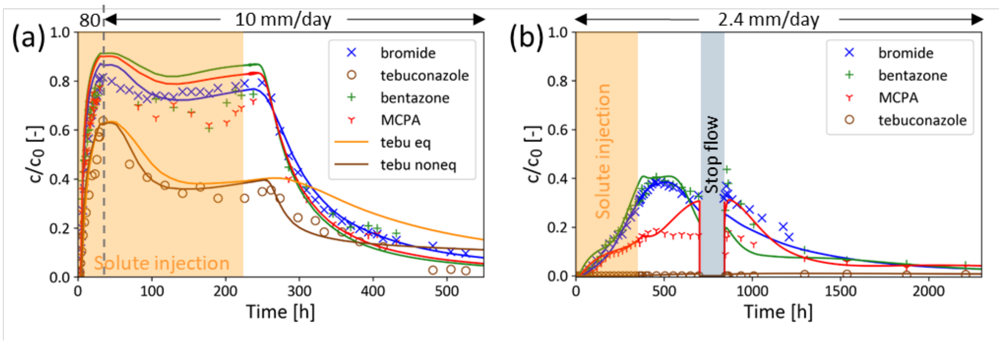

FIGURE 47. Simulated and measured breakthrough curves for a) Holbæk LUC-top and b) Havdrup-Salløv LUC-bottom. Comparison of the measured breakthrough curves of bentazon, MCPA, tebuconazole and bromide (symbols) with the simulated concentrations (lines). For tebuconazole in Holbæk LUC-top, the simulated curves with an equilibrium sorption model (tebu eq) and a nonequilibrium sorption model (tebu noneq) are shown. The infiltration rates are reported on top of each figure.

With the large fracture aperture in Holbæk LUC-top, the influence of the clayey-till matrix on the solute transport through the column was very small, and very accurate values of the matrix hydraulic conductivity were not necessary to capture the breakthrough curve with the model. Transport and exchange with the matrix happened mostly due to diffusion, and sorption influenced the leaching behaviour of the pesticides. Bentazon and MCPA showed a similar breakthrough behaviour as bromide. Their diffusion coefficients are a factor of 5-7 times lower, leading to less matrix diffusion. However, bentazon and MCPA are slightly sorbing and determined sorption coefficients (K_d) of 0.05 L/kg (bentazon) and 0.2 L/kg (MCPA) were used (see chapter 4.2 and 5.2). Sorption has a similar effect on the breakthrough curve as matrix diffusion, and that is why the breakthrough curves of these two pesticides are similar to the one of bromide with less matrix diffusion under the given flow conditions. For tebuconazole, a sorption coefficient of 11 L/kg was used, which reflects a strong sorption of the pesticide to clayey till. This is in the range of sorption coefficients that was determined in Albers et al. (2019). However, with an equilibrium sorption model, the breakthrough curve of tebuconazole could not be accurately reproduced (figure 47 and 46), particularly in the flushing period. It was observed that tebuconazole exhibits a nonlinear sorption behaviour. It sorbs relatively quickly to the clayey-till matrix, but then it is quite strongly bound, and desorption happens at a much lower rate. To account for this behaviour, a nonlinear sorption model was employed, which allows to specify different kinetic parameters for sorption and desorption. The inclusion of a nonlinear sorption model lead to a better fit of the simulated breakthrough curve with the measured one. This also means that a linear sorption model for tebuconazole would overestimate leaching concentrations after the application of the pesticide (when desorption would happen), and the strong sorption with slow desorption would lead to a much longer residence time of the pesticide.

The solute transport through Havdrup-Salløv LUC-bottom was influenced by both fracture transport and advective and diffusive transport through the matrix. In that column, a sandy clayey till with a relatively high hydraulic conductivity and horizontal sand layers were found, which contributed to the overall solute transport. The breakthrough curve of bromide could only be reproduced when the sand layers and the higher-conductive clayey till were included. The relatively high outflow concentrations that were measured after the stop flow could not be well reproduced. A reason might be that the stop flow caused a change in the pressure conditions in the LUC column, which led to a redistribution of the solutes within the column. Bentazon shows a similar transport behaviour as bromide. It has a lower diffusion coefficient which leads to less matrix diffusion, but bentazon slightly sorbs to the matrix, hence yielding a similar breakthrough behaviour in this experiment. The MCPA concentrations are lower than bromide and bentazon concentrations in this experiment. Due to the longer residence time and more contact with the matrix by diffusion and advection, sorption to the matrix has a stronger influence on the transport. MCPA seems to also show some nonlinear desorption behaviour in the flushing period. Tebuconazole sorbed very strongly to the clayey till and it was hardly observed in the effluent water in the period of the experiment.

The model setups that were used to simulate the two LUC experiments are not unique. Due to the complexity of the clayey-till systems, different combinations of parameters and geometric setups could lead to similar results.

5.4.3 Investigation of the influence of different parameters

Besides the interpretation of field and laboratory experiments, a model-based analysis was performed to investigate the influence of a variety of parameters on the pesticide transport behaviour through fractured clayey tills. Models with different configurations and parameter combinations were setup and run. These included a variation of fracture features, matrix features, and others features such as embedded sand lenses and macropores. Specifically, the following parameters were considered:

- Fracture features
    a. hydraulic fracture aperture
    b. fracture spacing
    c. fracture angle and continuity
    d. fracture narrowing (bottleneck behaviour)
- Matrix features
    a. hydraulic conductivity
    b. sorption and diffusion coefficients
- Other features
    a. sand lenses + angle
    b. fractures + macropores
    c. constant flow and seasonal flow pattern

Fracture features

Simulations over large parameter ranges were run to quantify the contributions of fractures to the total water flux depending on fracture hydraulic apertures, fracture spacings and matrix hydraulic conductivities. These flux contributions give an indication of the risk of fast advective solute transport through clayey till with the water flow through fractures.

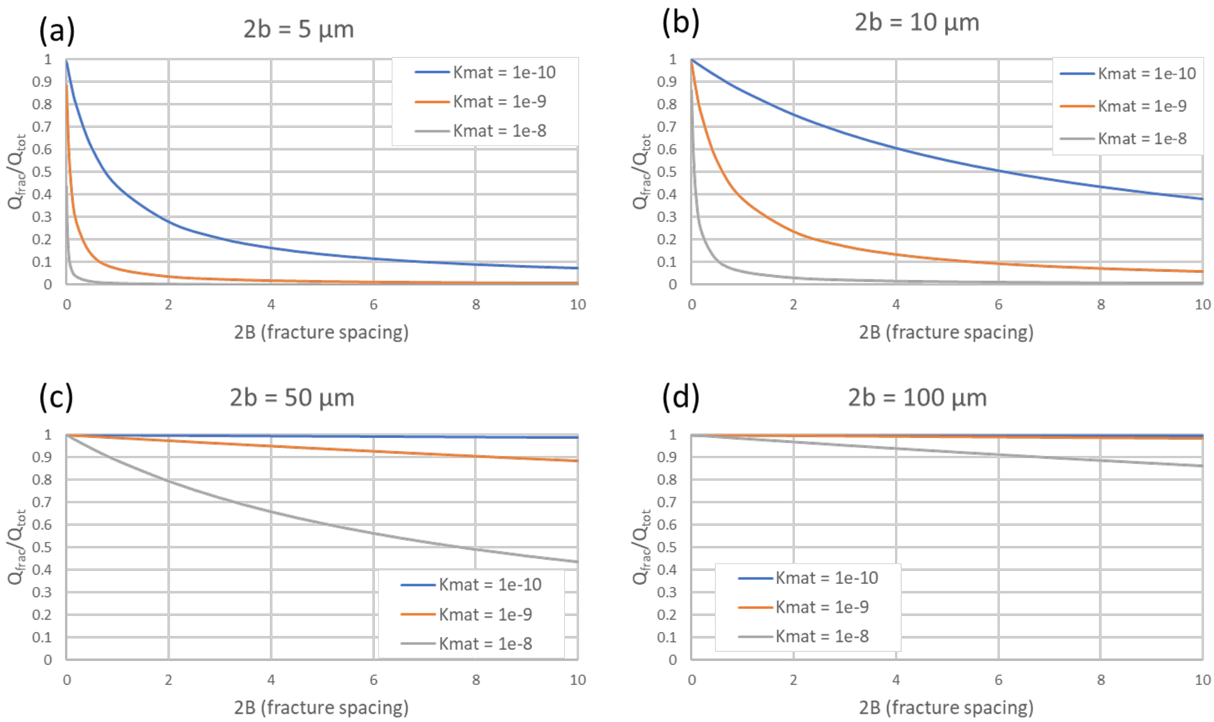

FIGURE 48. Flux contribution of fractures to the total water flux through a vertical profile with different fracture apertures (2b), spacings (2B in m) and matrix conductivities (Kmat in m/s). The share of the fracture flux (Q_{frac}) of the total flux (Q_{tot}) is shown for hydraulic apertures of (a) 5 µm, (b) 10 µm, (c) 50 µm and (d) 100 µm.

Figure 48 shows the flux contribution of the fractures to the total water flux through a vertical clayey till profile for different fracture spacings and matrix hydraulic conductivities. $Q_{frac}/Q_{tot}=0$ means that all water flux is attributed to the matrix while for $Q_{frac}/Q_{tot}=1$, all water flux is happening through the fractures. The ratio of the flux contributions is strongly dependent on the fracture aperture and spacing. When fracture hydraulic apertures are small (less than about 20 µm for the simulated setup), the flow contribution through the fractures is also small. Then, the fractures only contribute substantially to the total water flux when they are closely spaced and when the matrix hydraulic conductivity is low. For a large spacings and small apertures, most flow and thus advective solute transport is happening through the clayey-till matrix. This is different for larger-aperture fractures (e.g., 50 µm, figure 48c): the fractures can dominate the water fluxes over spacings of tens of meters, particularly for low matrix hydraulic conductivities. Such large-aperture fractures with a low hydraulic matrix conductivity entail a high risk of advective transport of pesticides through the macropores/fractures and a low residence time of the pesticides with only little sorption and diffusion into the matrix. This also applies to the clayey till above the plough layer, particularly when macropores like worm holes or root channels are present. The flux in such rather cylindrical features scales even with the fourth power of the hydraulic pore radius, allowing for a fast transport of pesticides. However, the influence of unsaturated conditions must be accounted for at such shallow depths.

Simulations were also run to determine bulk hydraulic conductivities (hydraulic conductivity for a bulk sample comprising both fractures and matrix) for different combinations and ranges of fracture apertures, matrix hydraulic conductivities and fracture spacings. This is shown in figure 49. For low fracture apertures (e.g., 5 and 10 µm, figure 49a-b), the bulk hydraulic conductivity is mostly determined by the matrix conductivity and hardly changes with the fracture spacing. The influence of the fractures is only visible for a small spacing between the fractures in combination with a low matrix conductivity, e.g., for fractures with hydraulic apertures of 10 µm, a matrix hydraulic conductivity of 10^{-10} m/s, and a fracture spacing below 5 m (Figure 49b).

However, for larger apertures, the fractures contribute most to the bulk hydraulic conductivity and strongly influence the determined bulk hydraulic conductivity values. The curves for the three matrix hydraulic conductivities shown for a hydraulic fracture aperture of 100 µm, for example, are almost on top of each other, i.e., the contribution of the matrix conductivity to the bulk hydraulic conductivity is insignificant.

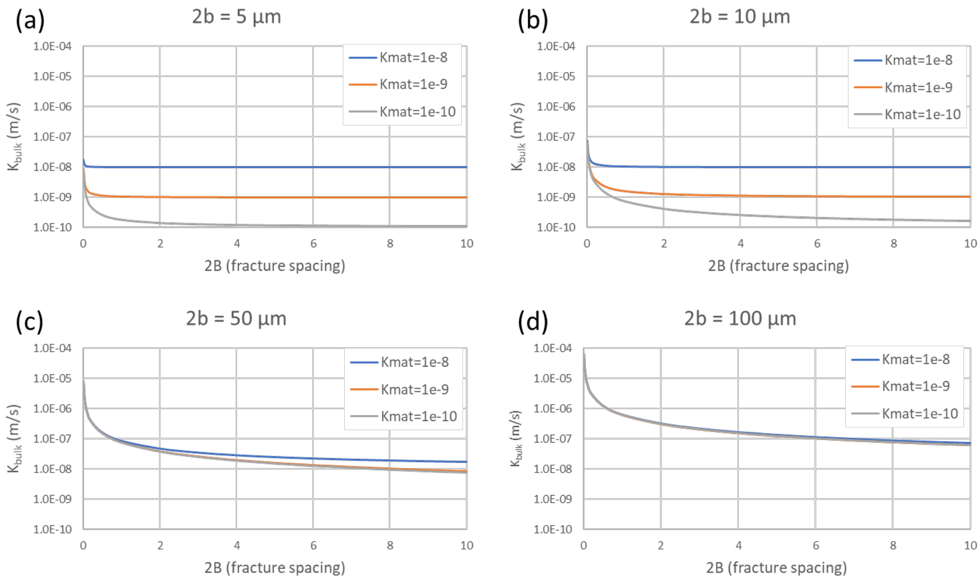

FiGURE 49. Computed bulk conductivity (fractures + matrix, K_{bulk}) for different fracture apertures (2b), spacings (2B in m) and matrix conductivities (Kmat in m/s).

As the analysis of the water flux contributions of the fractures for different apertures already demonstrated, the hydraulic fracture aperture (fracture width) has a very strong influence on the resulting total water fluxes for a given hydraulic gradient. The strong influence is based on the approximately cubic relation between hydraulic fracture aperture and water flux through the fracture, i.e., for a fracture with double the aperture, the flux is about eight times stronger. This also applies to the advective pesticide transport through clayey tills. However, matrix diffusion and sorption can also strongly influence pesticide transport. This is further investigated in the following parts.

The influence of the hydraulic fracture aperture on transport was analysed by running a series of simulations and determining the arrival time of a solute flux (defined as time when 10 % of the injected concentration is reached at the outlet) through the bottom plane of a 5 m deep clayey-till cross section with vertical fractures with uniform properties. In the underlying simulations, the water flux was kept constant and the hydraulic fracture aperture and matrix hydraulic conductivity were varied. As for the water flux contributions, this was done for three different matrix hydraulic conductivities (10^{-8}, 10^{-9} and 10^{-10} m/s). The results are shown in Figure 50.

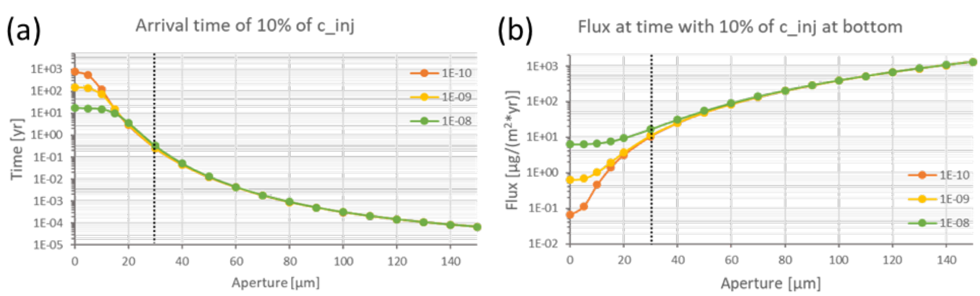

FIGURE 50. (a) Arrival times and fluxes when 10% of the injected concentration arrive at the bottom of a 5 m vertical cross section for a fixed flux and for three different matrix hydraulic

conductivities. Note that the time axis is logarithmic. The dashed vertical line at around 30 µm shows the range of apertures, where the matrix has an influence (left of the line) and where the fracture transport is governing. (b) Contaminant fluxes when 10% of the injected concentration arrive at the bottom of the vertical profile for the three different hydraulic conductivities.

For fracture apertures of less than about 30 µm (dashed line in Figure 50), the value of the matrix hydraulic conductivity influenced the arrival time at the bottom boundary, and matrix advection was important in the chosen setups. Further, for fracture apertures below 10 µm, the influence of the fracture aperture on the arrival time or the resulting fluxes is relatively small, and the matrix is mostly determining the solute fluxes. However, for apertures >30 µm, the contrast between fracture and matrix hydraulic conductivity is so strong, that solute transport is governed by fracture advection and the exact value of the matrix is less important. This is consistent with the observations from the two flow-through transport tests in Holbæk LUC-top and Havdrup-Salløv LUC-bottom, where the matrix hydraulic conductivity of Holbæk LUC-top (>30 µm) did not influence the transport behaviour much, whereas in Havdrup-Salløv LUC-bottom (<30 µm), the choice of the matrix hydraulic conductivity had an impact on the resulting breakthrough curve.

The effluent solute fluxes (Figure 50b) show a corresponding behaviour. Again, from fracture apertures of about 30 µm on, the influence of the matrix on the resulting solute fluxes is negligible. Naturally, higher fracture apertures would come along with a stronger water flux for the same hydraulic gradient, while in the presented simulations, the water fluxes were kept constant. After analysing the influence of apertures and hydraulic conductivities on the solute fluxes and breakthrough times of conservative pesticides, the influence of different fracture properties was analysed with the help of 2D DFM models, where fracture advection was dominating (hydraulic fracture apertures of 50 µm and matrix hydraulic conductivity of 10-8 m/s). This is further described in Lanters (2019) and several figures in the following are from the thesis. The influence of the fracture angle was analysed by varying it between 90 degrees to the ground surface (vertical fractures) and 40 degrees (diagonal). The effect of the fracture angle on vertical transport is mainly to prolong the leaching pathway (Figure 51). For the same flow conditions (e.g., the same vertical hydraulic gradient), angled fractures lead to a later arrival time and slightly lower breakthrough concentrations at the bottom boundary of a soil profile. This is due to the longer flow path through the fractures, which also allows for more matrix diffusion. For fractures that are oriented almost vertically (>75 degrees), the effect of the fracture angle on the computed breakthrough curve was very small.

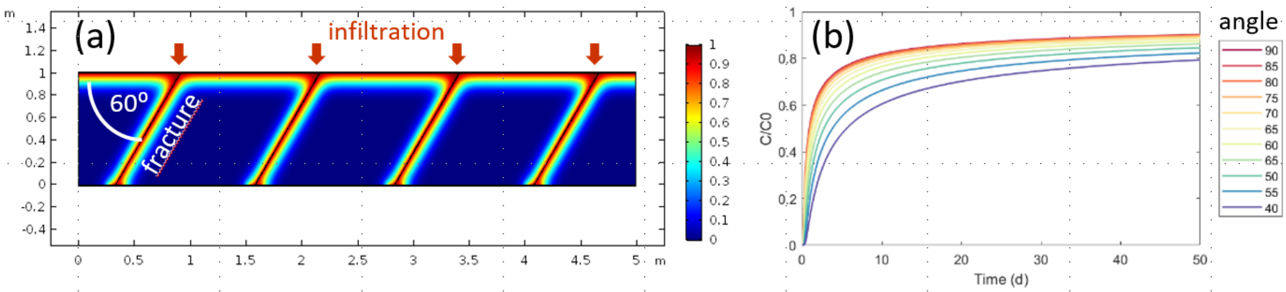

FIGURE 51. Influence of the angle of the fractures (a) Vertical cross section showing the concentration distribution into a system with fractures angled by 60 degrees to the top surface and infiltration from the top for 50 days. (b) Breakthrough curves for differently angled fractures.

The investigation of dead-end fractures (figure 52a-b) showed that for the given setup, solutes are primarily transported through the continuous fractures. The arrival time of the solute (Figure 52c) was similar for continuous fractures and the set of continuous and discontinuous fractures. However, the concentrations at the bottom boundary were lower if discontinuous fractures were included because parts of the solute are transported through and stored in the dead-end fractures, where the solute also diffuses further into the matrix. The discontinuous fractures slowly fill with solute (figure 52a), and the unfractured part must be overcome by matrix diffusion or matrix advection, which is usually slow in clayey tills.

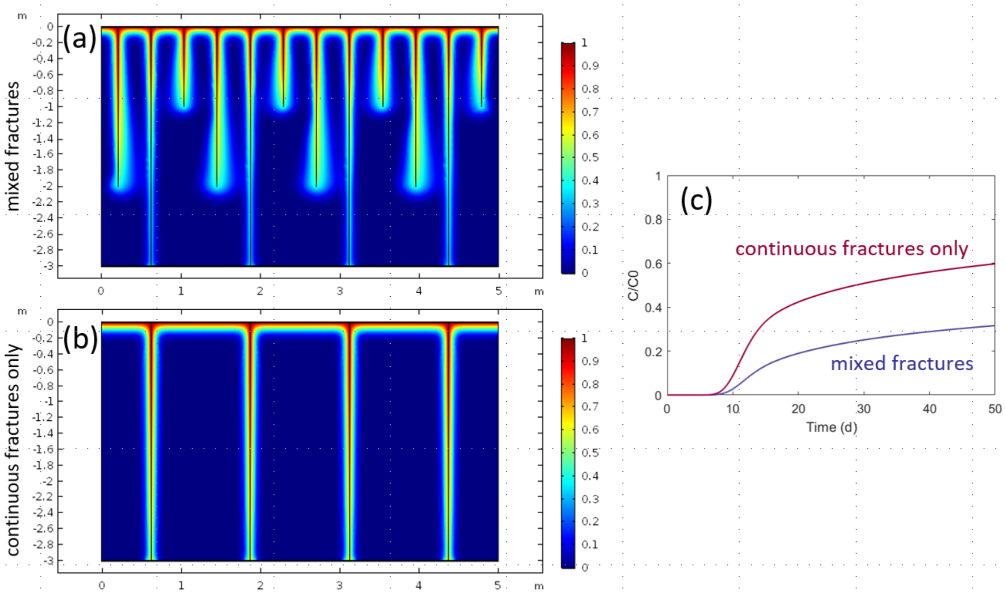

FIGURE 52. Solute infiltration into a vertical soil profile with a set of continuous and discontinuous fractures. (a) Concentration distribution for a setup with both continuous and discontinuous fractures. (b) Concentration distribution for continuous fractures only. (c) Breakthrough concentrations at the bottom boundary for the two setups.

We considered fractures with an abrupt change in the hydraulic fracture aperture in a 4 m deep soil profile to investigate if the narrow section poses a bottleneck to solute transport. The aperture was changed after 1, 2 and 3 m from the large aperture (110.6 µm) to the lower aperture (18.5 µm). The different cases were named according to the length ratio of the large aperture to the small aperture. For example, 1:3 means 1 m large fracture aperture (110.6 µm according to LUC Holbæk-top) on top followed by 3 m small aperture (18.5 µm according to LUC Havdrup-bottom) below (see figure 53). We also considered a linear variation of the hydraulic fracture aperture from large to small (case lin).

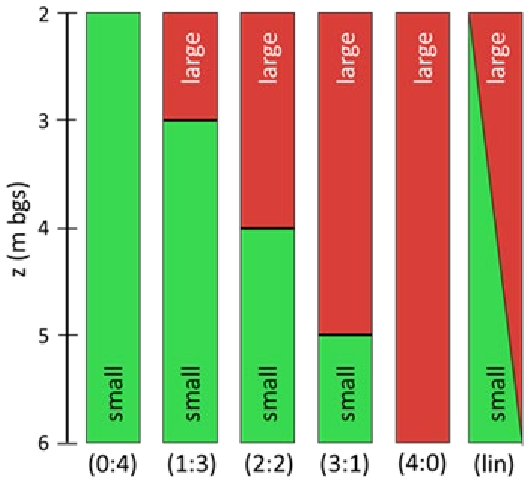

FIGURE 53. Schematic overview of the different setups and their names, showing the proportion of the domain where a small aperture (18.5 µm) or a large aperture (110.6 µm) was used. The case 'lin' employs a linear variation of the aperture from large (top) to small (bottom).

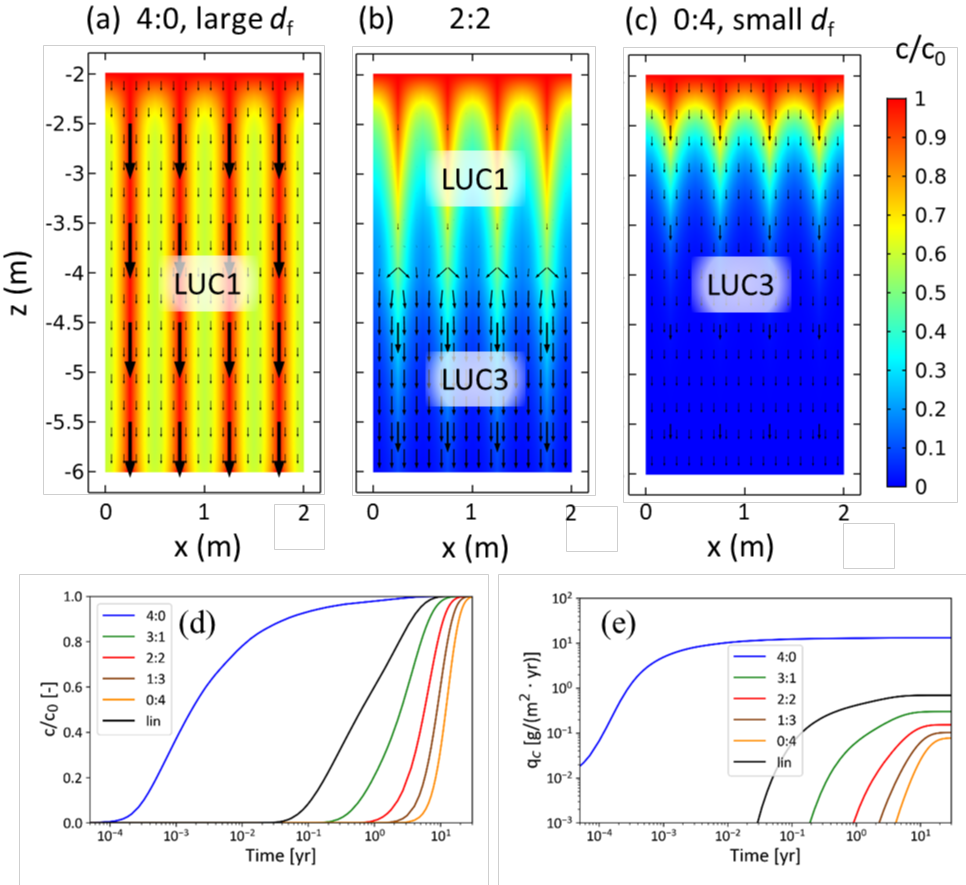

FIGURE 54. Analysis of influence of vertical fracture aperture variations on transport. LUC1 has fracture apertures according to LUC Holbæk-top and LUC3 according to LUC Havdrup-bottom. (a)-(c) flow field and relative concentration distributions after two years of injection for three different aperture distributions: (a) constant large aperture (110 µm, case 4:0), (b) abrupt aperture decrease after 2 m (case 2:2), and (c) constant small aperture (18.5 µm, case 0:4). The black arrows visualize the flow velocities and directions in fractures and matrix (d) Breakthrough concentrations in the effluent (bottom) of the vertical profile. (e) Fluxes at 10% of the injected concentration at the bottom. The black line 'lin' shows the simulated results for a linear variation of the fracture aperture from top (large aperture) to the bottom (small aperture). Modified after Mosthaf et al. (2020).

Figure 54a-c shows the concentration distribution on vertical profiles at the same time, after 2 years of injection from the top boundary. The solute has infiltrated furthest into the domain in the case of continuous large hydraulic aperture fractures. In the case with an abrupt change in the aperture from large to small (Figure 54 b), the solute has already reached the bottom boundary after 2 years. However, the concentration distribution is closer to the case with a continuous small fracture aperture. An interesting aspect is shown by the velocity vectors (black arrows). When the aperture becomes smaller, a part of the flow is redirected to the matrix. Furthermore, the flow velocity is slower in the large aperture part and becomes considerably higher in the lower part of the domain. The analysis of the vertical variation of the fracture aperture (18.5 µm – 110.6 µm) showed a very strong influence of the aperture along the fracture on pesticide leaching. For a fracture with a constant aperture of approximately 110 µm (case 4:0) the breakthrough at the bottom boundary through the considered profile happened in a few hours, whereas for a hydraulic aperture of about 18.5 µm (case 0:4), the breakthrough happened after several years. As can be seen in Figure 54d, already the breakthrough curve with 1 m of smaller aperture leads to a strong delay of the breakthrough (months instead of hours, the x-axis is logarithmic). This shows that lower apertures in deeper parts of the clayey till have an important influence on the pesticide leaching. Using a large fracture aperture observed at a shallower depth to model an entire profile could lead to poor predictions of the pesticide leaching. Figure 54e shows the respective fluxes through the bottom boundary. Again, the fluxes for a fracture with a constant thickness is significantly stronger than for the ones with a lower aperture section.

Matrix features

The influence of the matrix hydraulic conductivity in a fractured clayey-till setting is addressed in the previous section, e.g. figure 48, Figure 49, and Figure 50. When fracture apertures are high, the matrix hydraulic conductivity of the clayey till does not influence the flow and transport much. However, with low fracture apertures and a large fracture spacing, a higher matrix hydraulic conductivity will lead to an earlier breakthrough time and stronger pesticide fluxes.

A higher diffusion coefficient of the pesticide leads to a later breakthrough in a fractured clayey till and to lower breakthrough concentrations (Figure 55a). The solute is retarded due to diffusion of the pesticide from the fractures into the matrix. A diffusion coefficient of 2E-9 m^2/s corresponds to bromide, while bentazon , MPCA and tebuconazole have aqueous diffusion coefficients of 2E-10 to 4E-10 m^2/s. Solute in the matrix can also later on diffuse back, when the concentration in the fracture decreases (so-called back diffusion), which can considerably prolong the occurrence of a pesticide after it has been applied. Higher sorption coefficients lead, like the diffusion coefficient, to a later breakthrough and lower breakthrough concentrations since part of the solute is sorbed to the matrix. In Figure 55b, a linear sorption model was employed and the linear sorption coefficient (K_d) was varied. The effect of diffusion and sorption on the leaching behaviour is also well visible in the previously described LUC experiments with bromide and pesticides. Some pesticides show a non-linear sorption behaviour.

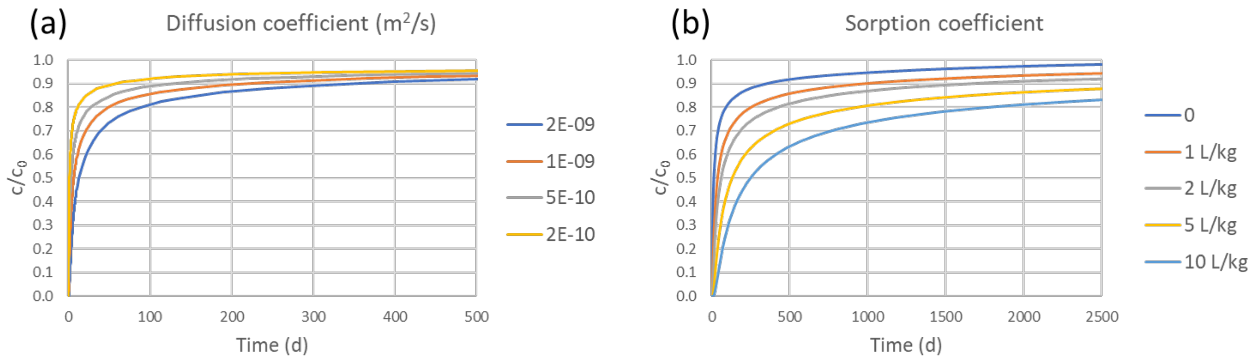

FIGURE 55. Influence of (a) the diffusion coefficient and of (b) the sorption coefficient on the leaching of a solute through a vertical cross section.

Other features

The influence of the fracture spacing on computed breakthrough curves was analysed based on a series of simulations with a constant vertical hydraulic gradient. Therefore, a 5 m vertical cross section with a set of 1 m long fractures with a hydraulic aperture of 10 μm was simulated. The spacing between neighbouring fractures was varied from 0.25 to 10 m. As can be seen in Figure a, larger fracture spacing leads to a later breakthrough time for the given contrast between fracture and matrix hydraulic conductivity.

Furthermore, the same setup was slightly modified, by adding a 2 cm section with a higher aperture (50 μm) on a 1 m long fracture, mimicking a vertical macropore within a fracture plane. This had a very strong influence on the breakthrough times, reducing them from decades to a few days (Figure b). This shows the relevance of macropores in the context of risk evaluation for clayey tills. The computed mass fluxes through the simulated cross sections are also strongly influenced by fractures and macropores – there is a strong difference between the fluxes in the small-aperture fractures (Figure c) and fractures with the macropores (Figure d). Macropores or large-aperture fractures can act as highway for pesticides, thus reducing the travel times drastically and increasing the pesticide fluxes to an aquifer considerably. Clayey tills are often very heterogeneous and such small-scale features are difficult to determine.

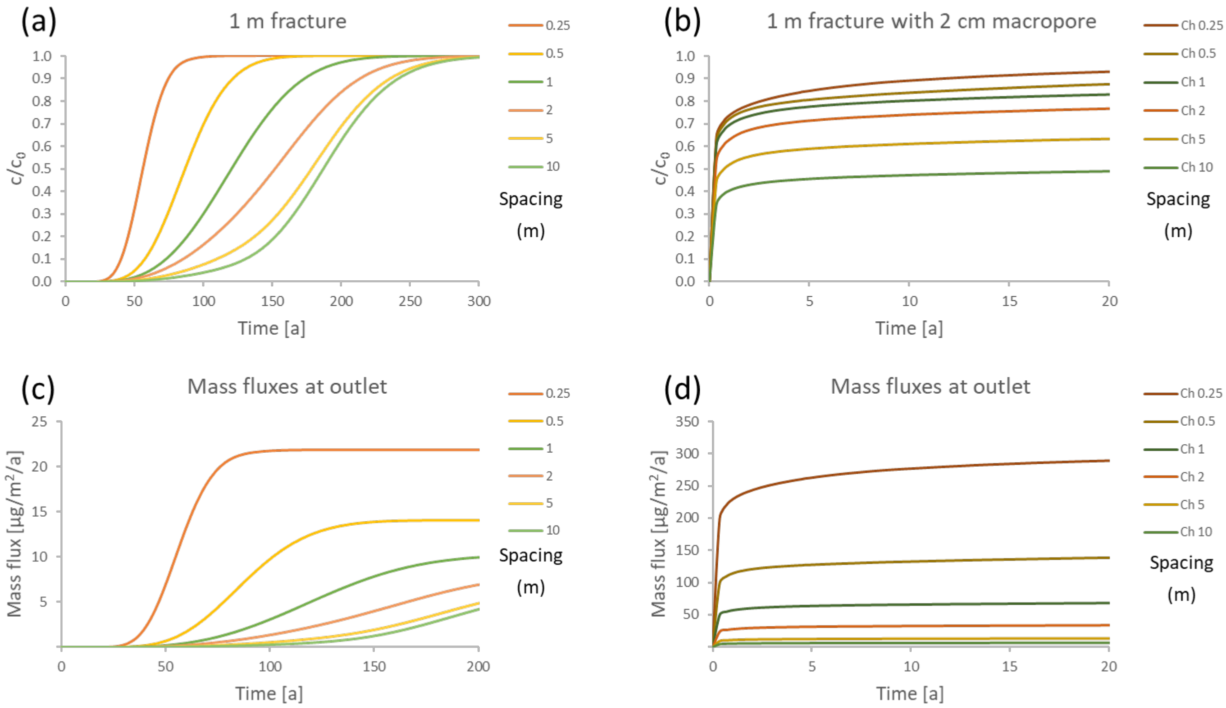

FIGURE 56. Influence of fracture spacing and macropores on pesticide leaching. (a) and (b) show computed breakthrough concentrations at the bottom of a 5 m x 1 m x 1 m vertical soil profile for a fracture with a constant aperture (a) and a fracture with a constant aperture and a vertical macropore of 2 cm length (b). (c) and (d) show the respective solute fluxes at the bottom boundary. Note that the values on the x- and y-axes differ for the different figures.

Sand lenses can connect isolated macropores and fractures and provide additional preferential flow paths. This was observed in the Havdrup-Salløv LUC-bottom experiment. To investigate the influence, we created a model setup with vertical discontinuous macropores. One setup was run with horizontal sand inclusions that link the macropores. The discontinuous fractures provide a preferential flow path, however, the solute did not penetrate through the simulated clayey-till cross section (Figure 57a). When the sand lenses are included, they connect isolated macropores and lead to a much faster transport. First, the solute is transported in the fractures until it hits a sand layer. There, it spreads along the sand lens to the next vertical macropore (Figure 57b). The resulting breakthrough curves show the different transport behaviours. With connected sand lenses, the solute arrives after about 15 days at the bottom of the simulated cross section, whereas the solute has not arrived after 150 days when the macropores are not connected by the sand lenses. This visualizes the importance of connected hydrogeological features and indicates that isolated features and dead-end pores have a smaller influence on the solute transport. However, when fractures are connected with sand layers, they can have a major impact on the risk of pesticide leaching.

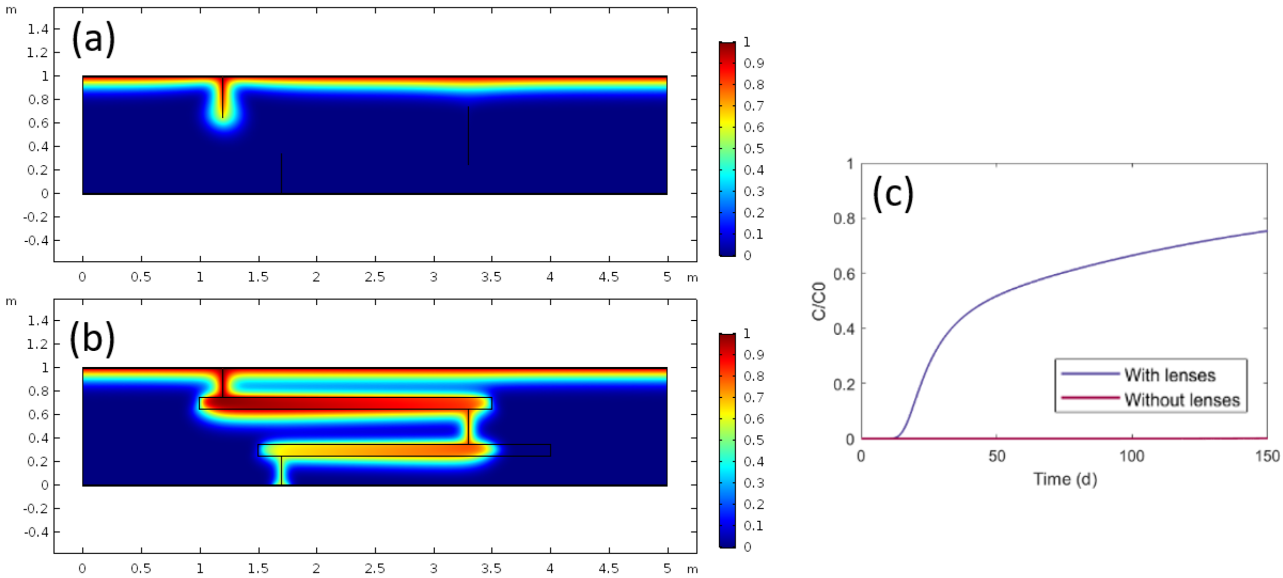

FIGURE 57. (a) Solute infiltration into a dead-end fracture. (b) Solute infiltration into a fracture connected through sand lenses to deeper fractures. (c) Simulated breakthrough curves for the two cases.

The influence of the orientation of embedded sand lenses was investigated by rotating the sand layers by 0 to 20 degrees from horizontal and applying a vertical hydraulic gradient. Macropores, that cross through horizontal sand layers (0 degrees) lead to little spreading in the sand lenses (Figure 58a). The solute follows the path of the least resistance and spreads only little within the sand lenses. This is different when the sand lenses are not perpendicular to the hydraulic gradient, leading to a gradient component along the sand lenses (figure 58b). Then, the solute spreads more within the sand lenses and slows down the transport. However, in the considered cases, the influence of the sand lens orientation on the breakthrough behaviour was small.

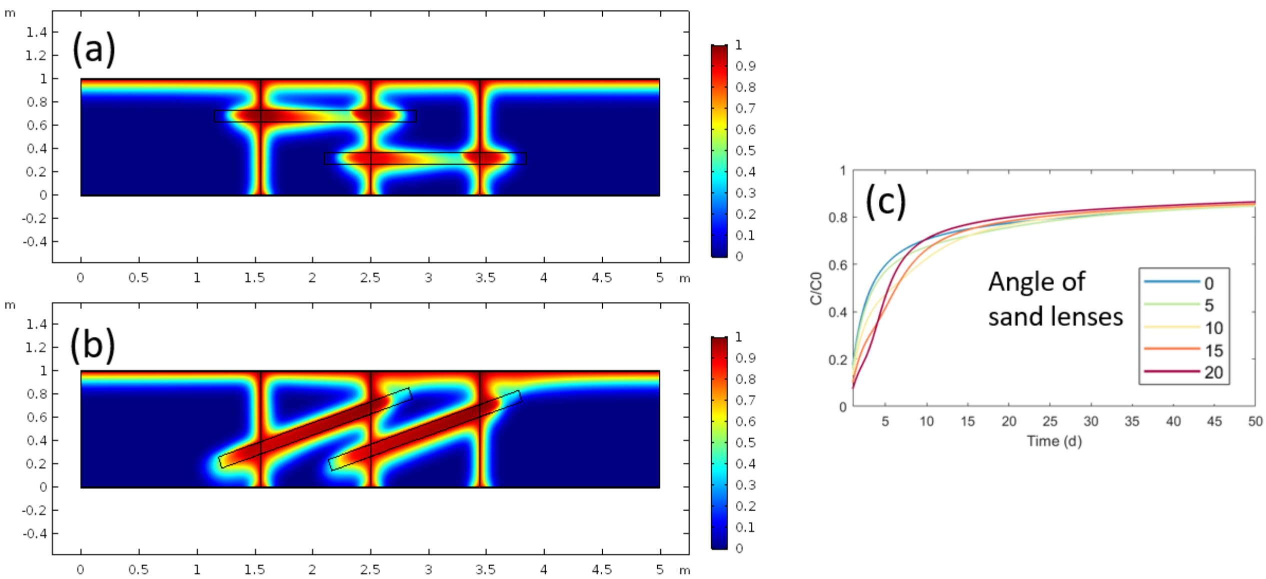

FIGURE 58. Solute infiltration from the top through three continuous fractures that cross (a) horizontal sand lenses and (b) inclined sand lenses. (c) Breakthrough curves for solute that infiltrates in such system with sand lenses, which are angled by 0 to 20 degrees to the horizontal surface.

It was tested, how seasonal flow variations (200 mm/year in the winter half of the year, 40 mm/year in the summer half) influences the simulated breakthrough behaviour in comparison to a constant influx (120 mm/year, same cumulative annual water flux). As can be seen in Figure , there are short-term effects, particularly during the high flow rate the concentrations at the bottom boundary increase stronger. Over a longer time period, the overall leaching behaviour is showing the same trend. The concentrations at the outlet with the seasonal flow are oscillating around the outflow concentrations obtained with constant flow. For long-term analyses (several years to decades), using the average infiltration rate instead of a variable infiltration rate leads to comparable results as using a variable flow rate with the same cumulative annual flow.

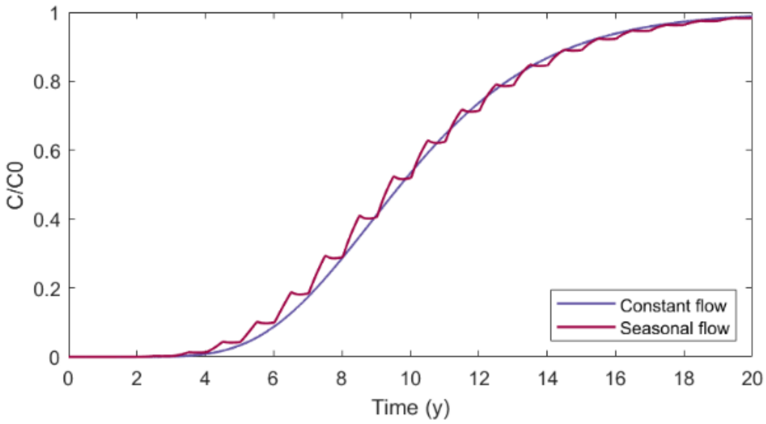

FIGURE 59. Seasonal variation of the infiltration rate over a period of 20 years.

6. DISCUSSION

6.1 Parameters controlling pesticide leaching in clayey tills

The laboratory and field data and the modelling from the CLAYFRAC project showed the high complexity of pesticide leaching through fractured clayey till geologies. LUC columns were excavated at two different sites (Holbæk and Havdrup-Salløv) with different PM types showing very different hydraulic properties. Even the LUCs sampled at the same PM type showed very different transport behaviours, despite being from apparently similar geologies. This leads to the conclusion that the vulnerability of a location depends strongly on the presence and hydraulic properties of macropores and fractures in the clayey till. Due to the cubic relation between flow and hydraulic fracture aperture, small variations of the aperture have a strong influence on the resulting fluxes, leading to a very different risk for pesticide leaching. Moreover, few larger-aperture fractures can dominate flow and transport over distances of several meters.

We conclude that the local variations seen within one field with one PM type are so strong, that a single vulnerability index cannot be identified and generalized to a specific PM type that involves clayey till with fractures and macropores. The possible pesticide fluxes can be in a wide range and are too strongly influenced by local small-scale features and heterogeneities.

Instead, an in-depth characterization of two sites, namely Havdrup-Salløv and Holbæk, with similar glacial till geologies was made involving field and laboratory experiments (e.g., hydrogeological characterization, sorption tests, LUC experiments) as well as detailed modelling. Furthermore, the lithology, fracture orientation and spacing were characterised at two more sites namely Tokkekøb and Farum. In addition, the influence of a variety of parameters on the risk of pesticide leaching was studied based on a series of simulations with generic setups and realistic ranges. Table 13 gives an overview of the considered parameters and their influence on the risk of pesticide leaching.

Macropores like wormholes, burrows, and root channels have a strong influence on water flow and transport of pesticides in upper clay tills. Especially, wormholes may be present in large numbers penetrating the clay till to greater depth. The highest number was counted at Tokkekøb with > 1000 per m^2 at 25 cmbs, but high numbers were also counted for the other sites though always decreasing with depth. At Tokkekøb wormholes were observed down to 2 mbs often following the fractures. Due to the cylindrical feature of macropores their cross-sectional area scales with the fourth power of the hydraulic pore radius. As macropore radiuses may be in the mm range compared to fractures being in the µm range they are allowing for a fast transport of pesticides depending on their inherent properties. This was further demonstrated by model simulations of pesticide breakthrough via a vertical fracture plan (10 µm) with a macropore of 50 µm. The inclusion of the macropore had a very strong influence on the breakthrough times, reducing them from decades to a few days. Though with depth, as the macropores decrease in number, their role as preferential flow paths becomes less important and fracture and matrix flow becomes more dominant.

The hydraulic fracture aperture is a strong determent of pesticide leaching as, the water flux through a fracture scales with the third power of the hydraulic fracture aperture according to the cubic law. This means that doubling the fracture aperture leads to eight times stronger flux. The largest aperture of 110.6 µm was calculated for the Holbæk LUC- top. Here the breakthrough of bromide and of the three pesticides happened after a few hours, while it took much longer (>60 hours) in the Havdrup-Salløv LUC-bottom with a calculated aperture of 18.5 µm. It must be noted though that the aperture of Havdrup-Salløv LUC-bottom is uncertain due to the occurrence of rim flow. Model simulations showed that in practise all waterflow in Holbæk LUC-top happened through fractures and macropores, while in the deep Havdrup-Salløv column this was reduced to 83 %. However, towards the outflow (bottom of the excavated clayey-till column, the aperture was assumed even smaller (10 μm) due to almost no observed staining after the Brilliant Blue injection giving a simulated water flow via the fractures of 18% only, The contribution of fractures to waterflow, obviously depends on the matrix hydraulic conductivity, but in general for apertures >30 μm, the contrast between fracture and matrix hydraulic conductivity is so strong, that solute transport is governed by fracture advection and the exact value of the matrix is less important. In contrast, fractures with apertures below 10 μm have little influence on water flow, and a larger part of the transport happens by advection in the matrix. In these cases, the matrix hydraulic conductivity becomes more important as a low conductivity results in more transport through the fractures and less rapid transport through the matrix. In general fracture apertures decrease with depth and may become a bottleneck for flow, which are then forced to occur either as matrix flow or via other structures like e.g. sand lenses.

The spacing between fractures or fracture density also has a strong influence on water flow and pesticide transport. Like the fracture apertures, which are often getting smaller with depth also the fracture density decreases, i.e., the spacing between the fractures increases. Both parameters all else being equal leaves the clay more protective against pesticide leaching. It should be noted that a high fracture density is not always present in upper clay tills. Thus, fractures were not present at all in the clay till above 1.4 mbs at Tokkekøb.

Increased fracture spacing with depth may imply the presence of discontinuous or dead-end fractures which to a certain extent may impact pesticide leaching. Model simulations showed that dead-end fractures hardly impacted the arrival time of a pesticide to a given depth, but the concentration was lower if dead-end fractures were included. The dead-end fractures slowly fill with solute and further transport will rely on matrix diffusion or advection, which is usually slow in clayey tills.

Discontinuous fractures are however not necessarily dead-end fractures but connect to sand lenses or layers as was observed at e.g. Farum (See figure 23). The model-based simulation of fractures connected to sand layers showed that such connections have a major impact on the risk of pesticide leaching. With connected sand lenses, a solute arrived after about 15 days at the bottom of the simulated cross section, while the solute did not arrive after 150 days when macropores were not connected to the sand lenses. Sand lenses or layers were indeed present at all locations contributing significantly to the great heterogeneities of the sites. This was most significant at the Holbæk site where surprisingly, one half of the excavation was dominated by sand and not clay. At the other locations sand was more present as dispersed sand lenses or laminated layers between the clay layers often inclined with a specific orientation. The model simulations, however, showed that the degree of inclination had little effect on pesticide leaching as rapid breakthrough was obtained both with horizontal and inclined sand layers.

The effect of sorption and degradation on pesticide leaching depends on the specific pesticides. In this project MCPA and bentazon were selected representing low-sorbing pesticides. Tebuconazole was further included in the LUC experiments to show the effects of more sorbing pesticides with low degradation potentials on pesticide leaching. Degradation may have a great effect on pesticide leaching via biopores in clayey tills as it has been demonstrated by Rosenbom et al., (2014) in model simulations of MCPA degradation in a biopore with a biofilm of MCPA degrading bacteria. We observed rapid degradation of MCPA, but only in the plough layer and biopores. Below 1 m depth degradation was negligible and without practical importance for pesticide leaching to the groundwater. Sorbing pesticides will be retarded during transport, but unless degraded on their way through the clayey tills they will eventually enter the groundwater. Sorption and degradation are important parameters determining the leaching potentials of specific pesticides; however, for MCPA and bentazon the results of this project show that at depths below the plough layer in clay tills they are not likely to play a key role for groundwater vulnerability. This is consistent with other studies that have similarly shown low sorption and degradation potentials of pesticides below the plough layer (Albers et al., 2019).

TABLE 13. Overview of the influence of several parameters on the risk of pesticide leaching through fractured clayey tills.

Parameter	Potential effect	Comment
Macropores	++	Mostly in uppermost meters
Hydraulic fracture aperture	++	water flux scales with the aperture cubed
Fracture spacing	++	less fracture transport with larger spacing
Discontinuous fractures	0/+	small influence on overall transport
Matrix (clayey till) hydraulic conductivity	-	leads to more transport through the matrix and less rapid transport through the fractures (if present)
Sand lenses	0/+/++	can be preferential flow paths and connect fractures/macropores; small influence when perpendicular to continuous fractures
Matrix porosity	-	provides more storage in the matrix, more matrix diffusion, and delays pesticide migration
Sorption coefficient	0/-/--	dependent on species, can substantially delay pesticide transport and prolong time frames
Degradation	0/-	was mostly observed in plough layer (upper 1-2 m), small to no influence below

++ strongly increasing effect on vulnerability with larger parameter value

+ increasing effect with larger parameter value

0 no effect with smaller / larger parameter value

- decreasing effect with larger parameter value

-- strongly decreasing effect on vulnerability with larger parameter value

6.2 Hydrological parameters determined by LUC

We conducted flow experiments with 6 LUCs and investigated pesticide transport with 2 LUCs. One LUC represented shallow grey fractures (Fe-oxide reduced, type A in figure 36) and 5 LUCs represented red fractures (Fe-oxide infilled, type C and D in figure 36) collected to 5.9 m depth.

The grey fractures (type A) had large hydraulic apertures caused by dense root channels located inside the fractures. The deep root channels in the sub-soil were extensively weathered and precipitated with Fe/Mn-oxides indicating an old origin. This was confirmed by radiocarbon and ancient DNA (aDNA) analyses of supposed root channels in the Havdrup-Salløv LUC-bottom and other investigations at the Havdrup-Salløv site, which also suggested an origin from pre-historic forests (Jørgensen et al, 2021 in review). Consequently, similar relic root systems must be expected widely in the clayey tills. These root channels may facilitate very rapid preferential flow and high pesticide fluxes. Preferential flow was largely absent in the red fractures due to Fe-oxide infillings of the fractures (type D) leading to tracer migration rates, which were only 2-4 times higher than in the unfractured matrix. In one of the type D LUC, solitary root channels (type B) were present. These however, terminated halfway through the column and therefore did only marginally contribute as preferential flow paths. In the deep LUC from the Havdrup-Salløv site, partially Fe-oxide infilled root channels with low hydraulic activity were encountered in the red fractures (type C).

The Holbæk and Havdrup-Salløv results were compared with nine previous studies of different tills types including a total of 34 LUC samples. This revealed that in general potential for very high water and pesticide fluxes is related with root channels in grey and to a lower extent red fracture. Especially the deep fracture root channels exhibited great variation with respect to flow and pesticide transport, which is well supported by field studies (e.g. Ruland et al. 1991, Jørgensen et al. 2002, 2003, 2017, 2020, and Rosenbom et al. 2008a 2008b).

In contrast, the red fractures that did not contain root channels had consistently a narrow range of very small hydraulic apertures despite they represented seven different sites and four different types of clayey till. This suggests that fractures without root channels in general have very minor influence as preferential flow paths below the upper 1-2 m depth in the clayey tills. This is emphasized by the observed tendency of the red fractures without root channels to collapse under simulated depositional overburden within the LUC system. Hence, the potential of very high water and pesticide fluxes in the LUC experiments were strictly confined to root channels located in the fractures or present solitarily in the matrix, while transport rates in the fractures were 2-3 orders of magnitude less in absence of root channels. This suggests that below the depth of open root channels, fractures alone are not determinants of preferential flow and pesticide mass transport into groundwater. Instead we suggest the association of fractures with root channels and/or their interconnection with embedded heterogeneities (e.g., sand layers and lenses) in the tills to be the key determinants of rapid pesticide transport into groundwater. Tectonied sands and micro-sand layers were previously shown to have similar potential for flow and pesticide transport as large aperture fractures (Jørgensen et al. 2004b).

6.2.1 Representing field scale fracturing and flow with the LUC method

Figure 60 compares the fracture spacings (2B) mapped at different field sites with spacings from this and previous LUC studies. The figure shows that in the upper few meters, the fracture spacings obtained in the LUC represent the overall fracture spacings observed in the field (fracture spacing, 2B = 0.03-0.5 m) with a few exceptions. Deeper, the LUCs seems more to represents minimum fracture spacings of those obtained by visual inspections of excavations at field sites. At many field sites the spacing between the fractures at greater depths were several meters or fractures were absent and hence much higher spacings were obtained than in the LUCs. Studies where fractures have been measured in adjacent excavations at the same site have shown that the spacing of deep fractures may vary significantly within the range of tens to hundreds of meters (Jørgensen et al 2004b).

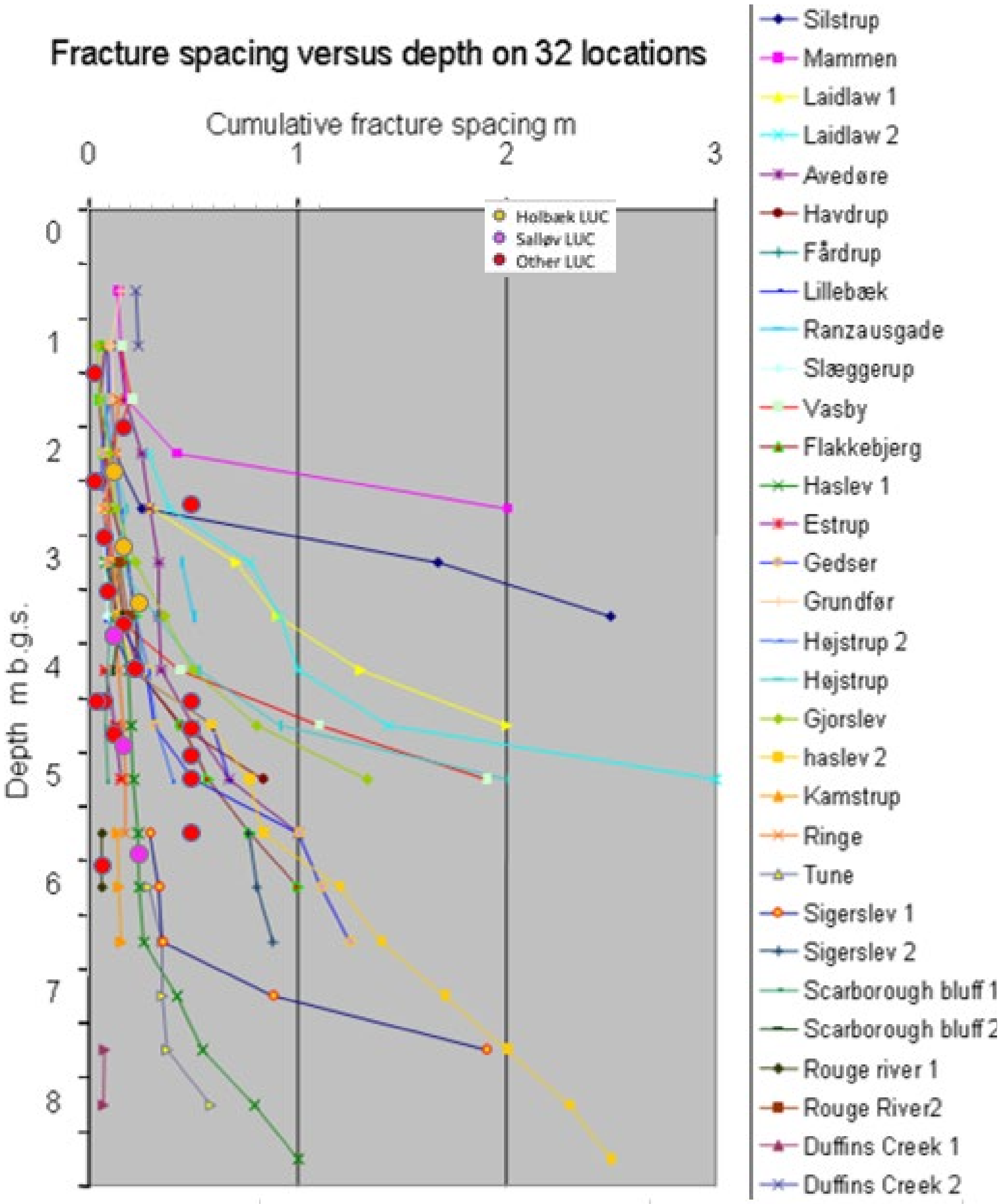

FIGURE 60. Fracture spacings in LUC samples compared with fracture spacings measured in field excavations (modified from Gravesen et al., 2014). The yellow and purple circles show spacings measured in LUCS from the Holbæk and Havdrup-Salløv sites respectively. The red circles show spacings from previous LUC experiments. Lines show spacings measured at excavations.

LUCs allow the quantification of clayey tills properties, water flow, and solute and pesticide transport. However, they are limited in connectivity which at larger scale may control flow and transport to underlying groundwater. This could be, for instance the case, of permeable features such as fractures and biopores identified in a LUC that terminate in a low permeability clay matrix. Therefore, a combined investigation approach including LUCs and field experiments is recommended for in-depth understanding of pesticide leaching in clayey tills.

6.2.2 Comparison with LUC from other study sites

Several LUC experiments have been performed previously in Denmark and Canada and in the following the results from these previous LUCs are discussed in relation to the results obtained in CLAYFRAC (figure 61). Figure 62 show the Ksat and fracture aperture 2b values for the current study compiled with previous LUC flow studies. The LUCs represented different types of clayey tills including lodgement till, melt-out till, hummocky till, and glacio-lacustrine till. The compilation reveals that the LUCs obtained in the current study (figure 60) show agreement with the previous studies. Figure 62a show that overall, the LUC Ksat-values decrease 2-4 orders of magnitude with depths from 1 to 6 mbs. For the LUCs from the upper 1-3 m depth there is several orders of magnitude difference between bulk Ksat-values of the columns and the unfractured matrix, which is due to closely spaced fractures and high frequencies of biopores inside and outside the grey fractures (fracture type A and B in figure 36). At greater depth, Ksat-values of most LUCs are decreasing mainly due to fewer fractures and root channels (fracture type C in figure 36). For the LUC, which contained fractures with no root channels (fracture type D in figure 36) the hydraulic conductivity is maximal one order of magnitude higher than for the unfractured matrix in the columns. It must be noted that, at greater depth the fracture spacings in the LUCs are representing local minimum spacings under field conditions as mentioned above (figure 60). This means, all other things being equal that at greater depths less fractures are present leaving the clay more protective against pesticide leaching.

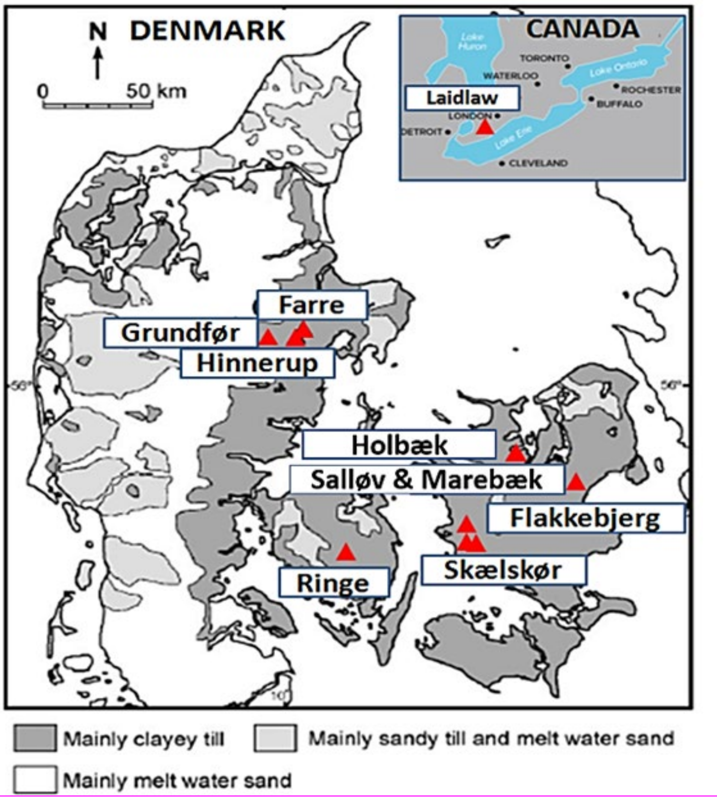

FIGURE 61. Locations of previous studies that have been performed using LUCs

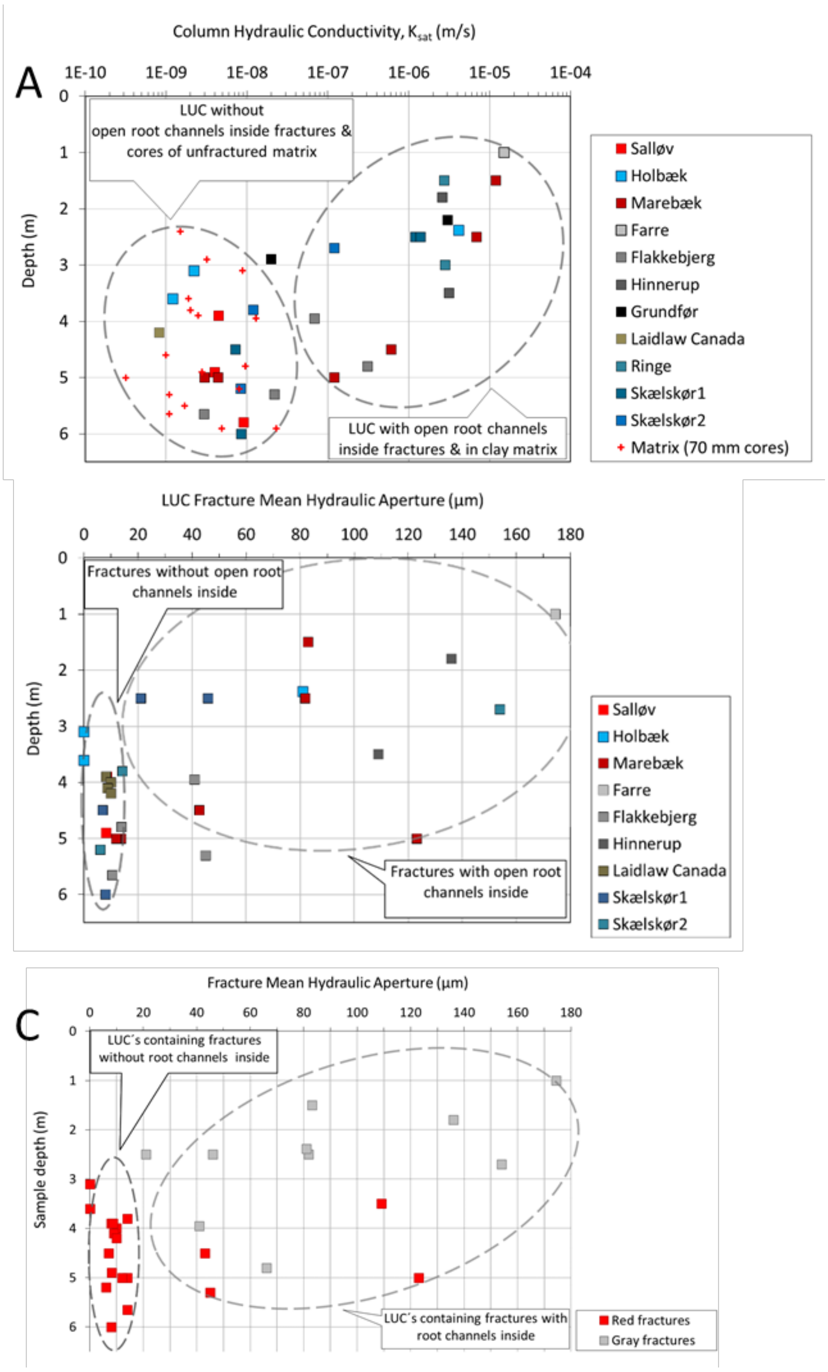

FIGURE 62. Compilation of hydraulic results from this and previous LUC studies. (A) LUC saturated hydraulic conductivities (B) LUC fracture hydraulic apertures (C) occurrence of enhanced fracture apertures by root channels in grey (Fe-oxide reduced) and red fractures (Fe-oxide filled). Notice that flow in the fractures varies with the hydraulic aperture cubed. Data from Jørgensen et al. 1993 (Marebæk), Hinsby et al. 1996 (Skælskør), Jensen et al. 1998, 1999, Jørgensen et al. 1999 (Farre), Jørgensen et al. 1998, 2002 (Marebæk), Broholm et al. 1999a,b (Ringe), O´Hara et al. 2000 (Laidlaw, Canada), Urup 2000 (Hinnerup and Grundfør), Jørgensen et al. 2004bc (Hinnrup and Grundfør), Butzbach 2007 (Flakkebjerg), Jørgensen and Spliid 2016, Jørgensen et al. 2001, 2016 (Skælskør), Mosthaf et al. (2020) this study (Salløv and Holbæk). Modified from Jørgensen et al., in preparation.

Figure 62B showing mean fracture apertures, reveals that the fractures that contains the biopore channels covers a great range of apertures with 2b = 37-173 µm, while the fractures without the root channels exhibit a narrow range of small apertures 2b =5-14 µm. Because fracture flow (volumetric flow pr. time unit) is proportional to the hydraulic aperture cubed (Snow 1968), the large aperture fracture root channels have potentials to dominate groundwater flow and contaminant transport fluxes, while the fractures without root channels is contributing with less than 1% of the flow per unit fracture width. The narrow range of small apertures represents seven different study sites and different till types, which suggests that fractures without root channels in general may have small influence on groundwater flow and pesticide transport. Hence, while the fractures without open root channels inside appear not to contribute significantly, there is a great pesticide transport potential related to the fractures with root channels. The large aperture variation for these fractures suggest that flow into shallow aquifers may be dominated by single vertically well-connected large aperture root channels, which agrees with previous field experiments (Jørgensen et al., 2002). Figure 62C summarizes the hydraulic properties of the grey and read fractures, i.e. flow related to fracture redox state. This shows that the grey fractures, which are typically occurring in the upper 3-4 m depth, are forming a dense network of preferential flow paths with a generally very high flow potential. As mentioned, this has potentially very high impact on pesticide transport in cases where those fractures are well-connected with underlying groundwater flow regimes with high hydraulic conductivity such as sand lenses or aquifers. The zone with root channels is locally extended further vertically by a smaller number of root channels, which have been observed to 5-6 m depth in the underlying red fractures. Field experiments suggest that such open channels in the red fractures are common, however, difficult to predict (Jørgensen et al. 2002, 1997, 2020). Below the rooting depth the LUC suggest very little potential of the red fractures as rapid preferential flow paths.

The role of deep fractures is further evaluated in figure 62, which show the contribution of the LUC fractures to aquitard bulk hydraulic conductivities (Ksat) below rooting depth (figure 62a). The LUC Ksat values are compared with field tested aquitard Ksat values of unweathered aquitards and unfractured matrix (Fredericia 1990). The data of Fredericia (1990) show that the field-tested aquitard Ksat values were 1-3 orders of magnitude higher than the unfractured matrix tests, which was originally interpreted as due to flow in deep fractures in the aquitards (Fredericia 1990). However, as shown, the LUC calculated aquitard Ksat values can only explain a minor part of the observed high aquitard Ksat values over the matrix. This suggests that fractures alone are not a major cause of the much higher Ksat of the aquitards than observed for the matrix. Instead, the combination of fractures and macropores, as well as their interconnection with sand lenses, sand layers, micro-sand layers, general textural heterogeneity all abundant features in aquitards (Kessler 2013), are the most likely to result in local high Ksat values. The latter probably responsible for preferential flow in deep aquitards.

6.3 Importance of sorption and degradation

Three model pesticides with different physio-chemical were selected: MCPA, bentazon, and tebuconazole. The herbicide MCPA represents pesticides that are easily degradable, rapidly mineralize to carbon dioxide, and with low sorption capacities (K_F ~ 0.94 and time for 50% disappearance (DT_{50}): 24 days; PPDB, 2019). The herbicide bentazon is also an easily degradable pesticide with low sorption capacity, (K_F 0.97 and DT_{50}: 20 days; PPDB, 2019), but the compound is mineralized very slowly. The fungicide tebuconazole has much higher sorption capacities than MCPA and bentazon and is less degradable (K_F ~ 12.69 and DT_{50}: 365 days (laboratory studies); PPDB, 2019). The K_F and DT_{50} values of the PPDB database are typically obtained from topsoil studies and they agree reasonably with the values we have obtained for MCPA and bentazon using topsoil from Havdrup-Salløv and Holbæk. However, in the subsurface below one mbs degradation was negligible and especially for MCPA sorption was much lower. This means that if the pesticides reach this depth their inherent properties make them prone to leaching. In contrast, tebuconazole will be retarded due to its higher K_F in accordance with the results of the LUC where much lower tebuconazole concentrations where measured in the outlet.

Degradation may have a great effect on pesticide leaching via biopores in clayey tills as it has been demonstrated by Rosenbom et al., (2014) in model simulations of MCPA degradation in a macropore with a biofilm of MCPA degrading bacteria. We observed clear difference in degradation potentials of both MCPA and bentazon, both regarding sediment depth and whether the sediments where from the clay matrix or potential preferential flow paths (compartments). The degradation was more than ten-fold faster in the topsoil and underlying biopores compared to matrix sediments, but at one mbs, degradation was negligible for both compounds and without practical importance for pesticide leaching. The sorption capacity of both MCPA and bentazon was in general low in all sediments, although the capacity was higher in the topsoils and biopores compared to the adjacent matrix sediments. Recently, sorption of tebuconazole was similarly shown to be higher in macropores compared to the surrounding matrix, and it was suggested that simulations of leaching should consider macropore sorption rather than bulk sorption properties as is the common practice. (Albers et al., 2019).

6.4 PM-type and vulnerability

In this project information and knowledge on potential development of fractures has been obtained from investigations within the MML, DM, DMS, and DR PM types on moraine flats (figure 63). Except for the MML these PM types has not been characterized previously regarding preferential flow pathways. The MMK is the most studied PM-type, often characterized by high fracture densities (low spacing) to depths of 4-5 mbs below which the spacing gradually increase. Though there are exceptions to this pattern as some sites (Sigerslev 1 and Haslev 1) showed high fracture densities even down to 7 mbs (figure 63a). The fracture pattern of the PM type MMS was comparable to the MMK with high fracture densities down to 7-8 mbs for some localities, while for other the density decreased at 4 mbs or even at 2 mbs (Mammen; figure 63b). The PM-types MML and MMR are much less studied. For the PM-type MML there were two previous studies only and the one (Havdrup) was very close to the Havdrup-Salløv site of this study (figure 63c). At Silstrup and Havdrup the fracture spacings increased at approximately 2.5 and 4 mbs, while the spacing at Havdrup-Salløv was below 0.5 m at all investigated depths down to 5.5 mbs. For the PM type MMR there were only one study of fracture densities and this single study showed increasing fracture spacing at depths below approximately 3.5 – 4 mbs, a pattern also seen for some sites belonging to the PM-types MMK, MMS, and, MML (figure 63d). Besides the MML(Havdrup-Salløv), three additional PM-types have been investigated in CLAY-FRAC namely DM (Holbæk), DMS (Tokkekøb), and DR (Farum) (figure 63e). The Holbæk and Farum sites both showed high fracture densities, but interestingly they were only observed in narrow depth intervals; 2-3 mbs at Holbæk and 4-5 mbs at Farum. Though at Farum and Holbæk the tills above the fracture zone contained many sand layers and sand lenses of which many were connected to the deeper fractures and thereby contributing to the preferential water transport network. The Tokkekøb site was characterized by fewer fractures with large spacings in between and again only present at a narrow depth interval of 1.4 and 2.5 mbs. Above this fracture zone was found a diffuse till layer with many wormholes also contributing to the preferential flow network.

It is geologically difficult to compare the different PM-types as the sedimentological heterogeneities are very high. The selected study sites may belong to the most heterogeneous clay till environments and based on this they are all potential vulnerable to pesticide leaching. The Farum, Holbæk, and Tokkekøb sites all had clay layers without tectonic fractures, however, heterogeneities like wormholes, sand lenses, and sometime desiccation fractures were present contributing to the vulnerability to pesticide leaching. At Farum the upper till was a melt-out till, with many sand lenses and the underlying basal till had low fracture spacings both giving a high hydraulic conductivity. At Tokkekøb, fractures were only present in a narrow till unit, but this unit was overlain by a soft sand-rich melt-out till with many wormholes and underneath lake deposits were observed with alternating sand and clay layers. The high degree of heterogeneity was further emphasized by data from a previous borehole two m from the excavation showing a very different build-up of lithology, and a high sedimentological variability.

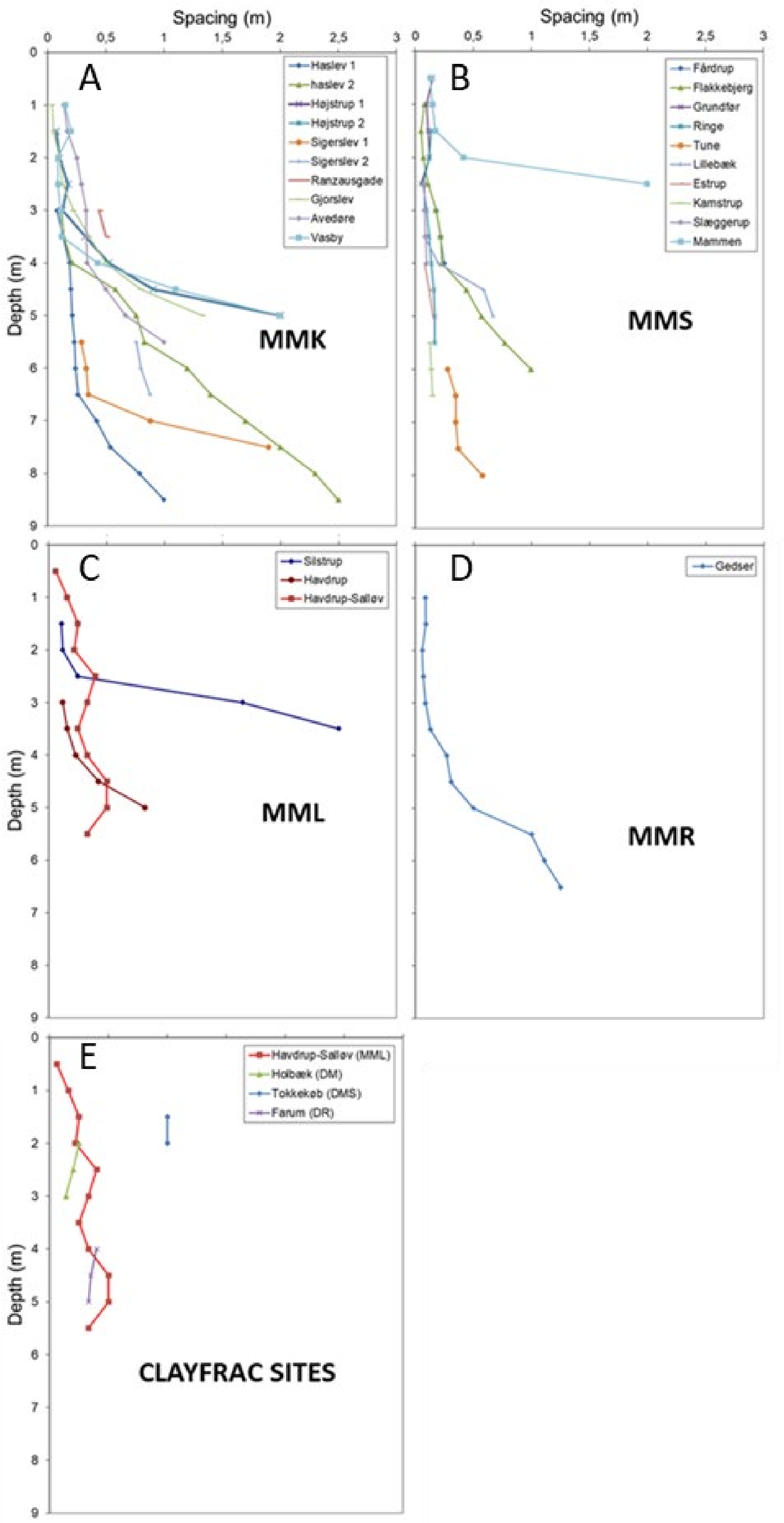

FIGURE 63. Fracture spacings at MMK (A), MMS (B), MML (C), MMR (D) and CLAYFRAC (MML, DM, DMS, and DR; E) PM-types (based on Klint et al. 2001).

The Holbæk site was sedimentological the most complex, with presence of both tills and lake deposits. The high sedimentological variability with several sandy units suggests a high potential vulnerability for this location. At the Havdrup-Salløv locality three till units were observed, separated by thin sand layers and fractures were observed in all tills.

It has been hypothesised that each PM type have unique geological heterogeneities and hydraulic properties that determines their vulnerability to pesticide leaching, however, based on the above it is concluded that it is not possible to relate PM-types to specific preferential flow patterns and thereby rank PM types according their vulnerability to pesticide leaching. The heterogeneity is simply too high concerning geological structures contributing to the overall preferential flow network including tectonic fractures, desiccation fractures, wormholes, and sand lenses the latter probably contributing significantly to the vulnerability of a site to pesticide leaching.

7. References

1. Albers, C. N., V. Ernstsen, and A. R. Johnsen (2019). Soil Domain and Liquid Manure Affect Pesticide Sorption in Macroporous Clay Till. Journal of Environment Quality, 48(1), 147. https://doi.org/10.2134/jeq2018.06.0222
2. Badawi N, A. E. Rosenbom, P. Olsen, and S.R. Sørensen (2015). Environmental fate of the herbicide fluazifop-P-butyl and its degradation products in two loamy agricultural soils: A combined laboratory and field study. Environ. Sci. Technol. 49:8995-9003
3. Badawi, N., A.R. Johnsen, K.K. Brandt, J. Sørensen, and J. Aamand (2013a). Hydraulically active biopores stimulate pesticide mineralization in agricultural subsoil. Soil Biology and Biochemistry 57: 533-541
4. Badawi, N., A.R. Johnsen, J. Sørensen, and J. Aamand (2013b). Centimeter-Scale Spatial Variability in 2-Methyl-4-Chlorophenoxyacetic Acid Mineralization Increases with Depth in Agricultural Soil. Journal of Environment Quality 42:683–689.
5. Bak, F., O. Nybroe, B. Zheng, N. Badawi, X. Hao, M.H. Nicolaisen and J. Aamand (2019). Preferential flow paths shape the structure of bacterial communities in a clayey till depth profile. FEMS Microbiology Ecology, 95, fiz008.
6. Batioglu-Pazarbasi, M., J. Bælum, A.R. Johnsen, S.R. Sørensen, H-J. Albrechtsen, J. Aamand (2012). Centimetre-scale vertical variability of phenoxy acid herbicide mineralization potential in aquifer sediment relates to the abundance of *tfdA* genes. FEMS Microbiology and Ecology 80: 331–341.
7. Beven, K., and P. Germann (2013). Macropores and water flow in soils revisited. Water Resource Research 49:3071-3092
8. Blessent, D., P. R Jørgensen, and R. Therrien (2014). Comparing Discrete Fracture and Continuum Models to Predict Contaminant Transport in Fractured Porous Media. Groundwater, 52:84–95. https://doi.org/10.1111/gwat.12032
9. Broholm K., P.R. Jørgensen, A. B. Hansen, E. Arvin, and M. Hansen (1999a). Transport of creosote compounds in a large, intact macroporous clayey till column. Journal of contaminant hydrology 39: 309-329.
10. Broholm, K., A.B. Hansen, P.R. Jørgensen, E. Arvin, M. Hansen (1999b). Transport and biodegradation of creosote compounds in a large, intact, fractured clayey till column. Journal of Contaminant Hydrology 39, 331–348.
11. Brüsch, W., A.E. Rosenbom, N. Badawi, L. Gudmundsson, F. Platten-Hallermund, C.B. Nielsen, F. Plauborg, T. Laier and P. Olsen (2015). The Danish Pesticide Leaching Assessment Programme Monitoring results May 1999–June 2013
12. Brusseau, M. L., P. S. C. C Rao, R.E. Jessup, and J. M. Davidson (1989). Flow Interruption: A Method for Investigating Sorption Nonequilibrium. Journal of Contaminant Hydrology, 4:223–240. https://doi.org/10.1016/0169-7722(89)90010-7
13. Chambon, J.C.C., I. Damgaard, C.M. Christiansen, G. Lemming, M.M. Broholm, P.J. Binning, and P.L. Bjerg (2009). Model assessment of reductive dechlorination as a remediation technology for contaminant sources in fractured clay: Modeling tool, Delrapport II Environmental Project No. 1296 2009, Environmental Protection Agency
14. Chambon, J.C.C., M.M. Broholm, P.J. Binning, and P.L. Bjerg (2010), Modeling multicomponent transport and enhanced anaerobic dechlorination processes in a single fracture-clay matrix system, Journal of Contaminant Hydrology, 112:77-90
15. Cherry J.A., B.L. Parker, K.K. Bradbury, T.T. Eaton, M.B. Gotkowitz, D.J. Hart, and M.A. Borchardt (2006). Contaminant transport through Aquitards: A-State-of-the-Science Review. Awwa Research Foundation, American Water Works Association, IWA publishing. p.126.

16. Cherry, J.A., (1989). Hydrogeological contaminant behavior in fractured and unfractured clayey deposits in Canada. In: Contaminant transport in groundwater, Kobus V., and Kinzelbach W., (eds) Balkema Rotterdam. 11–20.
17. Cuthbert M.O., R. Mackay, J.H. Tellam, and K.E. Thatcher (2010). Combining unsaturated and saturated hydraulic observations to understand and estimate groundwater recharge through glacial till. Journal of hydrology 391:263–276
18. DS3077 (2013). Representative sampling - Horizontal standard, vol. 44. Danish Standard Authority, pp. 1e38.
19. Ehlers, J. (1979). Fine gravel analyses after the Dutch method as tested out on Ristinge Klint, Denmark. Bull, geol. Soc. Denmark, vol. 27, pp. 157-165
20. Flury M., and M. Flühler (1995) Tracer characteristics of Brilliant Blue FCF. Soil science society of America. 59 (1). 22-27.
21. FOCUS (2014) Generic Guidance for Tier 1 FOCUS Ground Water Assessments. Version 2.2. May 2014
22. Fredericia J. (1990) Saturated hydraulic conductivity of clayey tills and the role of fractures. Nordic Hydrology, 21: 119-132.
23. Freeze R.A., and J. A. Cherry (1979) Groundwater. Prentice-Hall, Englewood Cliffs, NJ. 604.
24. Gates J.B., G.V. Steele, P. Nasta, and J. Szilagyi. (2014) Lithologic influences on groundwater recharge through incised glacial till from profile to regional scales: Evidence from glaciated Eastern Nebraska. Water Resources Research, 50, 466–481
25. GEUS (2007) Landskabets udvikling i Danmark. Geoviden, geologi og geografi nr.1. GEUS 2007. www.geocenter.dk/xpdf/geoviden-1-2007.pdf
26. Gravesen P., I.M. Balling, G. Vignol, K.E.S. Klint, W. Brüsch, B. Nilsson, C.L. Larsen, R. Juhler, and A.E. Rosenbom. (2014) Vurdering af mulighederne for udpegning af pesticidfølsomme lerområder (SFO-ler) på grundlag af eksisterende data. Udarbejdet for Naturstyrelsen. GEUS- rapport nr. 2
27. Hinsby, K., L. D. McKay, P. R. Jørgensen, M. Lenczewsk, and C. P. Gerba (1996) Fracture aperture measurements and migration of solutes, and Immiscible creosote in a column of clay-rich till. Groundwater 3: 1065-1075
28. Jensen, M.B., P.R. Jørgensen, H. C. B. Hansen, and N. E. Nielsen (1998) Biopore mediated subsurface transport of dissolved orthophosphate. Journal of environmental quality 27
29. Jensen, M. B., H. C. B. Hansen, P. R., Jørgensen, and J. Magid (1999) Subsurface transport of phosphate in structured soil - a two step process. Nordic hydrology 30: 361-378.
30. Jørgensen P.R., G. Felding, A. Helweg, N. H. Spliid, M. Thorsen, J. C. Refsgaard, and O. H. Jacobsen (1999) Validation and development of pesticide leaching models. Pesticides Research, 47, Danish Ministry of Environment.
31. Jørgensen P.R., K.Mosthaf, U. Pétursdóttir, J. Aamand, and M. Rolle (2020). Role of Root Channels, Fractures, and Textural Heterogeneity to Flow and Contaminant Transport in Clayey Till Aquitards. A Paradigm Shift. (Manuscript in preparation).
32. Jørgensen P.R., P.H. Krogh, S. Hansen, C. P. Petersen, M. Habekost-Nielsen, S. B. Rasmussen, K. Heinrichson and N. H. Spliid. (2017) Occurrence and hydraulic function of deep biopores and their influence on pesticide migration in glacial clayey till (in Danish with extended English summary), Danish Ministry of Food and Environment, BEKF 171, pp.159.
33. Jørgensen P.R., P.H. Krogh, J. Qin, L. Modesti, I.B. Nielsen, F. Seersholm, N. Wagner, A. J. Hansen, J. Olsen, B. Strobel, S. Hansen, J. Gudbjerg, C.T. Petersen, M. Lacoste, I. Cousin, E. Keaveney, and G. Barrett (2021) Ancient root macropores and fractures in glacial till and their contribution to pesticide vulnerability of groundwater in low and high-ground agricultural landscapes. Pesticides Research, Danish Ministry of Environment (2021 in review).
34. Jørgensen P.R., N. H. Spliid, M. Hansen, W. Harrar, H. Lindgreen, S. Outzen, and A. Brehmer (2001) Point and non-point source leaching of pesticides in a till groundwater water catchment. Pesticide Research no. 52 (2001). Danish Ministry of Environment, Copenhagen, Denmark. (2001).

35. Jørgensen P.R., P.H. Krogh, S. Hansen, C.T. Petersen, M. Habekost-Nielsen, S.B. Rasmussen, and N.H. Spliid (2015) Dybe biopores forekomst og betydning for pesticidudvaskning i moræneler. Miljøstyrelsens Bekæmpelsesmiddelforskning. 1. Rapportudkast godkendt til publiceringen med mindre rettelser.136 sider
36. Jørgensen, P. R., T. Helstrup, J. Urup, and D. Seifert (2004a) Modeling of non-reactive solute transport in fractured clayey till during variable flow rate and time. Journal of Contaminant Hydrology, 68(3–4), 193–216. https://doi.org/10.1016/S0169-7722(03)00146-3
37. Jørgensen, P. R., K. Mosthaf, and M. Rolle (2019). A large undisturbed column method to study flow and transport in macropores and fractured media. Groundwater, 57(6), 951–961. https://doi.org/10.1111/gwat.12885
38. Jørgensen, P.R., M. Hoffmann, J. P. Kistrup, C. Bryde, R. Boss, and K. G. Villholt (2002) Preferential flow and pesticide transport in a clay-rich till: Field, laboratory and modeling analyses. Water resource research., 28: 2801-2815.
39. Jørgensen, P.R., K.E.S Klint, and J. P.Kistrup (2003) Monitoring well interception with fractures in clayey till. Groundwater. Nov. – Dec. 2003, 772-779.
40. Jørgensen, P.R., L. McKay, and J. Kistrup (2004b) Aquifer vulnerability to pesticide migration through till aquitards. Groundwater. 42. 6. 841-855.
41. Jørgensen, P.R., L.D. McKay, and N.H. Spliid (1998) Evaluation of chloride and pesticide transport in a fractured clayey till using large undisturbed columns and numerical modeling. Water resource research 34: 539-553
42. Jørgensen, P.R., and N.H. Spliid (2016) Accumulation of pesticides in anaerobic clayey till - controls and implications to ground water Groundwater Monitoring and Remediation 36, no.3, 43-53
43. Jørgensen, P.R., N.H. Spliid, T. Laier, and S. Outzen (2016) Fate of point source pesticide spill in clayey till after 15 years. Groundwater Monitoring and Remediation 36, no.3, 33-42.
44. Jørgensen, P.R., and N. H. Spliid (1993) Mechanisms and rates of pesticide leaching in shallow clayey till. In: Integrated soil and sediment research: A basis for proper protection. Eds. H.J.P. Eijsackers and Harmers. p.247-253. Kluwer Academic Publishers
45. Jørgensen, P.R., J. Urup, T. Helstrup, M. B. Jensen, F. Eiland, and F. P. Vinther (2004c) Transport and removal of nitrate in clayey till underneath forest and arable land. Journal of contaminant hydrology 73:270 – 286.
46. Jørgensen, P.R., and J. Fredericia (1992) Migration of nutrients, pesticides and heavy-metals in fractured clayey till. Geotechnique 42: 67-77
47. Kardanpour, Z., O. S. Jacobsen, and K. H. Esbensen (2015) Counteracting soil heterogeneity sampling for environmental studies (pesticide residues, contaminant transformation) - TOS is critical. TOS forum 5, 209, 209
48. Kessler T.C., C. Alessandro, O. Fabio, P. Renard, B. Nilsson, K. E. S. Klint, and P. L. Bjerg (2013) Modeling fine-scale geological heterogeneity-examples of sand lenses in tills. Ground Water, 51: 692-705
49. Kitchen N.R., P.E. Blanchard, and R.N. Lerch (2015). Long-term agroecosystem research in the Central Mississippi River basin: Hydrogeologic controls and crop management influence on nitrates in loess and fractured glacial till. Journal of environmental quality 44:58-70
50. Klint K.E.S, and P Gravesen 1999. Fractures and biopores in Weichselian clayey till aquitards at Flakkebjerg, Denmark. Nordic hydrology. 30: 267-284
51. Klint K.E.S. (2001) Fractures in Glacigene diamict deposits: origin and distribution. PhD Thesis, Geological Survey of Denmark and Greenland Report 2001/129, GEUS, Copenhagen
52. Klint, K.E.S., B. Nilsson, L. Troldborg, and P. R. Jakobsen (2013) A Poly Morphological Landform Approach for Hydrogeological Applications in Heterogeneous Glacial Sediments. Hydrogeology Journal.
53. Krüger, J. 1979. Structures and textures in till indicating subglacial deposition. Boreas, Vol 8, No. 3, p. 323-40.
54. Lanters, C. A. (2019). Model-based investigation of solute transport in macropores and heterogeneous fractured clay till. Technical University of Denmark.

55. Larsen, G., J. Frederiksen, A. Villumsen, J. Fredericia, P. Gravesen, N. Foged, B. Knudsen, and J. Baumann (2009) Vejledning i Ingeniørgeologisk prøvebeskrivelse. Danish Geotechnical Society – Bulletin 1.
56. Mckay L.D., and J. Fredericia (1995) Distribution, origin, and hydraulic influence of fractures in a clay-rich glacial deposit. Canadian geotechnical journal, 32:957-975.
57. Meckenstock, R. U., M. Elsner, C .Griebler, T. Lueders, C. Stumpp, J. Aamand, S.N. Agathos, H.J. Albrechtsen, L. Bastiaens, P.L. Bjerg, N. Boon, W. Dejonghe, W.E. Huang, S.I. Schmidt, E. Smolders, S.R. Sørensen, D. Springael, and B.M. van Breukelen. (2015) Biodegradation: Updating the concepts of control for microbial clean-up in contaminated aquifers. Environmental science and technology 49: 7073–7081
58. Miljøstyrelsen (2002), Pesticider og vandværker. Udredningsprojekt om BAM forurening Miljøprojekt Nr. 732, Miljøstyrelsen
59. Mosthaf, K., M. Rolle, U. Petursdottir, J. Aamand, and P. R. Jørgensen (2020) Transport of tracers and pesticides through fractured clayey till: Large Undisturbed Column (LUC) experiments and model-based interpretation. Water Resources Research (accepted).
60. O´Hara, S.K., B. L. Parker, P. R. Jørgensen, J. A. Cherry (2000) Trichloroethene DNAPL flow and mass distribution in naturally fractured clay: 1. Evidence of aperture variability. Water resource research 36:135-147
61. OECD (2000) Guideline for the testing of chemicals 106. Adsorption–desorption using a batch equilibrium method. Org. Econ. Coop. Dev., Paris.
62. Pétursdóttir, U. (2019). Transport of tracers and pesticides in fractured clayey till : LUC flow-through experiments and model-based interpretation. Technical University of Denmark.
63. PPDB (2019) Pesticide properties database. available online: https://sitem.herts.ac.uk/aeru/ppdb/en/index.htm [accessed 2019.01.21]
64. Rosenbom A. E., P. J. Binning, J. Aamand, A. Dechesne; B. F. Smets and A. R. Johnsen (2014) Does microbial cm-scale heterogeneity impact MCPA degradation in and leaching from a loamy agricultural soil? Science of the total environment 472: 90-98
65. Rosenbom A.E, V. Ernstsen, H. Flühler, K. H. Jensen, J. C. Refsgaard, and H. Wydler (2008a) Flourescence imaging applied to tracer distributions in variably saturated fractured clayey till. Journal of Environmental Quality 37: 448-458
66. Rosenbom A.E., R. Therrien, J.C. Refsgaard, K.H. Jensen, V. Ernstsen, and K.E.S. Klint. (2008b) Numerical analysis of water and solute transport in variably-saturated fractured clayey till. Journal of Contaminant Hydrology 104:137-52
67. Rosenbom, A.E., P. Olsen, F. Plauborg, R. Grant, R.K. Juhler, W. Brüsch, and J. Kjær (2015) Pesticide leaching through sandy and loamy fields – long-term lessons learnt from the Danish Pesticide Leaching Assessment Programme. Environ. Poll. 201:75-90.
68. Ruland W.W., J. A. Cherry, and S. Feenstra (1991) The depth of fractures and active ground-flow in a clayey till plain in southwestern Ontario. Ground Water, 21, 3: 405-417.
69. Snow, D. T. (1968) Rock fracture spacings, openings and porosities, J. Soil Mech. Found. Div. Proc. Am. Soc. Civil Eng., 94, 73– 91
70. Sørensen S.R., G.D. Bending, C.S. Jacobsen, A. Walker, and J. Aamand (2003) Microbial degradation of isoproturon and related phenylurea herbicides in and below agricultural fields – a review. FEMS Microbial Ecology 45:1-11.
71. Thalund-Hansen, R. (2018). Assessment of pesticide transport in fractured clay till. Technical University of Denmark
72. Tuxen, N., S. Roost, J. L. L. Kofoed, A. Aisopou, P. J. Binning, J. Chambon, P. L. Bjerg, L. Thorling, W. Brüsch, and K. Esbensen (2013), Skelnen mellem pesticidkilder. Miljøprojekt nr. 1502, 2013, Miljøstyrelsen
73. Wang, L., M. B. Cardenas, W. Deng, and P. C. Bennett (2012). Theory for dynamic longitudinal dispersion in fractures and rivers with Poiseuille flow, 39, 1–5. https://doi.org/10.1029/2011GL050831
74. Witherspoon P.A., J. S. Y. Wang, K. Iwai, and J. E. Gale (1980) Validation of cubic law for fluid flow in deformable roch fractures. Water resource research. 16:1016-1024

75. Zheng, C., and G. D. Bennet (2002). Applied contaminant transport modeling. New York: John Wiley and Sons.
76. Åkesson M., D. Bendz, C. Carlsson, C.J. Sparrenbom, J. Kreuger (2014) Modelling pesticide transport in a shallow groundwater catchment using tritium and helium-3 data. Applied geochemistry 50: 231-239

Appendix 1.1 Soil extraction and analysis of bentazon and MCPA

Soil extraction

To find the most comprehensive extraction procedure for bentazon and MCPA, several extraction solvents were tested for solid-liquid extraction. All tests were performed before the actual field work started; thus, all tests were done on plough layer soil from the clay loam PLAP field, Silstrup and later confirmed with sediments from the Havdrup-Salløv and Holbæk sites. As both compounds are known to have low sorption coefficients, which are positively correlated to the soil content of organic matter and clay the Silstrup soil was considered a worst case soil sorbent and fit for the purpose of finding an extraction procedure covering the soil types of the Holbæk and Havdrup-Salløv sites.

For the solvent testing 2 g Silstrup soil were transferred to 12 mL pyrex glass tubes, added NaN_3 (0.1 M per 2-g soil) to stop microbial degradation, and spiked with ^{14}C-labelled MCPA and bentazon stock solutions, respectively. The pesticide concentrations were then adjusted with non-labelled stock solutions giving final concentrations of 100 µg/kg and 3000 DPM/2-g soil. All stock solutions were prepared in milli Q water. The test tubes were then stored at 4°C at least one day before addition of the different extraction solvents (table 1). All samples were shaken overnight before centrifugation and liquid scintillation counting of the ^{14}C-labelled content of MCPA and bentazon in the supernatant.

The percentage extraction recovery (REC) was determined in duplicate as

$$REC\ (\%) = (B/C) \times 100$$

where B and C is the content (Disintegrations Per Minutes; DPM) of MCPA or bentazon in the supernatant after the extraction and in the pure spike solution, respectively.

Table 1 Extraction solvents tested for solid-liquid extraction of MCPA and bentazon from 2-g soil samples and corresponding extraction recoveries (% REC). #13 represents the extraction solvent used for the degradation experiments at both the Havdrup-Salløv and Holbæk field sites. ACN: acetonitrile, MeOH: methanol, FA: formic acid, MQ: Milli Q water.

Treat no.	Extraction solvent	REC MCPA %	REC bentazon %
1	ACN 100%	68	90
2	ACN 100%	66	92
3	MeOH:MQ 0,1% FA 60:40	73	93
4	ACN:MQ 0,1% FA 60:40	83	92
5	ACN:CaCl2 0.01M, 50:50	86	94
6	MeOH:Acetone, 50:50	65	93
7	MeOH 100%	72	94

8	ACN, 100% + sonication (1 hour)	68	89
9	MeOH, 100% + sonication (1 hour)	76	81
10	ACN:MQ 0,1% FA, 20:80	79	90
11	ACN:0,01 M CaCl2, 20:80	84	95
12	MeOH, 100% + sonication (1 hour)	65	85
13	**ACN:MQ, 20:80 (+/- sonication, 1 hour)**	**82/84**	**88/92**
14	CaCl2 0,01M 100% + sonication (1 hour)	66	87
15	MQ 100% + sonication (1 hour)	71	88

Several of the tested extraction solvents performed well with extraction recoveries > 80 % for both compounds. Especially, the two treatments with acetonitrile and $CaCl_2$ (#5 and #11 in table 1) performed well. However, as it was favourable to keep the extraction procedure as simple as possible due to the high number of samples to be handled, we preferred not to include $CaCl_2$ as it is not advisable to use with direct injection and LC-MS/MS analysis. Instead we used the combination of acetonitrile and MQ + 1 hour sonication (table 1).

The solid-liquid extraction with acetonitrile and Milli Q water (ACN:MQ, 20:80, w:w) was used to extract MCPA and bentazon from all samples in the degradation experiments. The final procedure was in brief, 3800 µL ACN:MQ was added to each 2 g-sample, followed by whirly-mixing until all soil was in solution and sonication in an ultrasound bath for 60 min and then agitation at 160 RPM on a shaking-table overnight. The following day, samples were centrifuged at 2000 × g (20 min) and supernatants then filtered (PTFE filters, 0.22 mm, Titan Filtration Systems; Sun SRi, Wilmington, NC, USA) directly into HPLC vials for direct analysis of MCPA and bentazon concentrations. Prior to the extraction procedure, all samples were added a mixture of deuterium labelled MCPP (MCPP-d6) and bentazon (bentazon-d7) (internal standards, final sample concentration: 1 µg/kg; see section 4.2.1) to be extracted together with MCPA and bentazon.

Preparation of calibrator solutions and calibrator samples

A mix of bulk soil representing all compartments and depths was sieved and divided into 2-subsamples in Pyrex tubes like in the degradation experiment. The subsamples were spiked with MCPA and bentazon in varying concentration and used as calibrators for quantification of MCPA and bentazon in the degradation experiment. Five calibrators (2 g) were prepared on the day of solid-liquid extraction by adding bentazon and MCPA to final concentrations of 0, 0.05, 0.1, 1.0, and 20.0 µg/kg. The calibrators were further added deuterated bentazon and MCPA (1.0 µg/kg) as internal standards and extracted in parallel with the samples from the degradation experiment.

Chromatographic conditions

Chromatographic separation of MCPA and bentazon was performed using ultra-high-pressure liquid chromatography on a Waters ACQUITY UPLC system (Waters, Milford, USA) equipped with a Waters Acquity UPLC ™ BEH C_{18} 1,7 µm, 2.1x50 mm column and an inline filter (0.2 µm). The mobile phase consisted of (A) ACN and (B) Milli-Q water with 0.05% formic acid and was run as a gradient with increasing ACN content (table 2). A constant flow rate of 0.4 mL/min was used and total runtime was 6 min. The column temperature was 40°C and the injection volume was 10 µl.

Table 2 Inlet gradient program for analysis of MCPA and bentazon. ACN: acetonitrile, FA: formic acid. Total runtime: 6 min.

Time (min.)	% A: ACN	% B: MQ (0,05% FA)
0,00	10	90
3.0	60	40
3.1	90	10
5.0	90	10
5.1	10	90

Mass spectrometry

Mass spectrometry was performed using a Xevo TQ-S Micro triple quadrupole (Waters, Milford, MA, USA). Negative electrospray ionization mode was used for all mass spectrometric analyses. The ionization parameters were set as capillary voltage of 0.5 kV, and desolvation and source temperatures of 600 and 150 °C, respectively. Nitrogen (N_2) was used as cone and desolvation gas with a flow of 30 and 1000 L/h, respectively and argon was used as collision gas. Data acquisition of the analytes was done using the multiple-reaction monitoring (MRM). Data analysis was done using MassLynx 4.1 (Waters Corporation) software with automated data processing (TargetLynx). The analytes were identified by the ratio of two characteristic MRM transitions and the retention time. Quantification was performed by integration of the area under the curve from the specific MRM chromatograms of the analytes and the internal standards (figure 1). The response (the ratio of the integrated area of the analyte and the IS) was compared to the calibration curve generated from the calibrators. The retention times, MRM transitions and ionization energies for all compounds are shown in table 3.

Table 3 Retention time, MRM transitions, and operating parameters for MCPA, bentazon and internal standards, MCPP-d6 and bentazon-d7 (MRM transitions are listed for each analyte with quantifier transition on top and qualifier transition below).

Compound	ESI	Retention time (min)	MRM transitions (*m/z*)	Cone voltage (V)	Collision energy (eV)
Bentazon	Negative	2.11	239 > 131.9	40	24
			239 > 196.95		17
MCPA	Negative	2.36	198.95 > 140.9	25	12
			198.95 > 105		25
tebuconazole	Positive	3.12	308 > 69.9	45	18
			310 > 69.9		18
Internal standard:					
MCPP-d6	Negative	2.64	219 > 146.9	20	12
Bentazon-d7	Negative	2.09	246 > 131.9	50	25
Tebuconazole-d9	Positive	3.11	317 > 69.9	45	20

The LOD and LOQ for the quantification of MCPA and bentazon used for the degradation experiment was LOD 0.03 and LOQ 0.05 µg/kg.

For the LUC method (quantification of water samples), the LOD and LOQ for bentazon and tebuconazole were 0.005 µg/L and 0.01 µg/L, respectively and LOD was 0.01 µg/L and LOQ 0.05 µg/L for MCPA.

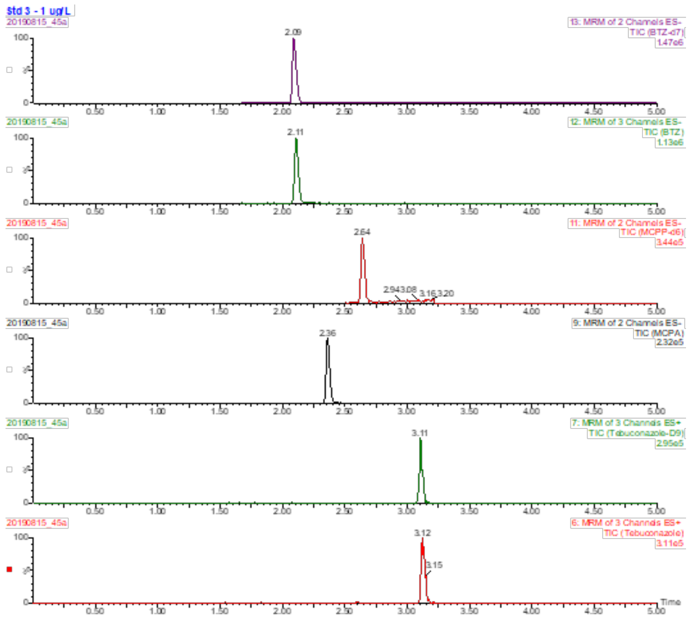

Figure 1 Chromatogram of bentazon, MCPA and tebuconazole. MCPP-d6 was used as internal standard for quantification of MCPA. Tebuconazole was not included in the degradation experiment but was included in the LC-MS/MS method for quantification of all three compounds in the LUC experiments (chap. 4.3 and 5.3)

Calculation of DT_{50}

Degradation curves from the degradation experiments following first order kinetics were used for calculation of DT_{50} (half-lives) values using:

$$C_t = C_0 \times e^{-kt} \qquad \text{(Eq. 1)}$$

where C_0 is the initially spiked concentration (µg/kg), C_t is the concentration (µg/kg) of pesticide remaining in the soil at time *t* (days), and *k* is the 1. order degradation rate constant (days^{-1}). The rate constant is then used for calculation of DT_{50} using:

$$DT_{50} = \frac{\ln 2}{k} \qquad \text{(Eq. 2)}$$

The measured concentrations for MCPA and bentazon were plotted against the incubation time and fitted with the model using the Solver (GRG non-linear) function in Microsoft Excel.

Degradation curves not following first order kinetics were fitted with linear regression and DT_{50} was calculated as the time required to achieve 50% removal:

$$C_t = A(t) + C_0 \qquad \text{(Eq. 3)}$$

Where *A* is the linear degradation rate constant.

For degradation curves not following first order or linear regression due to lack of degradation or not enough data points with degradation were not assigned a DT_{50} value but only a “no” or > 87 days, respectively depending on the curves.

Appendix 1.2 Drilling report from well situated about 600 m west of the Farum excavation

De Nationale Geologiske Undersøgelser for Danmark og Grønland — Udskrevet 4/7 2019 Side 1

GEUS

BORERAPPORT — **DGU arkivnr: 193. 3804**

Borested : Stavnsholt Gydevej 93
3520 Farum

Kommune : Furesø
Region : Hovedstaden

Boringsdato : 1/6 2018 — **Boringsdybde** : 15 meter — **Terrænkote** : 46.89 meter o. DNN

Brøndborer : Poul Hasbo A/S, Ishøj
MOB-nr :
BB-journr :
BB-bornr : F16

Prøver
- modtaget : 10/7 2018 **antal** : 17
- beskrevet : 17/9 2018 **af** : JWP
- antal gemt : 0

Formål : Råstofboring
Anvendelse :
Boremetode :

Kortblad : 1514 IISV
UTM-zone : 32
UTM-koord. : 711858, 6191935

Datum : EUREF89
Koordinatkilde : Brøndborer
Koordinatmetode : GPS

0 **MULD**, sandet, indh. af planterester, mørk brun, kalkfri. (muld). Prøve udtaget ved .1 m. Note: fyld ifølge brøndborer - evt muldfyld.

0.2 **SAND**, leret, siltet, svagt gruset, brun, kalkfri, "morænesand". Laggrænse skønnet. Prøve udtaget ved .5 m.

0.7 **LER**, siltet, mange slirer af sand, brun, kalkfri. (glacial vekslende små smeltevandslag). Prøve udtaget ved 1 m.

1 **SAND**, leret, siltet, svagt gruset, brun, kalkholdig, "morænesand". Laggrænse skønnet. Prøve udtaget ved 2 m.

2 **LER**, siltet, sandet, svagt gruset, brun, kalkholdig, "moræneler". Laggrænse skønnet. Prøve udtaget ved 3 m.

3 **SAND**, leret, siltet, svagt gruset, brun, kalkholdig, "morænesand". Laggrænse skønnet. Prøve udtaget ved 4 m.

4 **SAND**, leret, siltet, svagt gruset, brun, kalkholdig, "morænesand". Laggrænse skønnet. Prøve udtaget ved 5 m.

5 **SAND**, leret, siltet, svagt gruset, brun, kalkholdig, "morænesand". Prøve udtaget ved 6 m.

6.9 **SAND**, leret, siltet, svagt gruset, brun, kalkholdig, "morænesand". Prøve udtaget ved 7 m.

7.4 **SAND**, leret, siltet, svagt gruset, gråbrun, kalkholdig, "morænesand". Laggrænse skønnet. Prøve udtaget ved 8 m.

8 **SAND**, leret, siltet, svagt gruset, gråbrun, kalkholdig, "morænesand". Prøve udtaget ved 9 m.

9.9 **SAND**, mest mellem, slirer af silt, gråbrun, kalkholdig, "smeltevandssand". Prøve udtaget ved 10 m.

10.4 **LER**, siltet, sandet, svagt gruset, gråbrun, kalkholdig, "moræneler". Laggrænse skønnet. Prøve udtaget ved 11 m.

11 **LER**, siltet, sandet, svagt gruset, gråbrun, kalkholdig, "moræneler". Laggrænse skønnet. Prøve udtaget ved 12 m.

12 **LER**, siltet, sandet, svagt gruset, gråbrun, kalkholdig, "moræneler". Laggrænse skønnet. Prøve udtaget ved 13 m.

13 **LER**, siltet, sandet, svagt gruset, gråbrun, kalkholdig, "moræneler". Prøve udtaget ved 14 m.

14 **SAND**, mest mellem, siltet, brun, kalkholdig, "smeltevandssand". Prøve udtaget ved 15 m.

Appendix 1.3 **Drilling report from well 198.342 situated about 800 m northeast of the Holbæk excavation**

De Nationale Geologiske Undersøgelser for Danmark og Grønland

Udskrevet 24/1 2020 Side 1

BORERAPPORT

DGU arkivnr: 198. 342

Borested : VANDTÅRN NORDVEST FOR HOLBÆK LADEGÅRD
4300 Holbæk
2012-12-12: Sløjfet iflg. kommunen.

Kommune : Holbæk
Region : Sjælland

Boringsdato : 27/2 1964
Boringsdybde : 15 meter
Terrænkote : 39,7 meter o. DNN

Brøndborer :
MOB-nr :
BB-journr :
BB-bornr :

Prøver
- modtaget :
- beskrevet : **af** : G
- antal gemt :

Formål :
Anvendelse : Sløjfet/opgivet bor
Boremetode :

Kortblad : 1413 INØ
UTM-zone : 32
UTM-koord. : 669522, 6176752

Datum : ED50
Koordinatkilde :
Koordinatmetode : Dig. på koor.bord

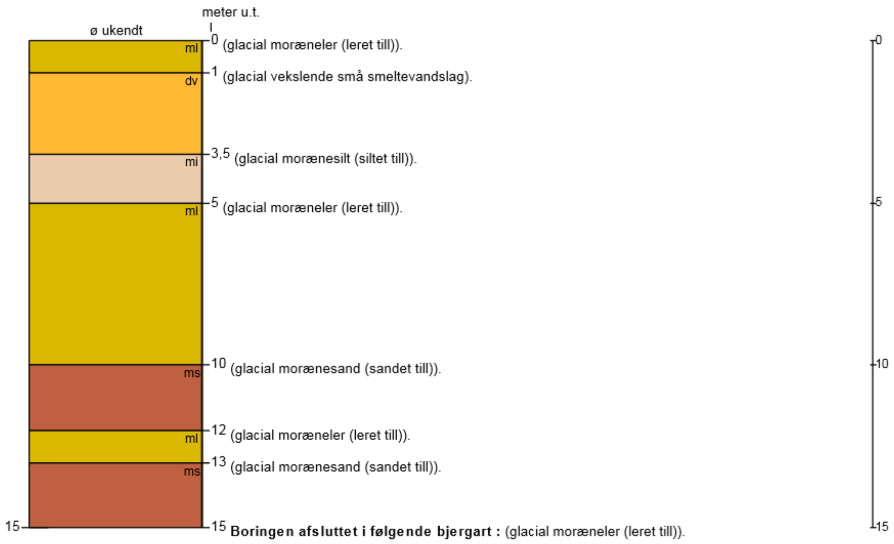

Mapping groundwater vulnerability to pesticide contamination

through fractured clays - CLAYFRAC

This report describes results from a project investigating possibilities to map or rank clay localities according to their vulnerability to pesticide leaching. The project entailed a combined and multiscale experimental and modelling approach starting from the polymorphological (PM) concept for ranking the heterogeneity of clay-till deposits. The PM concept separate clay-till deposits in landforms differing by their pattern of superimposed geomorphological units. Four large excavations have been established representing different PM landforms.

The lithology and presence of preferential flow paths, including macropores (wormholes, root channels, burrows etc), tectonic and desiccation fractures, and sand lenses were characterized at each excavation. All sites were geologically highly heterogeneous with different clay units being mixed with sand lenses and sand layers, implying that it may be difficult to attribute defined geological characteristics to PM types.

The geological characterization, though, showed the following general trends: 1) Macropores, including wormholes were present in all upper tills where they probably are the most dominant preferential waterflow routes, 2) fractures changed colour from grey to red due to iron precipitation at greater depths, and 3) sand deposits were present at all locations in the form of sand layers and sand lenses of different thicknesses.

In order to develop comprehensive vulnerability mapping methods, knowledge about heterogeneities at greater depths below the ‘fracture zone’ investigated in CLAYFRAC is needed as well as a systematic verification with pesticides contamination of groundwater aquifers underlying the clayey till aquitards.

The Danish Environmental
Protection Agency
Tolderlundsvej 5
DK - 5000 Odense C

www.mst.dk